

Bridge scour evaluation in cohesive soils using physical and geo-electrical soil properties

by

Md Zahidul Karim

B.S., Bangladesh University of Engineering and Technology, 2013

M.S., Kansas State University, 2016

AN ABSTRACT OF A DISSERTATION

submitted in partial fulfillment of the requirements for the degree

DOCTOR OF PHILOSOPHY

Department of Civil Engineering
College of Engineering

KANSAS STATE UNIVERSITY
Manhattan, Kansas

2019

Abstract

Scour accounts for 60% of all bridge collapses nationwide. There are two recommended methods for evaluating scour in cohesive soils, and both are flawed. The most common method is to use the scour evaluation manual from the Federal Highway Administration, Hydraulic Engineering Circular-18. The empirical equations, however, are based on the results of flume tests using cohesionless soils and are typically over conservative. The second alternative, performing site specific erosion testing, can be cost prohibitive, as erosion testing using available apparatuses is highly specialized and time consuming. Therefore, this research seeks to provide a new methodology that gives more accurate information than the equations based on cohesionless soils and is more cost effective than erosion testing. Various soil characteristics that affect the erosion of soil also influence in situ bulk electrical resistivity measurements. The objectives of this research were to develop a rapid methodology to predict soil erodibility using electrical resistivity and build an empirical equation to predict critical shear stress for erosion in cohesive soils using various soil properties. A total of 26 sites were used for in situ testing and soil sampling. Soil samples were used for erosion testing with the Erosion Function Apparatus and measuring geotechnical properties. The results indicate that electrical resistivity works as an excellent binary classifier for identifying soil with high erodibility. An electrical resistivity over 50 Ωm has a 93% probability of classifying the soil as high erodibility. As such, electrical resistivity tomography can be utilized to rapidly prioritize existing bridges where soils near the surface are classified as highly erodible. Regarding the second objective, multiple variable screening criteria determined percent fines, liquid limit, and electrical resistivity as the statistically significant model variables for predicting critical shear stress. Electrical resistivity is an increasingly common measurement by transportation agencies and this is the first time it has been identified as a variable for predicting critical shear stress. The use of electrical resistivity reduces the need for uncommon geotechnical, geochemical, and biological soil tests to predict critical shear stress. Design factors for

implementing the developed model for a practical design were also recommended based on probabilistic analysis. If adopted by transportation agencies, this research will reduce the need for cost prohibitive site specific testing and overconservative bridge scour designs.

Bridge scour evaluation in cohesive soils using physical and geo-electrical soil properties

by

Md Zahidul Karim

B.S., Bangladesh University of Engineering and Technology, 2013

M.S., Kansas State University, 2016

A DISSERTATION

submitted in partial fulfillment of the requirements for the degree

DOCTOR OF PHILOSOPHY

Department of Civil Engineering
College of Engineering

KANSAS STATE UNIVERSITY
Manhattan, Kansas

2019

Approved by:

Major Professor
Stacey E. Kulesza

Copyright

© Md Zahidul Karim 2019.

Abstract

Scour accounts for 60% of all bridge collapses nationwide. There are two recommended methods for evaluating scour in cohesive soils, and both are flawed. The most common method is to use the scour evaluation manual from the Federal Highway Administration, Hydraulic Engineering Circular-18. The empirical equations, however, are based on the results of flume tests using cohesionless soils and are typically over conservative. The second alternative, performing site specific erosion testing, can be cost prohibitive, as erosion testing using available apparatuses is highly specialized and time consuming. Therefore, this research seeks to provide a new methodology that gives more accurate information than the equations based on cohesionless soils and is more cost effective than erosion testing. Various soil characteristics that affect the erosion of soil also influence in situ bulk electrical resistivity measurements. The objectives of this research were to develop a rapid methodology to predict soil erodibility using electrical resistivity and build an empirical equation to predict critical shear stress for erosion in cohesive soils using various soil properties. A total of 26 sites were used for in situ testing and soil sampling. Soil samples were used for erosion testing with the Erosion Function Apparatus and measuring geotechnical properties. The results indicate that electrical resistivity works as an excellent binary classifier for identifying soil with high erodibility. An electrical resistivity over 50 Ωm has a 93% probability of classifying the soil as high erodibility. As such, electrical resistivity tomography can be utilized to rapidly prioritize existing bridges where soils near the surface are classified as highly erodible. Regarding the second objective, multiple variable screening criteria determined percent fines, liquid limit, and electrical resistivity as the statistically significant model variables for predicting critical shear stress. Electrical resistivity is an increasingly common measurement by transportation agencies and this is the first time it has been identified as a variable for predicting critical shear stress. The use of electrical resistivity reduces the need for uncommon geotechnical, geochemical, and biological soil tests to predict critical shear stress. Design factors for

implementing the developed model for a practical design were also recommended based on probabilistic analysis. If adopted by transportation agencies, this research will reduce the need for cost prohibitive site specific testing and overconservative bridge scour designs.

Table of Contents

List of Figures	x
List of Tables	xii
Acknowledgements	xiii
Dedication	xiv
Chapter 1 - Introduction.....	1
Chapter 2 - Predicting Soil Erodibility Using Electrical Resistivity Tomography.....	9
Abstract.....	9
2.1 Introduction.....	10
2.2 Electrical Resistivity Tomography	13
2.3 Methodology.....	15
2.3.1 Soil Sampling	15
2.3.2 Erosion Testing	16
2.3.3 Electrical Resistivity Field Survey	19
2.4 Results and Analysis.....	20
2.5 ER as a method to predict erodibility	26
2.6 Validation.....	31
2.7. Discussion.....	33
2.8 Conclusions.....	36
Chapter 3 - Electrical Resistivity as a Binary Classifier for Bridge Scour Evaluation.....	39
Abstract.....	39
3.1 Introduction.....	40
3.2 Methodology.....	44
3.2.1 Erosion Testing and Soil Analysis	44
3.2.2 In situ ERT Surveys	46
3.2.3 Laboratory ER Measurements	50
3.3 Results of Erosion Testing.....	52
3.4 Results of Laboratory ER Measurements	53
3.4.1 Laboratory ER measurements as an alternative to in situ ERT.....	54
3.4.2 Effect of Degree of Saturation on In Situ ER.....	58

3.5 Electrical Resistivity as a Classifier for Erodibility.....	61
3.5.1 ROC Curve for Evaluating a Binary Classifier	62
3.5.2 Interpreting an ROC Space.....	63
3.5.3 Efficiency of ER as a Binary Diagnostic Classifier	65
3.5.4 Selecting a Fixed Cut-off ER for the Binary Classifier.....	66
3.6 Discussion.....	68
3.7 Conclusions.....	71
Chapter 4 - Modeling Critical Shear Stress for Bridge Abutment Scour in Cohesive Soils	73
Abstract.....	73
4.1 Introduction.....	74
4.2 Methodology.....	79
4.3 Results and Analysis.....	82
4.3.1 Variable Selection	85
4.3.2 Model to Predict Critical Shear Stress in Cohesive Soils.....	89
4.4 Design Recommendations	91
4.5 Validation.....	95
4.6 Discussion.....	96
4.7 Conclusions.....	100
Chapter 5 - Scientific Contributions	102
5.1 Establishing resistivity as a measurable soil property	102
5.2 A binary classifier for rapid erosion monitoring	103
5.3 A new critical shear stress equation for cohesive soils.....	104
5.3 Implementing robust probabilistic and statistical approaches in geotechnical engineering	105
Chapter 6 - Conclusions.....	107
References.....	111
Appendix A - Full dataset.....	129

List of Figures

Fig. 1.1 Factors affecting erosion in cohesive soils (Grabowski 2011)	4
Fig. 2.1 EFA testing: (a) placement of the sample on piston head; (b) trimmed sample in flush with flume bottom (before the test); (c) sample with rough surface (after the test)	18
Fig. 2.2 Experimental setup at the bridge sites: (a) ER survey line; (b) potential position of 28th and 29th electrodes around borehole.....	19
Fig. 2.3 Typical site: (a) subsurface inverted ER of US-69; (b) erosion rate versus shear stress for US-69 samples	21
Fig. 2.4 Erosion rate versus shear stress for 14 sites: (a) USCS classification; (b) varying ER.....	25
Fig. 2.5 Predicting high edibility using ER: (a) ROC curve; (b) sensitivity and specificity for varying ER cut-off.....	28
Fig. 2.6 Erosion rate versus shear stress for two ranges of ER	30
Fig. 2.7 Validation site: (a) subsurface inverted ER of US-166A; (b) erosion rate versus shear stress for US-166A samples.....	32
Fig. 3.1 Map showing the bridge sites used for drilling and ERT survey.....	46
Fig. 3.2 Schematic demonstrating the dipole-dipole array.	48
Fig. 3.3 In situ ERT survey line including the data acquisition system.	49
Fig. 3.4 Resistance meter and soil box with C1, C2 current electrodes and P1, P2 voltage electrodes.	51
Fig. 3.5 Erosion rate versus shear stress for varying soil type of 72 samples in the study...	53
Fig. 3.6 Comparison of ER values: (a) bar chart comparing ER values as obtained from in situ ERT, laboratory ER (at the same S as in the field), and laboratory ER at fully saturated condition ($S \approx 100\%$); (b) laboratory ER (at in situ S) versus in situ ER; (c) laboratory ER ($S \approx 100\%$) versus in situ ER.....	55
Fig. 3.7 Characteristic ROC Space.....	64
Fig. 3.8 Probability density functions for both high and not high erodibility samples.	68
Fig. 3.9 Two dimensional ER and soil erodibility profile for US-24 site. (in color).....	69
Fig. 3.10 Two dimensional ER and soil erodibility profile for US-36 site. (in color).....	70

Fig. 4.1 Location of the 23 sites from eastern Kansas with their surficial geology	80
Fig. 4.2 Erosion rate versus shear stress with USCS classification for the 70 samples.....	83
Fig. 4.3 Heatmap showing the multicollinearity among independent variables; red and blue colors denote positive and negative correlations, respectively.....	86
Fig. 4.4 Predicted versus actual (measured) critical shear stress	90
Fig. 4.5 Cumulative density function plot for αd	92
Fig. 4.6 (a) Comparison of design scour depths with calculated scour depths for varying critical shear stress; (b) Design scour depths versus calculated scour depth	94
Fig. 4.7 (a) Subsurface resistivity distribution at K-10 site; (b) the EFA test result for the validation sample from K-10 site.....	96

List of Tables

Table 1.1 Typical ER values of different geo-materials (Knight and Endres 2005; Lucius et al. 2007)	6
Table 2.1 Erosion Test Results of US-69 samples	22
Table 2.2 Soil Properties and Classification of US-69 Samples	23
Table 2.3 Soil Properties and Classification of US-166A Samples	33
Table 2.4 Predicted Versus Actual Erosion Test Results for US-166A	33
Table 3.1 Comparison of in situ ER with laboratory ER at different degree of saturation.	54
Table 3.2 Sample of observations showing the differences between in situ and laboratory ER (with in situ S) (Column VI - Column VII of Table 3.1).	56
Table 3.3 Sample of observations showing the differences between in situ ER (with in situ S) and laboratory ER (with S \approx100%) (Column VI - Column VIII of Table 3.1).	60
Table 3.4 Diagnostic test results with respect to actual test results (adapted from Kumar and Indrayan 2011).	62
Table 3.5 TPR and FPR for various ER cut-off values as obtained from SPSS.	66
Table 3.6 Erosion test results with respect to recommended ER cut-off.	67
Table 4.1 Physiographic Origins of the Soil Samples	81
Table 4.2 Description of the Statistical Variables for Model Development for 70 Soil Samples	84
Table 4.3 <i>F</i> Scores of the Independent Variables for Predicting Critical Shear Stress	89
Table 4.4 Model Cross Validation Results	91

Acknowledgements

My graduate study at K-State has been a wonderful experience for me. First, I would like to express my deep sense of appreciation and gratitude to my major professor Dr. Stacey E. Tucker-Kulesza who has given me an exciting project to work on. Surely, the knowledge I have earned from her guidance, will make me a better research professional in the future. I am also grateful to her for providing me financial support throughout my graduate study.

I would also like to express my sincere gratitude to Dr. Dunja Peric, Dr. Gerard Kluitenberg, and Dr. Christopher Jones for their kind support as my committee members and Dr. Sunghun Park for kindly serving as the chairperson of the examining committee. Again, I would not be able to finish my research without the help my wonderful groupmates, Weston Koehn, Tri Tran, Ranojoy Chatterjee, Luke Augustine, and Mark Mathis II. I also acknowledge the kind help of Mr. Cody Delaney for helping me with all sorts of technical issues in my research.

Finally, this research was funded by the Kansas Department of Transportation. I would like to thank Bradford Rognlie, Michael Orth, James Brennan, Michael Noguera, and others with the Kansas Department of Transportation for supporting the project, providing feedback, selecting a variety of bridge sites, and collecting soil samples. Out of state samples were collected by the FHWA for a separate study. I would like to thank the FHWA for granting permission for use of these data in this study.

Dedication

I would like to dedicate my dissertation to my wonderful wife for her unconditional support throughout the days of preparing this dissertation and my beloved parents for their inspiration towards my graduate study.

Chapter 1 - Introduction

The Federal Highway Administration (FHWA) defines scour as the result of erosive action of flowing water, excavating and carrying away material from the bed and banks of streams and from around the piers and abutments of bridges (Calappi et al. 2010). Scour is the number one threat to the nation's bridge safety. Scour accounts for 60% of bridge failures, while earthquakes cause only 2% of bridge failures in the United States (Shirole and Holt 1991). From 1965 to 2005, over 1,500 bridges collapsed in the United States. Many of these collapses were due to extreme events. For example, 73 bridges collapsed during the 1985 floods in Pennsylvania, Virginia, and West Virginia (Richardson et al. 2001). While bridge collapses are costly loss of infrastructure, they can be dangerous for the traveling public. The 1987 interstate highway bridge failure over Schoharie Creek in New York that killed ten people was one of the primary motivators for the FHWA to establish scour monitoring procedures (Lin et al. 2014). Unfortunately, although preliminary protocol was put in place in 1988, the Hatchie River Bridge failed during the 1989 flood in Tennessee that killed nine people. In fact, these two catastrophic failures are considered as the driving force that motivated extensive scour monitoring research in the United States (Lin et al. 2014). Note that while this research focuses on scour design and monitoring in the United States, catastrophic bridges collapses due to scour are an international infrastructure issue.

Responding immediately to the 1987 Schoharie Creek Bridge failure, the FHWA published "Interim Procedures for Evaluating Scour at Bridges" in 1988. The procedures were reevaluated over time by the FHWA and Hydraulic Engineering Circular 18 (HEC-18) was published in 1991. Although it has been updated several times, the HEC-18 remains the state of the practice manual for evaluating bridge scour. State Departments of Transportation (DOTs) across the nation have relied on HEC-18 for evaluating the scour vulnerability of their bridges. There are 616, 096 bridges

currently listed in the National Bridge Inventory (FHWA 2018). Of these bridges, approximately 84% are built over waterways, of which, over 20,000 are classified as “scour critical”. Therefore, at least one out of every twenty-five bridges in the United States are vulnerable to scour. According to Nassif et al. (2002), about 80% of existing bridges require some sort of scour mitigation.

In 2005, all state DOTs were required to establish a plan of action (POA) to maintain scour critical bridges. Despite the overwhelming number of scour critical bridges, the FHWA specifically states that long-term monitoring is not an acceptable POA. This is a challenge for many states that have large numbers of scour critical bridges. For example, Wu and Chase (2010) identified over 1,000 of the 25,013 bridges in Kansas as scour critical but, many bridges have been labeled as scour critical based on calculations rather than observation, further exacerbating the issue. Because the HEC-18 is not accurate in all geologic and hydraulic conditions, many bridges are labeled as scour critical unnecessarily. For example, during the early 1990s’, the New Jersey Department of Transportation (NJDOT) analyzed nearly 2,400 state and county owned bridges using HEC-18 equations and identified 165 bridges as “scour critical”. However, in 2006, NJDOT launched a POA for the state’s scour critical bridges with the United States Geological Surveys (USGS) to conduct erosion monitoring. The USGS found that many of these bridges were not scour critical and were placed in the list solely based on HEC-18 analysis method (Schuring et al. 2010). Having bridges labeled as “scour critical” in the National Bridge Inventory requires plans for remediation or replacement. Since, the number of scour critical bridges is high nationwide, there is a need for every state to determine a feasible, cost effective and rapid methodology to identify the structures and prioritize the remediation or scour mitigation of these bridges. Hence, one of the motivations of this study is to establish a feasible POA methodology to identify scour critical bridges.

The HEC-18 is also used to estimate scour depths in new bridges, but the empirical equations are over conservative for cohesive soils. For example, these equations are applicable for a minimum median grain size of 0.2 mm (Arneson et al. 2012); however, median grain size is smaller than 0.075 mm for most cohesive soils. In cohesionless coarse grained soil, only gravity force resists the applied hydraulic stress to prevent erosion. Since this force is proportional to the size of the soil particle, median grain size predicts scour in cohesionless/non-cemented coarse grained soils reasonably accurately. On the other hand, soil particles in cohesive soils are mainly fine grained (i.e., smaller than 0.075 mm) and have a higher ratio of surface area to volume. In the presence of water these particles are subjected to interparticle forces. Cohesion and adhesion resulting from these interparticle forces, provide resistance against scour in addition to gravity forces. Thus, the resisting forces are more complex. According to Grabowski et al. (2011), the erosion in cohesive soils is dependent on a set of dynamically linked physical, geochemical and biological properties as shown in Fig. 1.1. Grabowski et al. (2011) reviewed a series of studies to correlate the erodibility of cohesive soils with the factors shown in Fig. 1.1; however, none of these studies were focused on bridge scour and few provided equations for calculating erodibility.

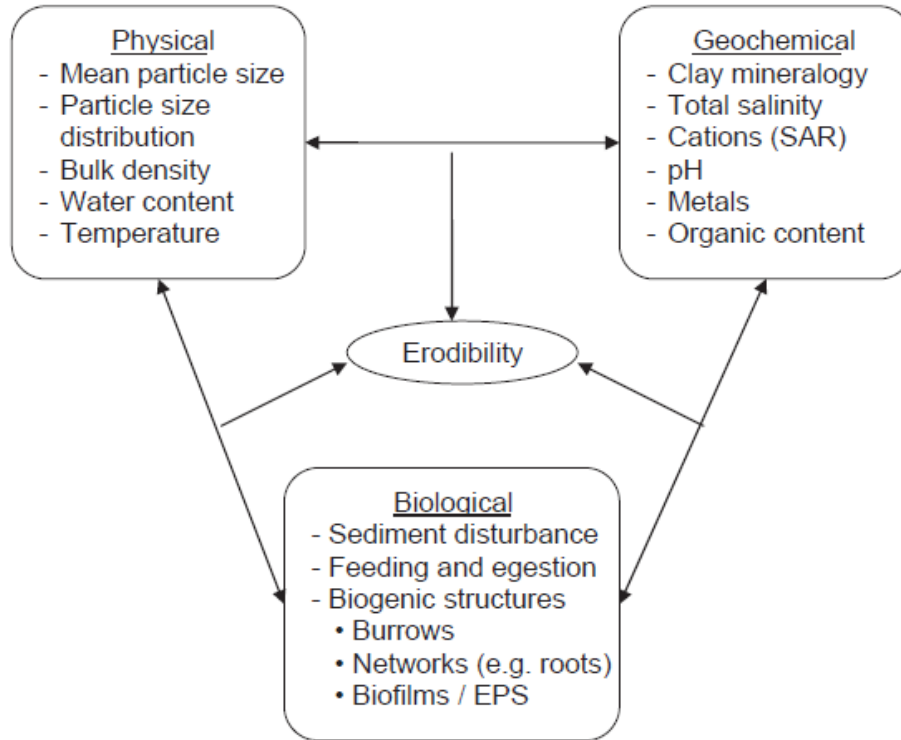


Fig. 1.1 Factors affecting erosion in cohesive soils (Grabowski 2011)

Because it was well established that the original HEC-18 scour equations were overly conservative for cohesive soils, Arneson et al. (2012) modified the scour estimation equation. These equations are now given as a functions of critical shear stress, which is the threshold shear stress (exerted by the flowing water) at which erosion occurs. However, there was no equation to determine the critical shear stress; rather site specific testing was suggested. In other words, the Arneson et al. (2012) recommends a direct measurement of critical shear stress. Numerous testing devices have been developed for directly measuring soil erosion (and critical shear stress) in the laboratory and in the field. Some of the recent apparatuses for erosion measurements include the Sediment Erosion Rate Flume (Crowley et al. 2012), the FLUME (Ravens 2007), the Jet Erosion Testing apparatus (Hanson and Cook 2004), and the Erosion Function Apparatus (EFA) (Briaud et al. 2001). Although this equipment list is not exhaustive, it represents the most common apparatus for bridge scour design. Still,

these equipments are not used for standard hydraulic or geotechnical tests making it a time consuming and cost prohibitive approach. Therefore, the common practice is to use the scour estimation equation for cohesionless soils irrespective of the soil type. As mentioned, the equation is valid for a minimum median grain size 0.2 mm, which is what is typically assumed. The resulting scour depths in cohesive soils become over conservative and inaccurate.

To address the need of an equation to predict the onset of erosion in cohesive soils, Shan et al. (2015) developed a critical shear stress equation (τ_c) (Pa) in the context of the FHWA's HEC-18 framework such that,

$$\tau_c = 0.1 \left(\frac{w}{F} \right)^{-2.0} (PI)^{1.3} q_u^{0.4} \quad (1.1)$$

where, w is the gravimetric water content (dimensionless), F is the fraction of fines (<0.075 mm) by mass (dimensionless), PI is the plasticity index (dimensionless), and q_u is the undrained shear strength (Pa). Although the regression equation corresponded to a R^2 of 0.71, it is only applicable to cohesive soils with plasticity indices between 4 to 25 and fraction of fines between 10 to 90. Furthermore, the shear stress range was limited to 3 to 15 Pa. In practice, these boundaries represent low plastic silts and clays which is only a portion of cohesive soils. Karim (2016) used the equation to predict critical shear stress in Kansas soils and found the equation to be unconservative at low stress (dangerous) and overconservative for many soils due to the smaller upper limit of the equation. Therefore, there is still a need to develop a robust equation to predict critical shear stress for a wide range of cohesive soils. This is the second objective of this study.

Many of the factors that affect the erosion in cohesive soils (Fig. 1.1) also influence soil bulk electrical resistivity measurements. Electrical resistivity is a measure of a material's ability to oppose the flow of electric current. Typical ranges of electrical resistivity for different geo-materials are

shown in Table 1.1. According to Friedman (2005), the factors that affect electrical resistivity can be divided into three categories. The first category describes bulk soil, in other words the respective volume fractions of solids and possible secondary structural configurations (aggregation): porosity, water content, and structure. The second category includes solid particles quantifiers such as particle shape, particle orientation, particle-size distribution, cation exchange capacity, and wettability. The third is the relevant soil solution attributes including ionic strength, cation composition, sodium absorption ratio, and temperature. Due to these common factors affecting both erosion and soil electrical resistivity, electrical resistivity was used in this study to characterize the soil erosion potential in cohesive soils.

Table 1.1 Typical ER values of different geo-materials (Knight and Endres 2005; Lucius et al. 2007)

Material	Resistivity (Ωm)
Clay	5-100
Dry Sand and Gravel	>200
Saturated Sand and Gravel	<50
Sandstone	50-1,000
Shale	5-50
Conglomerates	1,000-10,000
Limestone and Dolomite	>1,000
Igneous Rocks	>1,000
Metamorphic Rocks	>1,000

Electrical resistivity tomography (ERT) survey has gained popularity as a geophysical testing method due to improved data acquisition systems and inversion schemes. It is commonly used as a nondestructive testing method in geology, environmental science, archeology, and geotechnical engineering (Loke 1999; Dahlin 2001; Zonge et al. 2005). Applications within these fields include

determining depth to groundwater (Vaudelet et al. 2011), detecting varying subsurface geology (Chambers et al. 2013), the integrity of subsurface structures (Arjwech et al. 2013, Tucker et al. 2015), and locating seepage channels in levees (Karim et al. 2019). From geotechnical engineering perspective, although conventional soil test boring provides the ability to determine soil properties along a vertical line, borings cannot provide continuous soil data across the subsurface. In contrast, ERT is able to provide an image of the subsurface, including qualitative and quantitative information. ERT is considered one of the Advanced Geotechnical Methods in Exploration (A-GaME) by the FHWA and its use has been increasing by the transportation agencies for its capacity to obtain continuous subsurface data between soil borings and reduce the number of borings in geotechnical projects (FHWA 2019).

To improve the nationwide scour evaluation practices in the context of FHWA's HEC-18, there were five objectives of this dissertation. First, to develop a rapid methodology (classifier) to characterize the soil erodibility, which would allow transportation agencies to implement priority based POA for scour critical bridges. This would be done by distinguishing comparatively more scour vulnerable bridge sites from rest of the sites using ERT. The second objective was to develop an empirical model for critical shear stress in cohesive soils using various soil properties. As mentioned, utilizing geophysical methods such as electrical resistivity is not uncommon in geotechnical engineering; however, its use has mostly been for qualitative subsurface characterization. Hence, the third objective of this study was to evaluate electrical resistivity as a measurable soil property by using it as a variable in the models for both prioritizing scour monitoring as well as the predicting critical shear stress. The fourth objective was to recommend a design factor for practical use of the critical shear stress model with a probabilistic approach.

The final objective of this study was to validate both models using a bridge site selected by Kansas Department of Transportation (KDOT).

This study was funded by the KDOT and US Department of Transportation. As the project progressed, findings have been published in peer reviewed research articles to disseminate research findings and receive feedback from the engineering community to ensure meaningful recommendations. Three of these journal articles are compiled in this dissertation. This dissertation is organized in six chapters. The background, problem statement along with the research objectives are described in Chapter 1. The Introduction is followed by the first journal article (Chapter 2), where a binary classifier model to characterize the erodibility level of a bridge site was developed using electrical resistivity. One of the limitations of the first article was the soil samples were not fully saturated (as they were collected from stream banks). In the second journal article (Chapter 3) limitations of the previous article were addressed by comparing laboratory prepared fully saturated electrical resistivity measurements with in situ partially saturated samples. Chapter 3 also fully describes the statistical methodology for evaluating a binary classifier. The accuracy of the binary classifier model was evaluated using the receiver operating characteristics curve (ROC), which is a common tool for assessing the accuracy of a diagnostic test. Next, the model to predict the critical shear stress using various soil properties was developed and is discussed in the third article (Chapter 4). This article includes the variable screening for model development, design factor selection, and validation of the model. Next the novel scientific contributions of this dissertation research were described in Chapter 5. Chapter 6 includes the study conclusions and recommendations for future work based on this research.

Chapter 2 - Predicting Soil Erodibility Using Electrical Resistivity Tomography

This article was published in ASCE's *Journal of Geotechnical and Geoenvironmental Engineering* in January 2018. The full citation is:

Karim, M. Z., and Tucker-Kulesza, S. E. (2018). "Predicting soil erodibility using electrical resistivity tomography." *J. Geotech. Geoenviron. Eng.*, 10.1061/(ASCE)GT.1943-5606.0001857.

Abstract

Scour is responsible for roughly 60% of all bridge collapses in the United States. A large number of bridges are listed in the National Bridge Inventory as scour critical; however, evaluating scour potential based on soil sampling and laboratory testing can be uneconomic, as erosion testing using available apparatuses is time consuming. Various soil characteristics that affect the erosion of soil also influence in situ bulk electrical resistivity (ER) measurements collected using electrical resistivity tomography (ERT). The objective of this study was to predict soil erodibility using ERT. Fourteen bridge-sites were used for ERT and erosion testing. The results of this study indicate that an ER over 50 Ωm has a 93% probability of classifying as high erodibility. As such, ERT can be used to rapidly prioritize existing bridges where soils near the surface are likely highly erodible and require a more detailed investigation or to characterize soil erosion potential at proposed bridge sites. The application of using ERT to predict soil erodibility was validated using an additional experimental site.

Keywords: Scour; Electrical resistivity tomography; Erosion function apparatus; Receiver operating characteristic curve

2.1 Introduction

There are 614,387 bridges currently listed in the National Bridge Inventory (NBI) and over 500,000 are built over waterways (FHWA 2017). Scour is the most significant threat to these waterway bridges, where soils are eroded from around the structure. For example, over 1,500 bridges collapsed in the United States from 1965 to 2005, and scour was responsible for nearly 60% of these failures (Calappi et al. 2010). Bridge owners are required to maintain a bridge inspection program, which includes scour evaluation using the Federal Highway Administration (FHWA) Hydraulic Engineering Circular 18 (HEC-18) (Arneson et al. 2012). However, researchers have observed that the HEC-18 scour equations tend to over-predict scour depth for most geologic and hydraulic conditions because these empirical equations were developed from regression analysis of laboratory test results using coarse grained soils (Schuring et al. 2010). Soil sampling and testing yields more accurate scour predictions at sites where a HEC-18 analysis is not sufficient, but erosion testing is time consuming and costly. For example, Wu and Chase (2010) identified over 1,000 of the 25,013 bridges in Kansas as scour critical. Soil sampling and erosion testing at all 1,000 scour critical bridges is not feasible in a cost effective and timely manner. There is a need for a rapid methodology to establish priority where detailed bridge scour testing is necessary.

Scour, or more generally, erosion, occurs when hydraulic forces exerted by flowing water exceed the resistive forces at the soil surface. The hydraulic forces primarily include the shear forces of the flowing water acting parallel to the sediment plane. The resistive forces within the soil include gravity, friction, cohesion and adhesion depending on the type of soil (Grabowski et al. 2011). The threshold of applied hydraulic shear stress at which erosion initiates is the critical shear stress (Partheniades 1965; Ariathurai 1974; Hanson et al. 1999; Utley and Wynn 2008;

Bernhardt et al. 2011). The excess shear stress equation is the common simplified equation to estimate soil erosion rate, defined as

$$\dot{E} = k_d(\tau - \tau_c) \quad (2.1)$$

where \dot{E} is the erosion rate (mm/hr), k_d is the erodibility coefficient ($\text{m}^3/\text{N}\cdot\text{s}$), τ is the hydraulic stress (Pa), and τ_c is the critical shear stress (Pa) (Partheniades 1965; Hanson et al. 1999). The erodibility coefficient and critical shear stress are interrelated, soil specific and hydraulic parameters that are difficult to estimate; therefore, several researchers have developed apparatuses to directly measure soil erodibility. These apparatuses generally fall in four categories: rotating apparatus tests (Moore and Masch 1962; Bloomquist et al. 2012); jet erosion tests (Hanson and Cook 2004; ASTM D5852 2007a); internal erosion tests (Sherard et al. 1976; Wan and Fell 2004); and flume style tests (Briaud et al. 2001; Ravens 2007; Crowley et al. 2012).

This study utilized an Erosion Function Apparatus (EFA), which is a flume style test, for erosion testing. The EFA was originally developed for performing site-specific erosion testing for evaluating bridge scour. Briaud et al. (2001) proposed to use the erosion function (a plot of erosion rate versus shear stress) from EFA tests to estimate the scour depth, rather than depending on correlations to geotechnical properties. Briaud (2008) also proposed an erodibility categorizing graph by subdividing the erosion function based on the results of 15 years of testing in the EFA which was adopted in the latest edition of HEC-18 (Arneson et al. 2012).

Many researchers have investigated the relationship between measurable soil properties and erodibility (Dunn 1959; Smerdon and Beasley 1961; Carlson and Enger 1962; Reddi and Bonala 1997; Briaud et al. 2001; Léonard and Richard 2004; Meng et al. 2012; Bernhardt et al. 2011; McClerren et al. 2012). However, these relationships are not widely used in practice. A new

empirical equation to predict critical shear stress as a function of water content, percent fines, plasticity index, and unconfined compressive strength was proposed in an FHWA study (Shan et al. 2015). Although the coefficient of determination (R^2) of the correlation was 0.73, this equation is only applicable to soils having plastic limit 4 to 25, liquid limit 15 to 50, percent fines between 10 to 90, and a range of shear stresses from 3 to 15 Pa. The fine grained soils in this study contained over 95% fines and the applied shear stress was as high as 97 Pa before erosion initiated. Therefore, this relationship was not applicable for Kansas soils at scour critical bridges and it was shown to over predict critical shear stress, an unconservative prediction (Karim 2016). As such, there is still a need for a methodology to predict critical shear stress for soils at higher stresses.

Electrical resistivity (ER) is an intrinsic soil property which indicates a material's ability to oppose the flow of current. Electrical resistivity tomography (ERT) is a near surface geophysical technique to collect bulk ER measurements with depth. ERT surveys are rapid compared to erosion testing and there are several common factors that influence the ER of soil and soil erodibility including mean particle size, particle size distribution, soil unit weight, and water content (Abu-Hassanein et al. 1996; Kibria and Hossain 2012; Grabowski et al. 2011; Karim and Tucker-Kulesza 2017). Therefore, ERT was proposed as a method to prioritize bridges based on predicted soil erodibility. ERT has become a widely used geophysical method in fields such as geology, environmental science, geotechnical engineering, and archeology (Loke 1999; Dahlin 2001; Vaudelet et al. 2011; Hossain et al. 2011; Chambers et al. 2013; Snapp et al. 2017).

The objective of this study was to evaluate the applicability of ERT for prioritizing bridge scour evaluations. An overview of ER follows this introduction, then methodology of this research including field and laboratory work are discussed. The erodibility categorizing graph obtained from HEC-18 was used to identify the erodibility levels of soils from different sites. These data

were used for statistical analysis to determine the efficiency of ER as a diagnostic test and establishing probabilities for different levels of erodibility for specific ER ranges. This paper ends with the methodology validation, a discussion of the results and limitations of the study, and conclusions.

2.2 Electrical Resistivity Tomography

ERT utilizes at least four-electrodes in a straight line for each measurement: two induce current flow in the subsurface (A, B) and two measure the resulting voltage potential (P, Q). The source electrode (A) sends the current into the ground and the sink electrode (B) receives it, creating an electric field in the subsurface. If the measured voltage difference between electrodes P and Q is V_{PQ} , then the apparent resistivity is

$$\rho_a = \left(\frac{2\pi V_{PQ}}{I} \right) \left[\frac{1}{r_{AP}} - \frac{1}{r_{AQ}} - \frac{1}{r_{BP}} + \frac{1}{r_{BQ}} \right]^{-1} \quad (2.2)$$

where I is the induced current and r is the lateral distance between respective electrodes. The term apparent resistivity is used because initially the subsurface is assumed to be homogenous with uniform resistivity, ρ_a . An inversion process is required to determine the true resistivity of the subsurface from the measured apparent resistivity. The lateral distance between electrodes and the sequence of measurements affect the resolution of the data. Variables, including the depth of penetration of the signal, signal to noise ratio, and vertical and lateral resolution must be considered when determining the electrode configuration (Everett 2013). The primary goal of ERT in this study was to obtain subsurface ER data where samples were collected with 89 mm diameter Shelby tubes extending approximately to a depth of 3.35 m. The dipole-dipole array was used in this study. The dipole-dipole array is a configuration of electrodes in which the spacing between the two current sink/source electrodes and the two voltage potential electrodes are constant. The

dipole-dipole array is one of the most commonly used configurations because it provides good vertical and lateral resolution of the subsurface with minimal coupling effects between the current sink/source and voltage potential electrodes. This resulted in high resolution data surrounding the borehole with depth.

The measured apparent resistivity must undergo an iterative process that involves forward modeling and data inversion to determine the true resistivity of subsurface. Forward modeling mathematically calculates the apparent resistivity for given electrical properties and boundary conditions (Binley and Kemna 2005). The data inversion uses the measured apparent resistivity and calculated apparent resistivity data to determine the true resistivity distribution of the subsurface. The Advanced Geosciences, Inc. (AGI) EarthImager 2D commercial software was used in this research to determine the true resistivity of subsurface (AGI 2009). The starting model was a finite element mesh with each element assumed to be equal to the average of all the measured apparent resistivity data. Next, the apparent resistivity for each element was calculated (forward model). An Occam style smooth model was used for data inversion (Constable et al. 1987). The smooth model inversion utilized the data misfit between the calculated and measured apparent resistivity, determined by the root mean squared error, E_{RMS} , and the normalized $L2$ -Norm, $L2_{Norm}$, such that

$$E_{RMS} = \sqrt{\frac{\sum_{i=1}^N \left(\frac{d_i^{calc} - d_i^{meas}}{d_i^{meas}} \right)^2}{N}} * 100\%, \text{ and} \quad (2.3)$$

$$L2_{Norm} = \frac{1}{N} \sum_{i=1}^N \left(\frac{d_i^{calc} - d_i^{meas}}{W_i} \right)^2 \quad (2.4)$$

where d_i^{calc} is the calculated apparent resistivity by forward modeling, d_i^{meas} is the measured apparent resistivity from the field, N is the total number of data points, and W_i is the estimate of

data weights (E_{RMS}). The smooth model inversion produces the model that best fits the data with minimum roughness and optimum smoothness. The estimate of data weights, E_{RMS} , is chosen by the user. If the E_{RMS} is too high, the resulting model will be over smoothed. If the noise estimate is too low, the inversion will be forced to fit data noise and produce artifacts. The $L2_{Norm}$ is used to guide the error estimate. An $L2_{Norm}$ of one indicates the error estimate was appropriate for the measured data. If the $L2_{Norm}$ is above one, the error estimate was too low, if it close to zero the data are likely over smoothed. The inversion and forward modeling take place until they meet the data misfit criteria and the corresponding inverted resistivity section is selected as the true resistivity section for a site. The objective of the inversion process is to meet the data misfit criteria in as few iterations as possible. Typically, E_{RMS} less than 3.0 % and $L2_{Norm}$ less than 1.0 are considered as an excellent fit (Tucker et al. 2015); therefore, these data misfit criteria were chosen in this research.

2.3 Methodology

The Kansas Department of Transportation (KDOT) selected 15 bridge sites across eastern Kansas to categorize erosion in this study. Sites were selected considering the scour vulnerability and proximity to Kansas State University (K-State); 14 of the sites were used for model development and one site was used for validating the model. Fieldwork included soil sample drilling by the KDOT and the ERT survey. All samples were tested using the EFA at K-State for erosion data.

2.3.1 Soil Sampling

Thin-walled Shelby tubes were used following ASTM standard D1587 (ASTM 2015a) to collect soil samples at each bridge site. Five 89 mm, 610 mm long samples were collected at each of the 15 sites at a fixed drilling position. The top 0.3 m of soil was augered through to remove the surface

vegetation. As a result, the total drilling depth for five samples was typically 3.35 m. Drilling was performed as close to the stream as possible and at least 10 m from the pavement shoulder or the bridge abutment so that collected sample represented the native geology of the site, avoiding influence from the bridge on the measured resistivity. Drilling was not conducted in the streambeds as bridge abutment scour is critical in Kansas, particularly where there is no surface vegetation.

The Shelby tubes were pushed using the drill rig without rotation to the desired depth. This was repeated five times for five separate but continuous samples. ASTM standard D4220 (ASTM 2014a) was followed for preserving and transporting soil samples to maintain the in situ conditions. Samples were stored in a 100% humidity controlled room until erosion testing. The samples were designated according to their highway name and the order of sampling. For example, the top sample, collected from the 0.3 m to 0.9 m depth at US-400 was designated as US-400 #1.

2.3.2 Erosion Testing

The soil erosion rate was measured in the EFA. The Shelby tube was cut to remove the holes that connect to the drill head, and approximately 381 mm of soil was used for the erosion test. The rest of the sample was used for in situ soil water content and classification. One end of the Shelby tube containing the sample was placed over a piston [Fig. 2.1(a)] and the other end was passed through a circular opening in the bottom of the flume so that the soil was flush with the flume bottom [Fig. 2.1(b)]. Water flowed through a rectangular flume using a pump to control the water velocity. Larionov et al. (2014) showed that the temperature of water influences the erosion rate; therefore, water temperature during each EFA test was $15 \pm 2^\circ\text{C}$ maintained by continuous filling and sump pumping the water reservoir with cold tap water. Soil samples were tested at room temperature, 20°C . The erosion rate was measured at six different velocities for each sample.

The shear stress due to the flowing water that causes the erosion is calculated as

$$\tau = \frac{1}{8} f \rho v^2 \quad (2.5)$$

where f is the friction factor, ρ is the mass density of the flowing fluid (water) in kg/m^3 (999.1 to 999.4 kg/m^3 for water temperature $15 \pm 2^\circ\text{C}$), and v is the water velocity in m/s (Briaud et al. 2001). The friction factor was obtained from the Moody Chart (1944) and was a function of relative roughness of the eroding surface and Reynold's number. Relative roughness, ε/D , is the ratio of the average height of the roughness elements on the eroding surface (soil above and below the top of the Shelby tube), ε , and the diameter of the Shelby tube, D . Briaud et al. (2001) estimated ε as the half the median grain size assuming half of the particle protruded into the flow and bottom half was buried into the soil mass during testing. However, this approximation may lead to error in shear stress calculation, as during testing under each velocity the roughness of the eroding surface [Fig. 2.1(c)] was of higher magnitude than half of the median grain size. Therefore, ten measured roughness points were used calculate the average height of the roughness elements so that

$$\varepsilon = \sum_{i=1}^{10} \frac{h_i A_i}{A} \quad (2.6)$$

where, h_i , A_i are the height and corresponding area of i -th roughness element measured by calipers; and A is the cross-sectional area of the sample or Shelby tube. Reynold's number was calculated using the same method as described in Briaud et al. (2001).

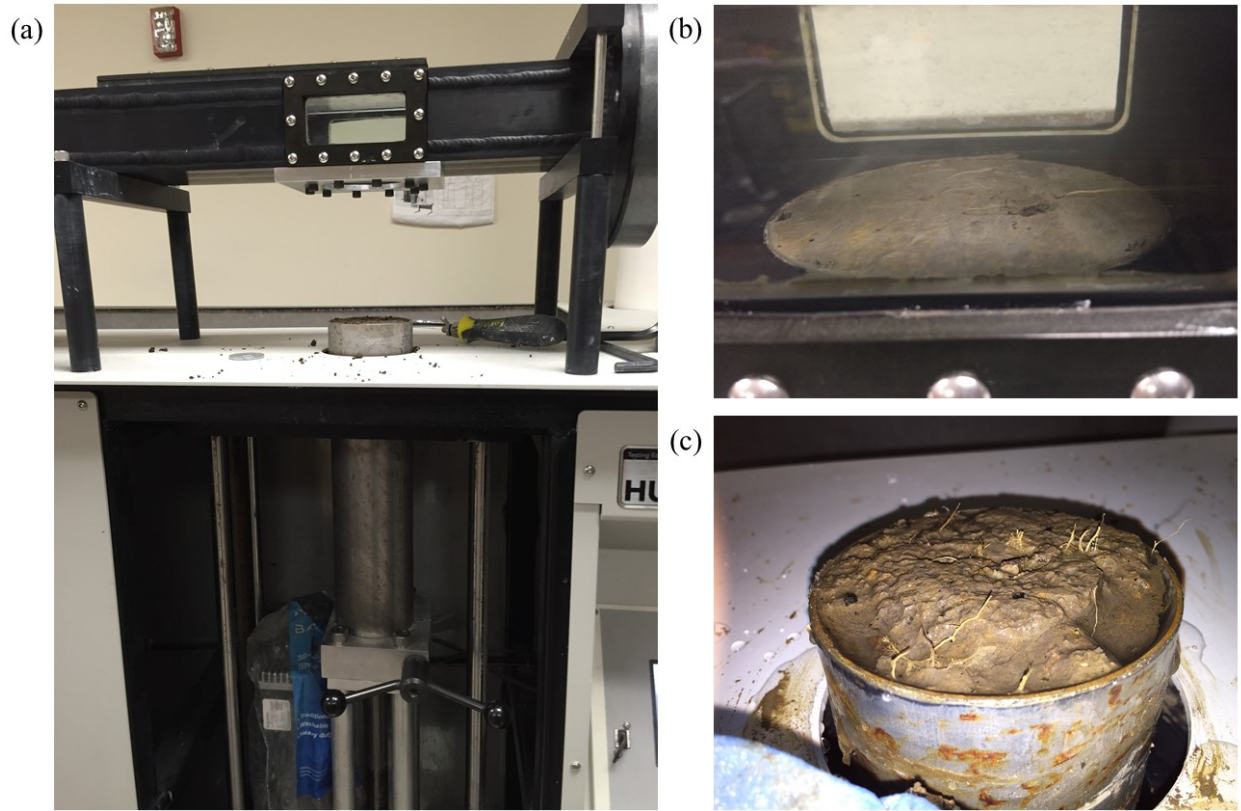


Fig. 2.1 EFA testing: (a) placement of the sample on piston head; (b) trimmed sample in flush with flume bottom (before the test); (c) sample with rough surface (after the test)

The remaining soil was used for classification using the Unified Soil Classification System (USCS). For this purpose, sieve analysis was performed using ASTM standards C117 (ASTM 2013) and C136 (ASTM 2014b) and hydrometer analysis was performed using ASTM standard D422 (ASTM 2007b). Plasticity Index (*PI*) for classification was determined according to ASTM standard D4318 (ASTM 2010). Although hydrometer analysis was not required for the classification of many samples, it was done for all samples to obtain the median grain size.



Fig. 2.2 Experimental setup at the bridge sites: (a) ER survey line; (b) potential position of 28th and 29th electrodes around borehole

2.3.3 Electrical Resistivity Field Survey

The AGI SuperSting R8/IP multichannel imaging system was used for the ERT. The SuperSting data acquisition (DAQ) was powered by two 12V deep-cycle marine batteries. The current and voltage measurements were obtained via electrodes on cables that were connected to the DAQ. The K-State system has 56 electrodes which were connected to metal stakes that were hammered into the ground to couple the electrodes to the subsurface. The metal stakes were 46 cm in length and 2.2 cm in diameter. With 56 electrodes and a spacing of 0.46 m, the length of survey line was 25.2 m. The survey line was oriented so that the position of the borehole was in the center of the ERT survey line (between the 28th and 29th electrode) and parallel to the creek or river [Fig. 2.2(b)]. This was also selected because more data points are in the central region of ERT measurements and consequently the highest resolution is obtained in that region. Relative elevations of each electrode were measured using a total station and a survey rod.

2.4 Results and Analysis

The US-69 site is located in Labette County in southeast Kansas and is shown as an example site to describe the data collection process. The US-69 bridge crosses Big Sugar Creek, where water flow was observed during the ERT survey on May 30, 2016. The inverted resistivity section for US-69 is shown in Fig. 2.3(a). The RMS error for the inversion was 2.25% and L2 norm was 0.45, which indicate excellent agreement of the measured and calculated resistivity. All inversion statistics in this research had an RMS error below 3% and L2 norm less than 1.0. The dashed line rectangle in Fig. 2.3(a) shows the location of the borehole corresponding to the five samples from US-69. Fig. 2.3(a) also shows the USCS soil types for these samples. A silt layer is evident near the ground surface with comparatively higher ER (above 37.8 Ωm).

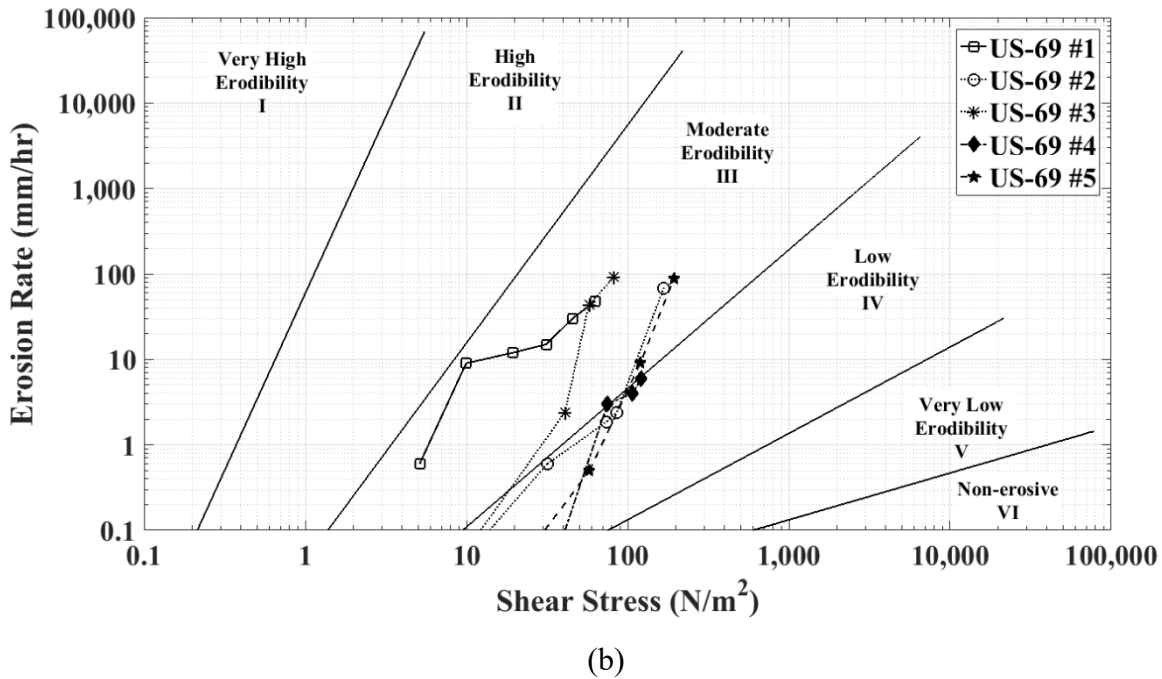
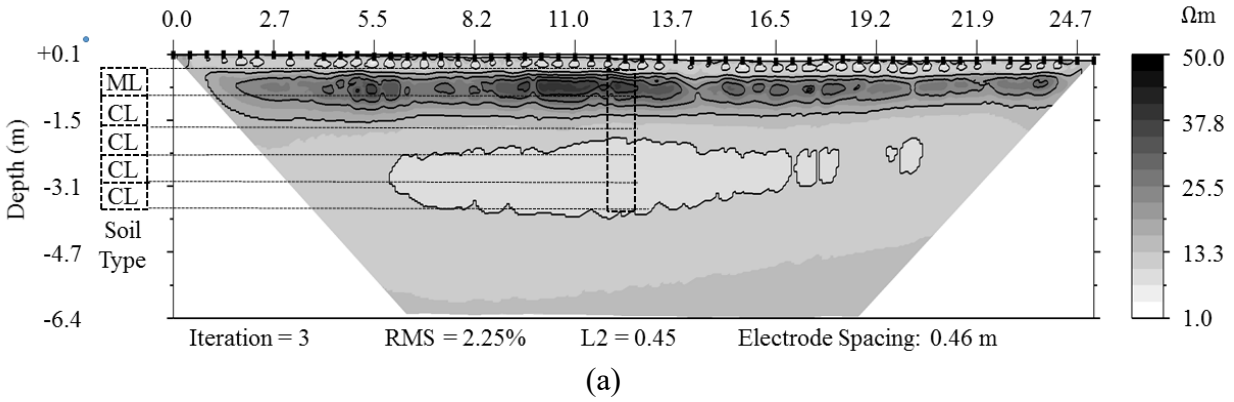


Fig. 2.3 Typical site: (a) subsurface inverted ER of US-69; (b) erosion rate versus shear stress for US-69 samples

Each sample was 610 mm long and 89 mm in diameter. In the 2D ERT profile this 610 mm x 89 mm area for a single sample corresponded to 16 elements of the finite element mesh of the true resistivity from the inversion. The average ER from these 16 elements was used as the ER for each sample. The ER measurements of the five samples from US-69 were between 7.5 to 39.8 Ωm and are shown in Table 2.1. Each erosion test was performed under six different water velocities and the erosion rate was measured for each velocity. Eq. (2.5) was used to calculate the corresponding

shear stresses for these water velocities. The critical shear stress for each sample was the minimum shear stress at which the sample started to erode. The erosion test results of US-69 are also shown in Table 1. US-69 #1 was the most erodible among the five samples from the site as the critical shear stress was the lowest (5.1 N/m²). These results were compiled using the HEC-18 erodibility categorizing plot [Fig. 2.3(b)], where the erosion rate is plotted against shear stress with erodibility boundaries (Arneson et al. 2012; Briaud 2008). Note that this a logarithmic plot; points below the critical shear stress have zero erosion rate and are not visible.

Table 2.1 Erosion Test Results of US-69 samples

Sample	ER (Ω m)	Erosion Test Results							Critical Shear Stress (N/m ²)
US-69 #1	39.8	Water Velocity (m/s)	1.0	1.5	2.0	2.5	3.0	3.5	5.1
		Shear Stress (N/m ²)	5.1	10.0	19.5	31.3	45.5	62.8	
		Erosion Rate (mm/hr)	0.6	9.0	12.0	15.0	30.0	48.0	
US-69 #2	14.6	Water Velocity (m/s)	1.0	2.0	3.0	4.0	5.0	6.0	31.7
		Shear Stress (N/m ²)	2.6	13.9	31.7	73.4	85.6	167.4	
		Erosion Rate (mm/hr)	0.0	0.0	0.6	1.8	2.4	68.6	
US-69 #3	7.8	Water Velocity (m/s)	1.0	1.5	2.0	3.0	3.5	4.0	40.8
		Shear Stress (N/m ²)	3.1	6.8	12.3	40.8	57.4	82.0	
		Erosion Rate (mm/hr)	0.0	0.0	0.0	2.4	43.1	91.4	
US-69 #4	7.5	Water Velocity (m/s)	1.0	2.0	3.0	4.0	5.0	6.0	75.0
		Shear Stress (N/m ²)	3.2	13.9	40.8	75.0	107.2	121.5	
		Erosion Rate (mm/hr)	0.0	0.0	0.0	3.0	4.0	6.0	
US-69 #5	9.3	Water Velocity (m/s)	1.0	2.0	3.0	4.0	5.0	6.0	58.0
		Shear Stress (N/m ²)	3.0	13.2	30.6	58.0	119.7	193.5	
		Erosion Rate (mm/hr)	0.0	0.0	0.0	0.5	9.0	88.0	

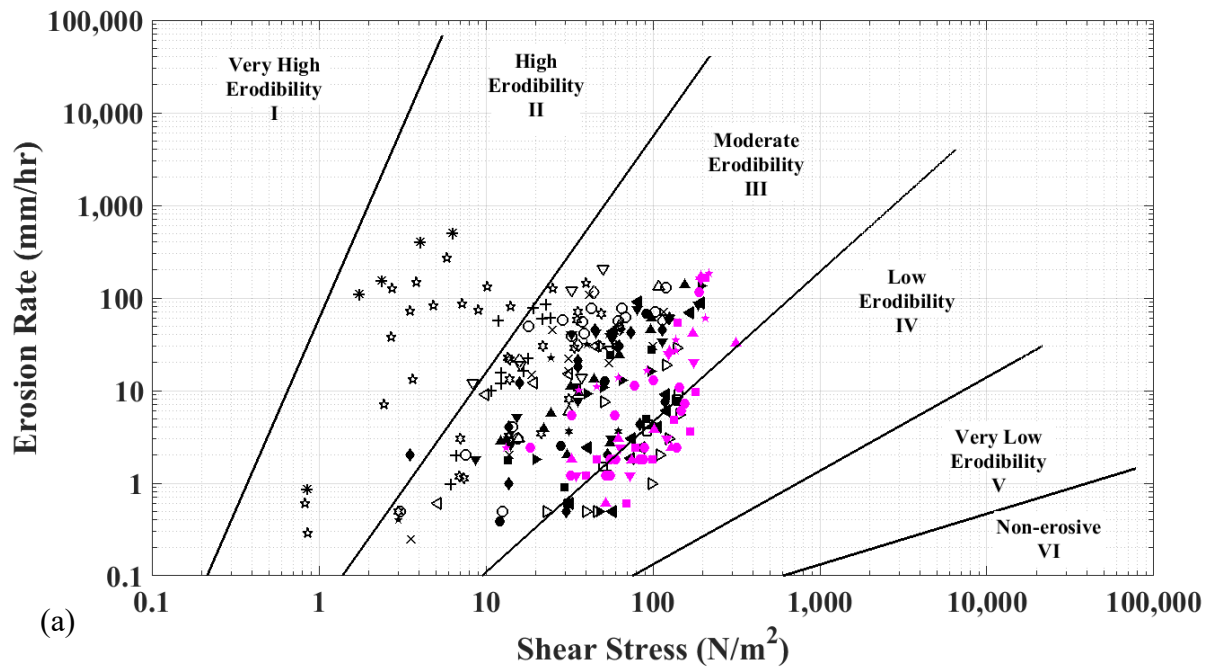
Fig. 2.3(b) shows that all points from US-69 samples were in the low to moderate erodibility zones according to the HEC-18 erodibility categorization. However, sample #1 was comparatively more erodible than the rest of the samples at the site. The material difference of sample #1 was distinguishable from the ERT shown in Fig. 2.3(a). The drilling for the first sample was performed from 0.3 to 0.9 m in the subsurface and a dark zone of high ER (above 37.8 Ω m) is evident in this layer. The remainder of each sample following the erosion test was used to determine the geotechnical properties needed for classification. Soil trimmings before starting the erosion tests were used for water content determination. Table 2.2 shows the soil parameters and the USCS classification of the five samples from US-69.

Table 2.2 Soil Properties and Classification of US-69 Samples

Sample	Sampling depth (m)	Water content (%)	% finer than 0.075 mm	Median grain size (mm)	LL	PL	PI	USCS Classification
US-69 #1	0.30-0.91	16	61	0.0310	32	29	3	ML
US-69 #2	1.07-1.68	31	98	0.0082	47	22	25	CL
US-69 #3	1.68-2.29	30	99	0.0052	48	20	28	CL
US-69 #4	2.29-2.90	29	99	0.0064	41	24	17	CL
US-69 #5	3.05-3.66	26	99	0.0103	48	17	21	CL

The soil parameters identify that the top layer is a low plastic silt with a median grain size of 0.031 mm, which is different from the four remaining lean clay samples with median grain size varying between 0.0052 to 0.0103 mm. According Shan et al. (2015) and Bernhardt et al. (2011), the comparatively higher erodibility of the top sample could be attributed to its higher grain size and lower plasticity. Because the different soil layer was also identified by ERT prior to soil classification, the statistical validity of ERT to rapidly identify soil erosion potential was studied.

The erosion test results of 65 samples from 14 of the sites were used for analysis and are shown in Fig. 2.4 using the HEC-18 erodibility categorizing graph. The site locations and the USCS classification of these samples are also included. US-166A was used for validating the model so it was excluded from the data set. Each of the 65 samples provided six points in the erosion rate versus shear stress plot; however, when expressed in logarithmic scale, the points with no erosion rate were not visible and were excluded from further analysis. Of the 251 visible points Fig. 2.4, 189 points (75%) were in the moderate erodibility zone; 40 points (16%) were in the low erodibility zone; and 22 points (9%) were in the high erodibility zone. Fig. 2.4(a) also shows that the highly erodible soils were mainly sands. Most samples tested in this study were low plasticity clay, CL. Although a wide range of soil types would be preferred, the bridge sites were selected by the KDOT considering proximity to K-State and if they were identified as scour critical.



K-9		K-4B		K-4A		US-400		US-75		K-126		
◆ CH	◇ MH	● CH	○ CL	★ CH	☆ CL	■ CH	□ CL	▲ CH	△ CL	★ CL	☆ SC	* SW-SC
US-73		K-58		US-69		US-166B		US-160		US-54	US-36	US-24
▼ CH	▽ CL	▶ CH	▷ CL	◀ CL	◁ ML	▽ CH	▲ CL	★ CH	◆ CL	● CL	X CL	+ CL

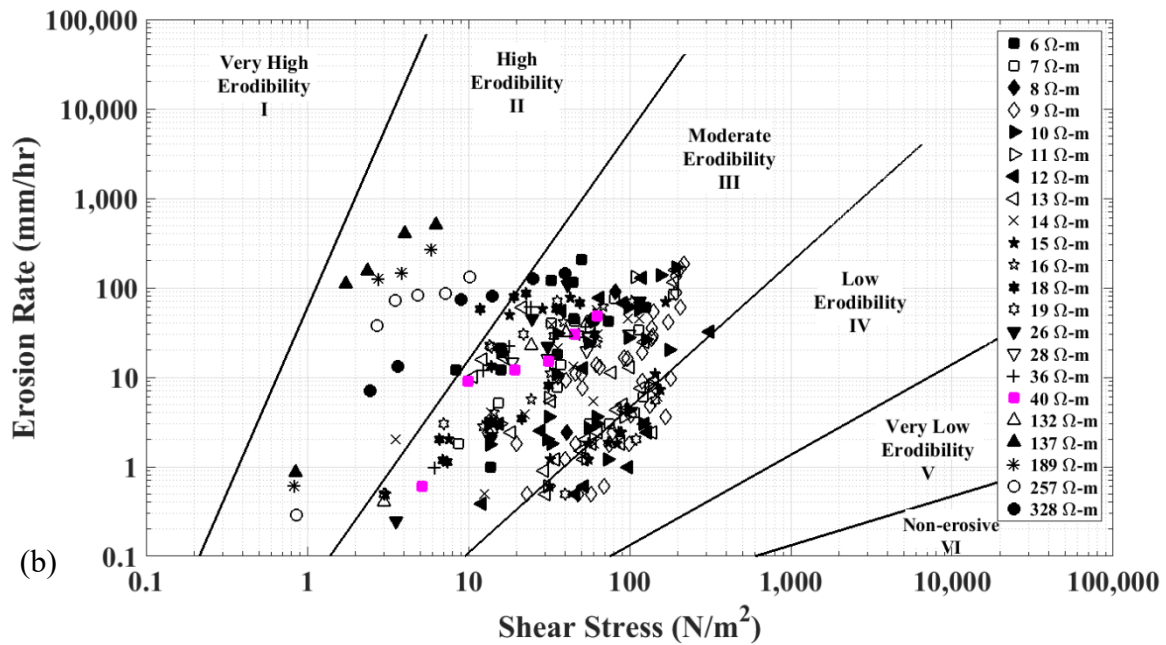


Fig. 2.4 Erosion rate versus shear stress for 14 sites: (a) USCS classification; (b) varying

ER

Soil parameters such as median grain size, plasticity index, percent of fines, and water content have been used to quantify the erosion before by many researchers (Hanson and Temple 2002; Clark and Wynn 2007; Bernhardt et al. 2011); however, no evidence of using geophysical methods, such as ER, to describe soil erosion was found in literature. In this study, the measured ER values varied from 6 Ωm to 328 Ωm . The erosion rate versus shear stress for varying ER is shown in Fig. 2.4(b). There were 22 different measured ER's from the 65 samples; 13 out of the 22 ER values corresponded to more than one sample. Samples with higher ER values tended to be in the high erodibility category as shown in Fig. 2.4(b). Therefore, ERT can be used to identify highly erodible soils. However, there are still uncertainties relating ER and erodibility, as there were highly erodible samples that corresponded to very low ER (6 Ωm from US-73), as well as moderately erodible samples corresponding to high ER (132 Ωm from K-126). The uncertainty of using ERT to identify scour critical bridges was determined by assuming the erodibility was likely high for an ER above a certain value (cut-off value), and the opposite was expected for an ER below that value. The effectiveness of this binary diagnostic test (detecting high erodibility based on a certain ER value) was validated using a Receiver Operating Characteristic (ROC) curve (Krzanowski and Hand 2009). Specifically, the effectiveness of ER was tested based on whether it can distinguish between samples classified as high erodibility from the other samples (low and moderate). All points in the erosion rate versus shear stress plot (Fig. 2.4) were divided into two parts based on erodibility: high and low/moderate.

2.5 ER as a method to predict erodibility

The ROC curve was used to evaluate the accuracy of ERT to predict whether a soil will be classified as high erodibility. ROC curve is a common tool for assessing the accuracy of a diagnostic test (Egan 1975; Swets 1988; Williams et al. 1999). ROC curve has been used to predict

landslides (Brenning 2005; Gorsevski et al. 2006) and major earthquakes in California (Holliday et al. 2006). The curve is constructed by plotting the sensitivity versus the difference of specificity from unity, as the cut-off value of ER varies. Sensitivity is the rate of true positive, predicting a soil to be classified as high erodibility when the soil is actually highly erodible. Conversely, specificity is the rate of true negative, predicting a soil to be low/moderate erodibility when this is actually the case. The accuracy of a predictive model or a diagnostic test (in this case, the ability of ER to identify high erodibility soil) is measured by the area under the ROC curve (AUC). In the ROC curve, each set of sensitivity and specificity is associated with a specific decision making criterion for the acceptable level of risk regarding the accuracy of prediction. This is done by selecting a number of cut-off values. Therefore, AUC is independent of any specific cut-off value and it represents the accuracy of the diagnostic test itself (Brenning 2005). The AUC value varies between 0.5 to 1.0 and a rough guide for classifying the accuracy of the diagnostic test using AUC value is: 0.5-0.60 = fail; 0.60-0.70 = poor; 0.70-0.80 = fair; 0.80-0.90 = good; and 0.90-1.0 = excellent (Swets 1988). There were 251 different erosion rates (22 points falling in the high erodibility zone and 229 points in the low/moderate zone) from 65 samples with corresponding ER varying between 5.54 to 327.67 Ω m. The ROC curve for different cut-off ER to determine the accuracy of the ER to identify high erodibility is shown in Fig. 2.5(a).

Since samples with a high ER value showed a tendency to be high erodibility; a cut-off value of a select ER assumes that any sample with ER value above the cut-off ER will be highly erodible. Sensitivity and specificity were calculated for these 65 increasing cut-off ER's (corresponding to 65 samples) to develop the ROC curve in IBM SPSS Statistics 24 (IBM Corp. 2016). The dashed line in Fig. 2.5(a) corresponds to an AUC of 0.5 that represents a diagnostic test with no capacity to diagnose. The ROC curve for ER to identify high erodibility is shown with

the solid line and the AUC value is 0.922 with standard error 0.047; therefore, the accuracy of ER to predict high erodibility is “excellent” according to Swets (1988). Moreover, at 95% confidence interval, the AUC value varies between 0.832 to 1.000; therefore, the accuracy of diagnostic test varies between “good” to “perfect” according to Swets (1988). The satisfactory AUC value showed that ER can be adopted to predict erodibility.

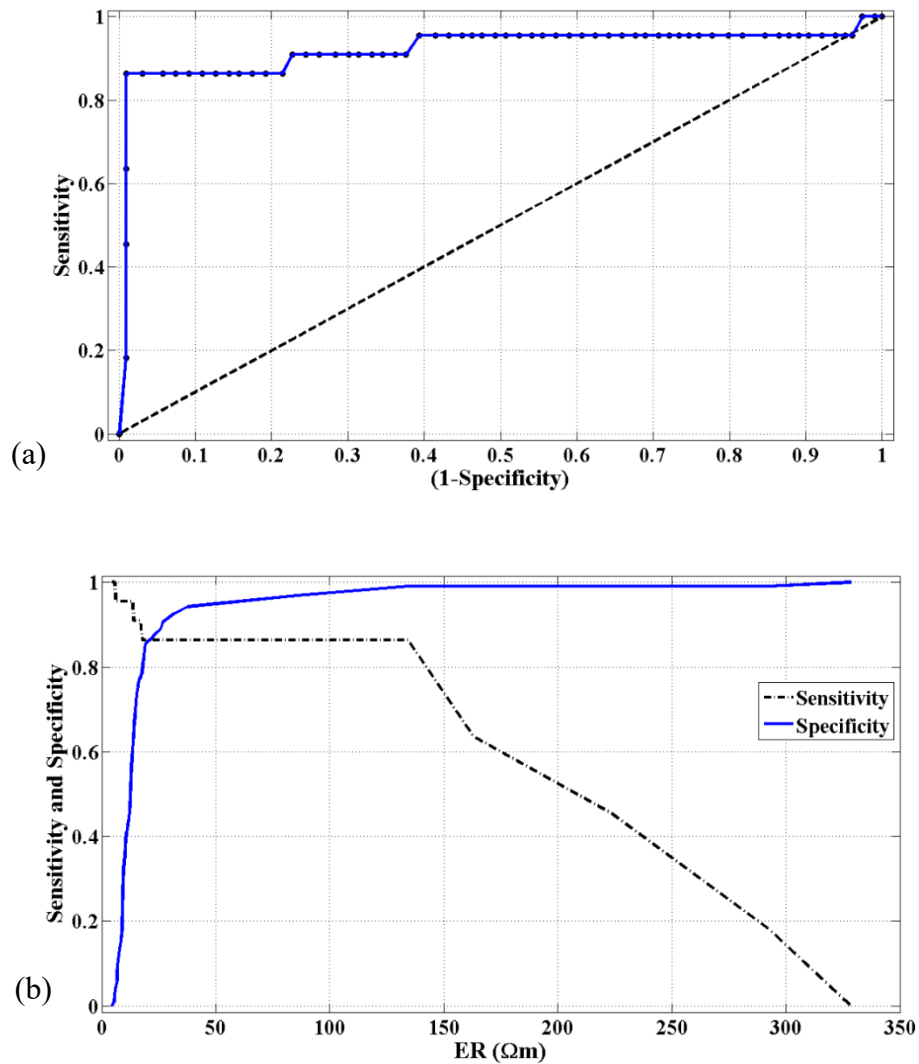


Fig. 2.5 Predicting high edibility using ER: (a) ROC curve; (b) sensitivity and specificity for varying ER cut-off

Next, the cut-off value of ER for predicting the erodibility was determined. Selecting a cut-off value depends on the acceptable level of risk regarding the accuracy of the prediction and requires knowledge of the contextual information (Gorsevski et al. 2006). Sensitivity and specificity values were plotted against the ER in Fig. 2.5(b) to choose an optimal cut-off value of ER. The goal was to select a cut-off ER that ensured high rate of true positive (high sensitivity) and/or high rate of true negative (high specificity). Fig. 2.5(b) shows high sensitivity values (such as 0.955) correspond to a lower cut-off value of ER (below 10 Ωm). Therefore, although most of the high erodibility samples will be considered as high erodibility for such low cut-offs of ER, many low erodibility samples will also be falsely treated as high erodibility leading to an uneconomic design. Conversely, high specificity (such as 0.969) will result in an unsafe design. In this case the corresponding high cut-off ER (over 85 Ωm) will falsely exclude potential highly erodible soils.

The cut-off ER was selected such that the probability of a false negative and false positive prediction were low and using geophysical judgement. The range of ER is typically 1-20 Ωm for clays (Everett 2013) and 20-200 Ωm for silts (Grisso et al. 2009). The ER of dry sand and gravel is over 200 Ωm (Lucius et al. 2007); however, ER of wet sands vary between 20-200 Ωm (Everett 2013). The cut-off ER of 50 Ωm was selected as it was expected to distinguish between most coarse grained soils (usually high erodibility) and fine grained soils (usually low/moderate erodibility) based on the typical ranges of ER for soils while not excluding either based solely on geophysics. If a higher cut-off value was selected (for example over 100 Ωm) the sediments would most likely be coarse, which are typically highly erodible. The lower cut-off allows the incorporation of fine-grained sediments that have lower resistivity but are highly erodible. The cut-off ER also considers where both sensitivity and specificity were high (0.864 and 0.950 respectively). The adaptability

of ER in predicting erodibility is better illustrated when the erosion rate versus shear stress for all samples were redrawn with respect to the cut-off ER (below and above 50 Ωm) in Fig. 2.6.

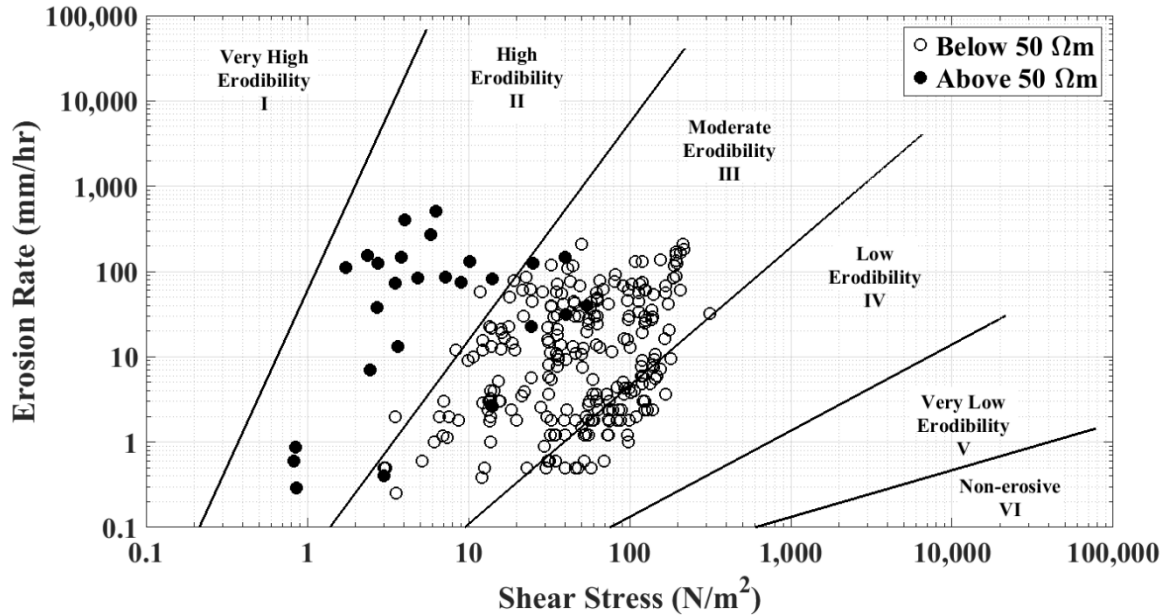
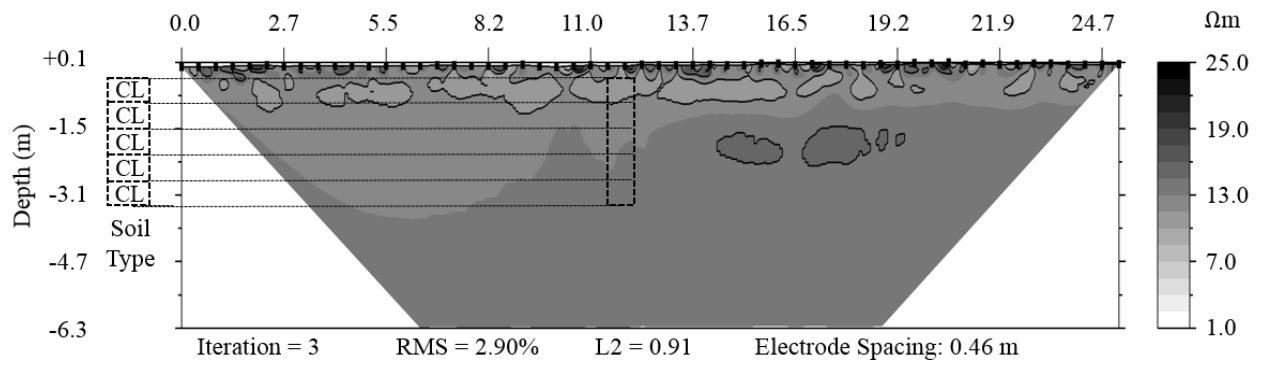


Fig. 2.6 Erosion rate versus shear stress for two ranges of ER

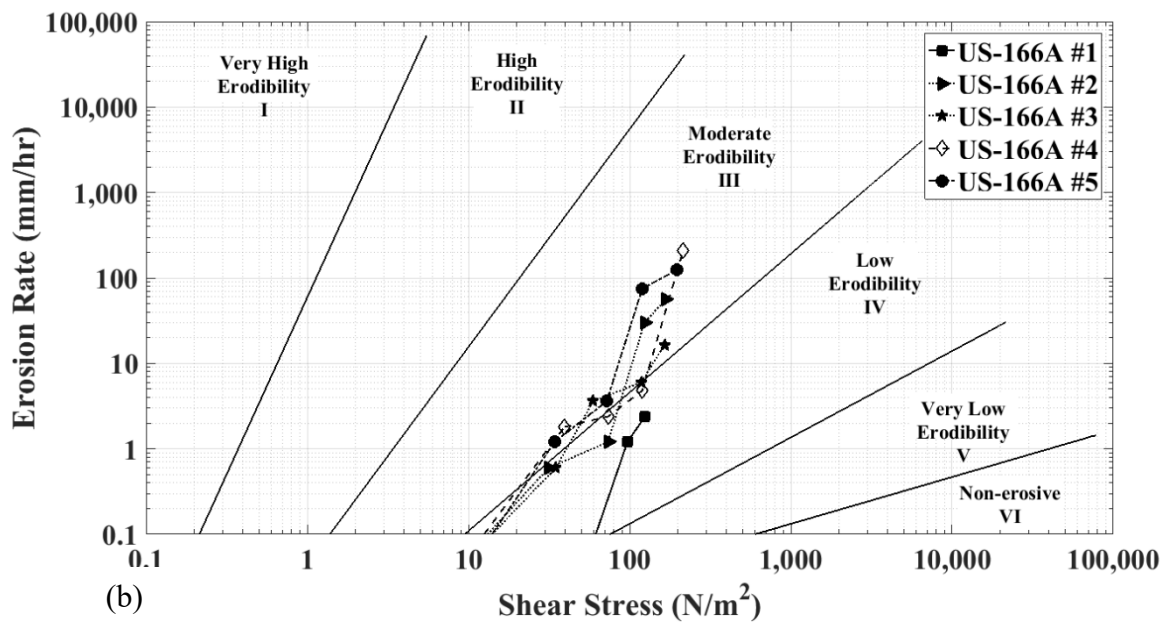
When ER values were below 50 Ωm , 99% (222 out of 225) points showed low/moderate erodibility. When ER values were above 50 Ωm , 73% (19 out of 26) points showed high erodibility. In order to develop a probabilistic model to determine level of erodibility, when the ER value is above and below the cut-off ER 50 Ωm , the probability distribution function (PDF) for both high and low/moderate erodible points were constructed. The average ER among the 22 high erodible points was 196.8 Ωm with a standard deviation of 97.8 Ωm . This corresponds to a 93% probability of high erodibility (using normalized z-value) when the ER is above 50 Ωm . On the other hand, the average ER among the 229 low/moderate erodible points was 18.8 Ωm with a standard deviation of 34.5 Ωm . This corresponds to an 82% probability of low/moderate erodibility (using normalized z-value) when the ER is below 50 Ωm .

2.6 Validation

The ERT and erosion test results from the remaining site (US-166A) were used to validate the methodology. As shown in in Fig. 2.7(a), the ER values of the five samples varied between 11.2 to 13.0 Ωm ; therefore, according to the probabilistic model, there is 82% probability for all five samples to show low/moderate erodibility. The erosion test results are presented in Fig. 2.7(b) and Table 2.4, which verified that all points were low/moderate erodibility. From a transportation agency's viewpoint, this site may be given lower priority in the initial evaluation for scour potential. The samples from US-166A were classified as CL with median grain size varying between 0.0038 to 0.015 mm (Table 2.3) which is also in agreement with the low ER values.



(a)



(b)

Fig. 2.7 Validation site: (a) subsurface inverted ER of US-166A; (b) erosion rate versus shear stress for US-166A samples

Table 2.3 Soil Properties and Classification of US-166A Samples

Sample	Sampling depth (m)	ER (Ωm)	Water content (%)	% finer than 0.075 mm	Median grain size (mm)	LL	PL	PI	USCS Classification
US-166A #1	0.30-0.91	11.2	24	98	0.0038	46	26	20	CL
US-166A #2	0.91-1.52	12.4	26	99	0.0042	45	21	24	CL
US-166A #3	1.52-2.13	13.0	27	99	0.0182	41	21	20	CL
US-166A #4	2.13-2.74	13.0	28	99	0.0100	39	19	20	CL
US-166A #5	2.74-3.35	13.0	30	90	0.0150	33	18	15	CL

Table 2.4 Predicted Versus Actual Erosion Test Results for US-166A

Sample	Electrical Resistivity (Ωm)	Predicted Erodibility	Actual Erodibility	Predicted Critical Shear Stress (N/m^2)	Actual Critical Shear Stress (N/m^2)	Variation (%)
US-166A #1	11.2	Low/Moderate	Low	21.2	96.9	78
US-166A #2	12.4	Low/Moderate	Low/Moderate	19.2	31.5	39
US-166A #3	13.0	Low/Moderate	Low/Moderate	18.4	34.9	47
US-166A #4	13.0	Low/Moderate	Low/Moderate	18.3	39.4	53
US-166A #5	13.0	Low/Moderate	Moderate	18.3	34.2	46

2.7. Discussion

The primary objective of this study was to develop a method to rapidly identify high erodibility soils for initial prioritization of scour critical bridges. Additional considerations, limitations, and improvements are discussed in this section, starting with limitations. The location of drilling at

each site was selected following the direction of the hydrology and geotechnical divisions of KDOT. The drill rigs did not have the ability to access within the channel cross section; therefore, drilling was performed at the stream banks. As such, one of the limitations of this study was that the samples may not be representative of the saturated stream bed soils. Among the three types of scour, namely, pier scour, contraction scour, and abutment scour (Briaud et al. 2011); soil samples of this study are representative of the latter two. Although hand sampling could have been performed in the stream bed; it was not used as the samples would likely be highly disturbed. The bank samples, however, still provided a means to estimate the erosion of unsaturated soils at the surface. This methodology can be extended to other near surface soil erosion failures such as earth embankments or slopes. There are over 160,000 km of levees in the United States (ASCE 2017); and levee breaches are caused due to the erosion of the dry side of the slopes (which is not saturated) during sudden flood events (Bernhardt et al. 2011). The top 0.3 m of surficial soils were not sampled; because, that portion often consisted of fills and foreign materials not representative of the native geology; however, this also removed most of the vegetative armoring. This was done to consider the worst case scenario of surface erosion.

An AUC value of 0.922 of the ROC curve indicated that ERT was an “excellent” method and the dataset showed a 93 % probability of classifying as high erodibility when ER was above the cut-off value of 50 Ω m. However, the dataset contained a narrow range of sediments predominantly of low and high plastic clays, with few sands, and only two silt samples. It would have been ideal to include a broader range of sediment types with very high or very low erodibility; but choosing such sites with varying scour behavior without prior erosion data was beyond the scope of this study. In addition to adding more sediment types to build the model; it should be

validated with randomly selected sites of different soil types before it is adopted by any transportation authority.

The potential of ER to predict critical shear stress was also evaluated in this study. Critical shear stress is an important curve fitting parameter for describing the erodibility of any sediment which can be used for estimating the total amount of scour by transportation agencies. The critical shear stress was determined by calculating the threshold shear stress at which the soils started to erode and Equation 5. Critical shear stress for erosion is a function of various soil parameters including plasticity index (Dunn 1959; Smerdon and Beasley 1961), dry density (Owen 1975; Thorn and Parsons 1980), median grain size (Briaud et al. 2001; Briaud 2008; Kimiaghalam et al. 2015), cohesion (Reddi and Bonala 1997), clay-silt fraction (Julian and Torres 2006), shear strength (Léonard and Richard 2004; Meng et al. 2012), and water content (Amaryan 1993; Bale et al. 2007). Again, factors affecting the ER of soils include median grain size (Inazaki et al. 2008), liquid limit, plasticity index, percent fines and percent coarse fraction (Abu-Hassanein et al. 1996), water content, and moist unit weight (Kibria and Hossain 2012). Due to the existing common factors, an effort was made to correlate the critical shear stress for erosion with the ER of soil.

The measured critical shear stresses did not vary linearly when plotted against the corresponding ER values of the 65 samples of this study and the coefficient of determination (R^2) was only 0.12. Other mathematical functions such as exponential, logarithmic, power, and polynomial relationship between the independent and dependent variables were considered. Ultimately the power relationship provided the best fit to the data with $R^2 = 0.50$, and therefore, was selected. Other researchers have evaluated if one measurable soil property can be used to estimate the critical shear stress. Kimiaghalam et al. (2015) obtained R^2 of 0.05, 0.11 and 0.20 for predicting critical shear stress using water content, median grain size, and plasticity index,

respectively. Briaud et al. (2001) obtained R^2 of 0.01, 0.03 and 0.35 using plasticity index, percent fines, and undrained shear strength respectively. McClerren et al. (2012) obtained R^2 of 0.53, 0.70, 0.77 using dry unit weights for three different river sediments. McClerren et al. (2012) likely calculated a higher R^2 because the regression was performed among the sediments from same rivers. As the R^2 for the preliminary predictive model in this study was improved over previous efforts using one variable from different sources, this shows that ER is likely a valuable parameter to predict critical shear stress. The relatively narrow range of soil types is a limitation of the current model, but as noted previously these sites were selected based on other criteria.

The poor correlation between critical shear stress and single soil properties from this and previous studies highlight that the critical shear stress for scour is a complex process and interaction among the different variables is needed. There are a limited number of studies that considered a combination of different variables (Knapen et al. 2007; Zhu et al. 2008; Debnath and Chaudhuri 2010; Shan et al. 2015). The FHWA adopted Shan et al. (2015) model that uses water content, percent fines, plasticity index and unconfined compressive strength for predicting the critical shear stress of fine grained soils has an R^2 of 0.73, however as noted in the introduction, the boundaries for this equation were not appropriate for the soils in this study. The authors are currently working on incorporating other measurable soil parameters including median grain size, plasticity index, and undrained shear strength along with ER for wide range of sediment types to construct a robust model predicting critical shear stress with a more reliable value of R^2 .

2.8 Conclusions

This study investigated the effectiveness of ERT as a tool for identifying high erodibility soil. ERT is a non-destructive, rapid, and cost effective methodology. If adopted by transportation agencies

for prioritizing scour critical bridges, the number of site specific erosion tests may be reduced by identifying soils that are likely not highly erodible. A threshold of 50 Ωm was determined based the sensitivity and specificity of a ROC curve for this data set. When ER measurements from an ERT survey are higher than the threshold, the corresponding soils had a 93% probability of classifying as high erodibility on the HEC-18 erodibility characterization graph. Thus, bridge sites with ER values typical of high erodibility soils can be prioritized for scour monitoring procedures and additional testing where necessary. Furthermore, ERT surveys provide spatial distributions of variability in the subsurface (Karim and Tucker-Kulesza 2017). For example, although the boreholes were 3.35 m deep with a diameter of 89 mm in this study, the ERT profiles contained the subsurface distribution of ER for a two-dimensional section of 25 m X 6.4 m. This methodology can be used to map the extent of highly erodible soils parallel to a bridge, future bridge site, or other infrastructure where surface erosion estimates are needed. When present at the surface, bridge designers may elect to consider the entire high erodibility layer thickness as the minimum potential scour zone. Localized zones of highly erodible soils that may have been missed with traditional boreholes will also be identified using the continuous ERT profiles.

A predictive model for critical shear stress using ER as the only independent variable was also developed. This preliminary model showed a better correlation between one measurable property, ER, and critical shear stress than previous studies that used soil samples collected from a range of sites; however, it is not strong enough to be used for design purposes. The weak correlation for critical shear stress may be due to factors that affect soil erodibility but not ER, or vice versa. For example, Grabowski et al. (2011) identified physical, geochemical, and biological factors that affect soil erosion. While there is direct overlap between the physical properties (i.e. particle size, particle size distribution, water content), the influence of biological and geochemical

factors that affect soil erosion may not influence ER. The authors are conducting an ongoing study to incorporate other measurable soil properties with ER using a robust statistical analysis to improve the predictive model. The proposed ER threshold of 50 Ωm was validated with a bridge site selected by the KDOT.

Chapter 3 - Electrical Resistivity as a Binary Classifier for Bridge

Scour Evaluation

This article was published in Elsevier's *Transportation Geotechnics* in June 2019. The full citation is:

Karim, M. Z., Tucker-Kulesza, S. E., and Bernhardt-Barry, M. (2019). "Electrical resistivity as a binary classifier for bridge scour evaluation." *Transportation Geotechnics*, 19, 146–157. <https://doi.org/10.1016/j.trgeo.2019.03.002>.

Abstract

Scour is responsible for approximately 60% of all bridge collapses in the United States. Evaluating scour using empirical equations has proven inaccurate, particularly in fine-grained soils. Furthermore, evaluating scour potential based on site specific erosion testing can be uneconomic as erosion testing is time consuming. Many soil characteristics that affect soil erosion also influence soil electrical resistivity (ER) which can be measured in the field or in the laboratory. The objectives of this study were to assess if field and laboratory ER measurements can be used interchangeably for characterizing soil erodibility and the impact of saturation as expected during a flood event, on the ER based soil erodibility model. Twenty-one bridge sites were used for in situ electrical resistivity tomography (ERT) surveys and erosion testing. Supplementary ER measurements at varying degrees of saturation were also conducted using a soil box in the laboratory. It was found that ER values do not differ significantly when ERT is conducted on streambanks as opposed to fully saturated conditions. A receiver operating characteristic curve and probability density function (PDF) were used to determine that soils with ER over 50 Ωm had an 87% probability of classifying as highly erodible based on this data set. Statistical tests also

suggested that laboratory ER can be used as an alternative to field ERT surveys. While in situ ERT provides more information in terms of spatial variation in the subsurface, laboratory ER measurements on retrieved samples will allow transportation agencies to utilize the developed erodibility classifier model without the capital investment of an ERT system. Given the large number of bridges with scour susceptible foundations in the National Bridge Inventory, ER can be used to rapidly prioritize them for additional testing to measure the erosion potential or to characterize the soil erosion at proposed bridge sites.

Keywords: Soil erosion, Bridge scour, Electrical resistivity (ER), Erosion Function Apparatus (EFA), Receiver operating characteristic (ROC) curve

3.1 Introduction

Scour is the number one threat to the nation's bridge safety. Scour accounts for 60% of bridge failures, while earthquakes cause only 2% of bridge failures in the United States (Shirole and Holt 1991). Following the catastrophic bridge failure over Schoharie Creek in New York, which killed ten people in 1987, the Federal Highway Administration (FHWA) established scour evaluation as an integral part of the National Bridge Inspection Standards (Lin et al. 2014; Arneson et al. 2012). The subsequent scour evaluation technical advisory was updated as Hydraulic Engineering Circular (HEC-18) in 1991. The FHWA and State Departments of Transportation (DOTs) continue to use HEC-18 for bridge scour evaluations to date. Briaud (2008) developed an erodibility categorizing graph based on the results of erosion testing using the Erosion Function Apparatus (EFA) which was later adopted into HEC-18 (Arneson et al. 2012). This graph divided the erodibility of all geologic materials into six categories (non, very low, low, moderate, high, and very high erodibility). Furthermore, in 2005, all state DOTs were required to establish and maintain a mandatory plan of action (POA) to maintain scour critical bridges. The overarching motivation

for this research is establishing a feasible POA methodology to identify scour critical bridges nationwide.

Karim and Tucker-Kulesza (2018) established that electrical resistivity tomography (ERT) could be used as a method to rapidly identify bridges with high erosion potential and prioritize scour critical bridge monitoring. Electrical resistivity (ER) is an intrinsic property of a material that measures its ability to oppose the flow of electrical current and is calculated using:

$$ER = \frac{R \cdot A}{L} \quad (3.1)$$

where, ER is the electrical resistivity (Ωm), R is the resistance (Ω), A is the cross-sectional area (m^2), and L is the length (m) of the material. While resistance may vary depending on the dimensions of the material, ER is a normalized material property. ER varies between 1 to 20 Ωm for clays (Everett 2013), 20 to 200 Ωm for silts and wet sands (Grisso et al. 2009, Everett 2013), and over 200 Ωm for dry sands and gravel (Lucius et al. 2007). While these are common ranges of ER, there can be variability in these values for each soil type due to the spatial and temporal variation of the factors controlling ER including the degree of saturation, porosity, and concentration of dissolved salts in porewater (Rinaldi and Cuestas 2002).

ER can be measured in the field and in the laboratory. Field based ER, ERT, has become a popular geophysical methodology to capture the spatial and temporal variation of subsurface soil properties. In addition to geophysics, ERT has been utilized in fields such as geology, environmental science, archeology, and geotechnical engineering (Loke 1999; Dahlin 2001; Zonge et al. 2005; Sirieix et al. 2015). Applications within these fields include determining depth to groundwater (Vaudelet et al. 2011), depicting groundwater-surface water interactions (Koehn et al. in press), detecting varying subsurface geology (Chambers et al. 2013), and evaluating

unknown foundations (Arjwech et al. 2013; Tucker et al. 2015). The advantages of ERT are that it is non-destructive, and it can capture extensive amounts of data rapidly. However, the data acquisition system needed to conduct ERT surveys is expensive, and data processing and interpretation can be complex.

In the laboratory, ER is used to monitor samples during strength testing (Bai et al. 2013), characterize soil samples for index properties (Abu-Hassanein et al. 1996; Kibria and Hossain 2012; Kouchaki et al. 2018), and predict the corrosive potential of soil (AASHTO T 288-12). Typically, resistance meters are connected to standard soil boxes or cylinders which are filled with soils for laboratory ER measurements following the demonstration of ASTM G187 (ASTM 2018a). The advantages of a laboratory ER measurement are that the experimental setup is inexpensive, the testing and data processing are simple compared to in situ ERT, and the use of disturbed samples is similar to index property testing. Moreover, laboratory ER can be conducted on remolded samples allowing the user to get the ER values at a predetermined target density or degree of saturation based on project requirements. Although laboratory ER and field ERT measure the same soil property, measurements must be conducted at similar densities and water contents to achieve comparable results due to the physical properties previously described which affect ER. Still, researchers have utilized both field and laboratory ER to broaden a research study. For example, Brady et al. (2017) developed a new laboratory ER method that would yield representative ER of coarse aggregates, because the original method was believed to be too conservative. The new method was validated with ERT (Snapp et al. 2017). Additionally, laboratory ER was used in conjunction with in situ methods for monitoring sediment consolidation (Liu et al. 2013), soil characterization (Siddiqui and Osman 2013), and monitoring hydrocarbon pollution (Arato et al. 2013).

Karim and Tucker-Kulesza (2018) used ERT to predict soil erosion potential; however, there were several limitations which are addressed herein. All soil sampling and ERT testing were conducted along streambanks. Hence, the measured ER represented partially saturated soil at most of the bridge sites depending on the depth to the groundwater table. Karim and Tucker-Kulesza (2018) focused on the streambanks because the primary interest for erosion potential was around the bridge abutments. One objective of this study was to address the limitation of the field conditions and determine if ER based soil erosion predictions were still valid under fully saturated conditions. Additionally, implementing in situ ERT for identifying scour critical bridges may require a substantial capital investment if equipment is not available, as well as expertise in data processing for transportation agencies. Laboratory ER measurements were conducted in this study at the same degree of saturation and density as in situ conditions to evaluate if laboratory ER and in situ ERT measurements could be used interchangeably for predicting soil erodibility. Although previous researchers have used both field and laboratory ER, there has been limited research where both methods were used for the same means (i.e., Siddiqui and Osman 2013). No studies have evaluated if there is a statistical difference between the two measurements and if they can be used interchangeably for the same purpose. Finally, Karim and Tucker-Kulesza (2018) did not fully describe the hydrogeologic conditions where the ER based binary classifier for soil erodibility is valid (i.e., based on the factors that control ER). Seven sites were added to broaden the range of soil types and critical soil properties (i.e., density, degree of saturation, porewater conductivity) were presented herein to highlight the boundaries of the proposed methodology.

Whether measured in the field or laboratory, the ability for ER to identify or distinguish bridge sites containing highly erodible soils from the rest of the sites is a binary problem. A Receiver Operating Characteristics (ROC) curve is a popular statistical tool for illustrating the

diagnostic ability of a binary classifier (Egan 1975, Swets 1988, Williams et al. 1999). This methodology was first developed for radar signal detection during the 1940s and has since been utilized in fields like machine learning, atmospheric sciences, geosciences, biosciences, finance, experimental psychology and sociology (Krzanowski and Hand 2009). Despite many binary problems in geosciences, few studies were identified in the literature where ROC curves were used (Brenning 2005, Gorsevski et al. 2006, Holliday et al. 2006). Therefore, the statistical methodology establishing that ER (measured in the field or laboratory) can be used as binary diagnostic classifier for scour evaluation was included herein based on the new comprehensive dataset to contribute to probabilistic methods in transportation geotechnics and allow for future applications.

The research methodology, including erosion testing, in situ ERT, and laboratory ER measurements, follows this introduction. Next, the results of the laboratory ER measurements are compared to that of in situ ERT results and analyzed. The statistical methodology to evaluate the efficiency of ER as a binary classifier to predict the level of erodibility is then described. This paper ends with a discussion of the results, and conclusions and recommendations going forward on the use of ER as an erosion predictor.

3.2 Methodology

3.2.1 Erosion Testing and Soil Analysis

Based on the scour vulnerability and the travel distance from the origin of the research, Kansas State University, a total of 21 bridge sites across eastern Kansas were selected by the Kansas Department of Transportation for this study. Fig. 3.1 shows a map of Kansas containing the locations of the 21 sites. An ERT survey and conventional soil sampling were conducted at each bridge site. Up to five 610 mm long samples were collected using 89 mm diameter thin-walled

Shelby tubes. These samples were drilled continuously and at a fixed drilling location using hollow stem augers. ASTM Standard D4220 (ASTM 2014a) was followed for transporting and preserving the samples until erosion testing commenced. Each 610 mm sample was cut down to 381 mm for the erosion test specimen. The remaining soil was used for determining the water content and soil classification according to the Unified Soil Classification System (USCS) (ASTM 2017d). The bulk density of all samples was measured to obtain in situ geotechnical properties including void ratio and degree of saturation. The specific gravity values for specific USCS soil types were utilized from ASTM D854 (ASTM 2014c). Additionally, the sample pore water conductivity was measured following the saturated paste method (Whitney 1998).

A total of 72 samples from the 21 sites were used for erosion testing with an erosion function apparatus (EFA). The EFA is a flume style apparatus that measures the rate of erosion (mm/hr) at different water velocities (m/s) (Briaud et al. 2001). Each sample was allowed to erode at six different water velocities and the corresponding amount of erosion (mm) was recorded to determine the rate of erosion (mm/hr) for that velocity. The shear stress (N/m^2) (applied tangentially by the water to the eroding soil surface) corresponding to each velocity was calculated using

$$\tau = \frac{1}{8} f \rho v^2 \quad (3.2)$$

where, τ is the shear stress (N/m^2), f is the friction factor, ρ is the density of water (kg/m^3), and v is the water velocity (m/s) (Briaud et al. 2001). The dimensionless friction factor, f , is a function of relative roughness of the eroding surface and Reynold's number, and was obtained from the Moody Chart (1944). The final results include up to six applied shear stresses and the corresponding erosion rates from each sample. A more detailed description of sampling and erosion testing can be found in Karim and Tucker-Kulesza (2018).

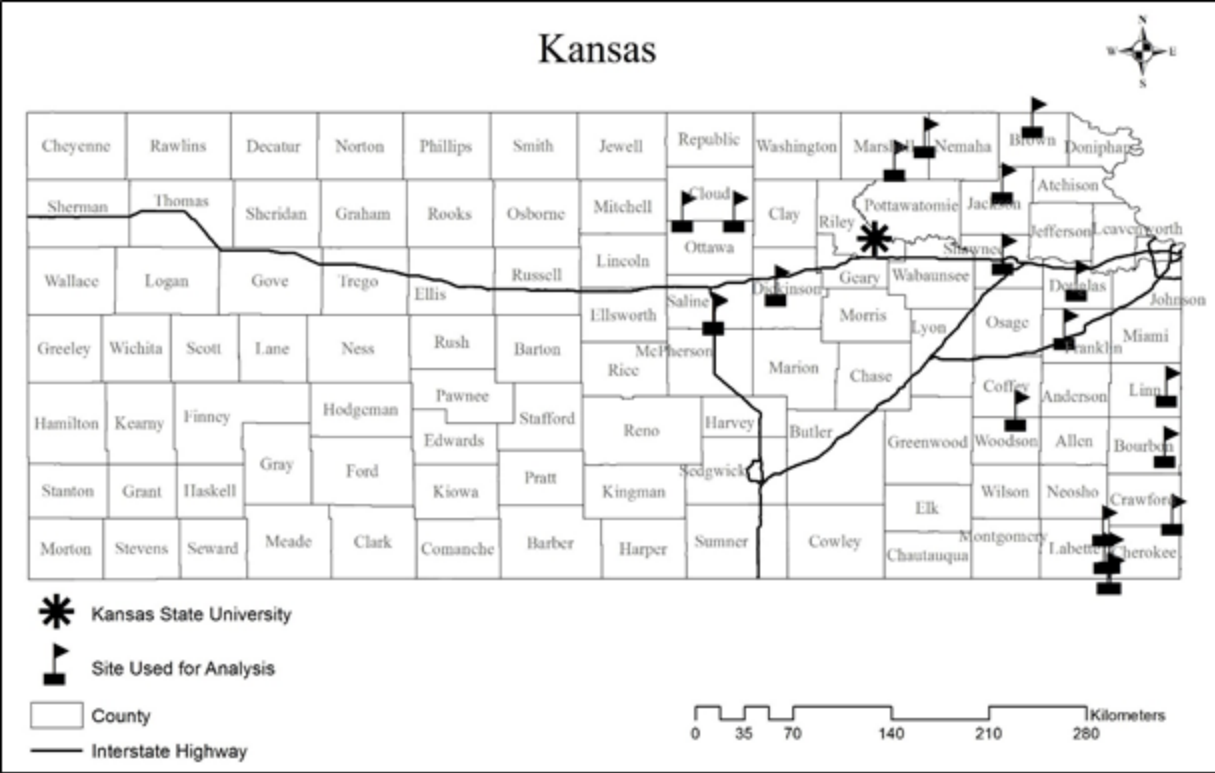


Fig. 3.1 Map showing the bridge sites used for drilling and ERT survey.

3.2.2 *In situ* ERT Surveys

ERT typically utilizes four electrodes: two current electrodes, and two voltage electrodes. The current electrodes (A, B) create an electric field within the subsurface from an external direct current source while the voltage electrodes (P, Q) measure the voltage potential between two subsurface points. For a measured voltage potential and an induced current, the apparent ER, ρ_a (Ωm), is obtained using

$$\rho_a = \left(\frac{2\pi V_{PQ}}{I} \right) \left[\frac{1}{r_{AP}} - \frac{1}{r_{AQ}} - \frac{1}{r_{BP}} + \frac{1}{r_{BQ}} \right]^{-1} \quad (3.3)$$

where, I is the electric current (amperes), V is the voltage potential (volts), r is the lateral distance between respective electrodes (m), and A/B/P/Q represent electrodes used for current or voltage measurements. Note that the term “apparent” is used because ERT measurements assume the entire

subsurface is homogenous (Everett 2013). A larger number of electrodes can be used simultaneously to expedite the data collection and cover a longer stretch of land. The configuration of these electrodes and the sequence at which different electrodes operate as current or voltage electrodes are called array. The type of array in this study was selected based on two criteria. First, the ER signal had to penetrate beyond the maximum borehole depth of 3.35 m (i.e., to obtain good vertical sounding). Second, a high lateral resolution was required for constructing the two-dimensional (2-D) soil erodibility profile. Pilot studies were conducted to determine the best configuration among the three traditional and commonly used array types: Schlumberger, Wenner, and dipole-dipole. The Schlumberger provides excellent vertical sounding beneath a single location, because the voltage electrodes are kept centered at a fixed location and the separation of the current electrodes increases about the common center during data collection. However, the Schlumberger was not selected due to its poor lateral resolution. In the Wenner array, the potential electrodes are also centered between the current electrodes. Unlike the Schlumberger, the whole voltage and current electrode assembly moves during data collection, thus increasing data collection time. The Wenner provides high lateral resolution of ER at a roughly constant depth of penetration. However, due to lateral constraints between the structure and private property, the signal could not penetrate to the intended depth with the Wenner array.

The dipole-dipole array offers advantages of both the vertical sounding of the Schlumberger and the lateral profiling of the Wenner array. The configuration of the voltage and current electrodes in the dipole-dipole array also allows for multiple voltage measurements in multi-electrode systems, thus reducing data acquisition time. The dipole-dipole array also minimizes coupling effects (an electric link between the current and voltage pairs), compared to other arrays (Binley and Kemna 2005). Therefore, the dipole-dipole array was selected for this

study. In the dipole-dipole array, the spacings between the current electrodes (A, B) and the voltage electrodes (P, Q) remain constant (a); however, the spacing between the current electrode pair and voltage electrode pair, na is variable (Fig. 3.2). The dipole-dipole array can have signal to noise ratio issues as the separation between current and voltage pairs (i.e., na in Fig. 3.2) increases; however, the maximum separation was 3.6 m and therefore data quality were not affected. Note that as n increases, the depth to the measured apparent resistivity point also increases.

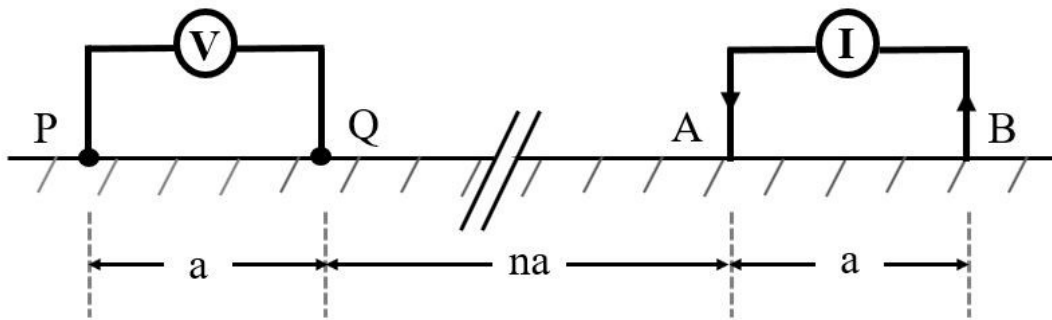


Fig. 3.2 Schematic demonstrating the dipole-dipole array.

A total of 56 electrodes were used for data collection at a uniform 0.46 m spacing, resulting in a 25.1 m survey. Because most data points were in the central region of an ERT survey line using a dipole-dipole array, and because the best resolution was obtained in that region, the survey line was oriented so that the sampling borehole was located between the 28th and 29th electrodes (Fig. 3.3). Visible sources of cultural noise (e.g., utilities, power lines, fiber optic cables, cell phone towers) were avoided near the survey line at the sites. A contact resistance test was run prior to data collection at each site to ensure that all electrodes were installed properly so that the maximum current was induced into the subsurface. The data collection for each ERT survey took about 30 minutes at each site. The relative elevation of each electrode was taken with an optical level and leveling rod which was later used in data processing to incorporate the exact topography in the ERT profile of the site.



Fig. 3.3 In situ ERT survey line including the data acquisition system.

All resistivity data were processed with AGI *EarthImager 2D* software (AGI 2009). Prior to inversion, erroneous data (e.g., negative apparent resistivities or extreme outliers) were filtered from the raw data set. Note that no more than 6% of the data were removed by filtering the erroneous data at any of the sites. The inversion of the measured apparent resistivity from the ERT surveys to the true resistivity of the subsurface was iterative, starting with a subsurface resistivity distribution where all elements of the finite element mesh were assigned the average of all apparent resistivity values measured in the field. The apparent resistivity was then calculated for given electrical properties and boundary condition using a process called forward modeling (Binley and Kemna 2005). Following this, the calculated data were inverted based on the estimated misfit between the measured and calculated apparent resistivity (Constable et al. 1987). An Occam style smooth model data inversion was used. In this inversion process, two data misfit criteria must be fulfilled simultaneously ensuring minimum roughness and optimum smoothness of the model before iteration stops and the final inverted (true) ER section of the subsurface is determined. The final ER section is approximately a $6.5 \times 25 \text{ m}^2$ 2-D section of the subsurface, which is actually a

contour plot of ER with over 45,000 elements of a finite-element mesh. As mentioned, each sample for erosion testing was 381 mm long with a diameter of 89 mm. The projected area of 381x 89 mm² contained 16 elements of the ER mesh in the 2-D section. The average ER of these 16 elements was assigned as the ER for that soil sample. Note that at least two mesh elements between two consecutive electrodes are needed for analyzing the measured data. Increasing the number of elements results in more accurate forward modeling, but with a longer run-time. Because the dipole-dipole array data are sensitive to near surface heterogeneity, a sensitivity analysis was conducted on the mesh discretization. The default mesh of two elements between electrodes was increased to six per 0.46 m (electrode spacing) to reduce the likelihood of mathematical artifacts. Further discretization of the mesh did not improve the quality of the inversion (Karim 2016).

3.2.3 Laboratory ER Measurements

A *Nilsson Resistance Meter Model 400* was used for the laboratory ER measurements. An *M.C. Miller Large Soil Box* (with a volume of 270 cm³) was used as the soil box holding the soil specimen at the in situ density. As shown in Fig. 3.4, the resistance meter was attached to the four terminals (or electrodes) of the soil box. The system uses a Wenner array, where the outer two electrodes work as the current electrode pair and the inner electrode pair measures the voltage potential between two points within the soil. The resistance meter shows the corresponding resistance of the soil. To convert the measured resistance to the soil resistivity, the dimensions of the soil box are required. The cross-sectional area (cm²), and the distance between the voltage electrodes (cm) of the soil box used in this study are such that the resistivity (Ωcm) has the same numerical value as the measured resistance (Ω) from the resistance meter.



Fig. 3.4 Resistance meter and soil box with C1, C2 current electrodes and P1, P2 voltage electrodes.

Two experiments were conducted with the soil box. In the first experiment, specimens were dried and then mixed with required amount of water to bring them to the in situ water content. All laboratory ER water contents were within 0.2% of the in situ value. Next, each specimen was compacted into three equal layers following ASTM G187 (ASTM 2018a) to fit within the soil box at the in situ density. Finally, the laboratory ER reading was taken, and the temperature was noted. In the second experiment, additional water was added to the specimens to ensure 100% degree of saturation ($S = 100\%$). All fully saturated specimens were compacted into three equal layers at the same density as in the field within the soil box and ER was measured. Due to the air entry potential (negative pore water pressure) it was not possible to achieve full saturation for eight specimens at the in situ density (very little air was entrapped in these specimens). However, 98-100% saturation was achieved for all specimens and considered satisfactory. Note that Kouchaki et al. (2018) showed that for all soil types, the change in laboratory ER with the change in degree of saturation

was negligible beyond 60% degree of saturation as long as the density remained constant. Also, note that the laboratory measurements are temperature dependent, and thus all ER values were adjusted to accommodate for the differences between the laboratory temperature and the in situ soil temperature according to ASTM G187 (ASTM 2018a) for valid comparison. In situ soil temperatures were obtained from *Kansas Mesonet* (<http://mesonet.k-state.edu/agriculture/soiltemp/>).

3.3 Results of Erosion Testing

The erosion test results of the samples from the 21 bridge sites in this study were compiled using the HEC-18 erodibility categorizing graph, which is a plot of erosion rate versus shear stress (Arneson et al. 2012). Fig. 3.5 presents the erosion rate versus shear stress data for the 72 samples marked according to their USCS classifications. As mentioned, each sample was tested under six different velocities (i.e., six corresponding shear stresses) in the EFA, therefore a total of 432 points in the erosion rate versus shear stress plot were compiled. Among these 432 points, 271 points were above the critical shear stress (shear stress at which erosion initiates) and were visible in the logarithmic plot. Since rate of erosion is zero below the critical shear stress, the rest of the points were not visible in the logarithmic plot. Among these 271 visible points, 196 points (72%) were located in the moderate erodibility zone; 49 points (18%) were located in the low erodibility zone; and 26 points (10%) were located in the high erodibility zone. The in situ ER of these samples, measured with ERT, ranged from 5.5 Ωm to 327.7 Ωm . As previously mentioned, these experiments were measured on the streambanks. The natural conditions may not be representative of the electrical response when the streambanks are inundated, such as during a flood event. Therefore, laboratory ER measurements were used to evaluate the soil samples under fully saturated conditions.

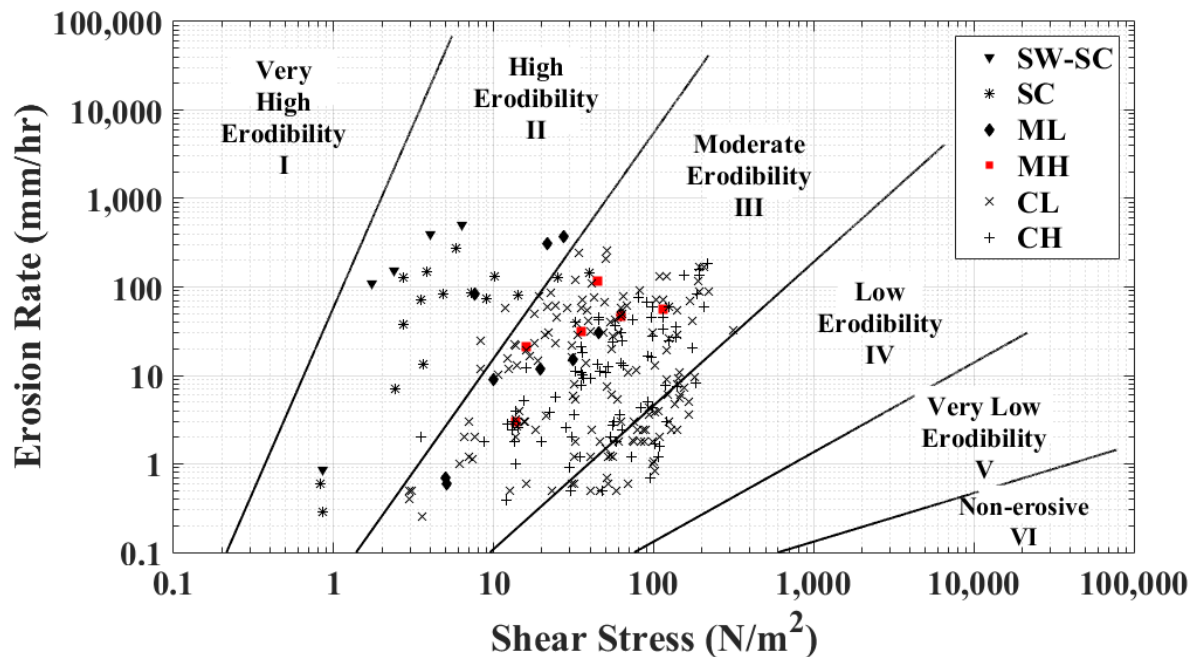


Fig. 3.5 Erosion rate versus shear stress for varying soil type of 72 samples in the study.

3.4 Results of Laboratory ER Measurements

Ten samples were selected for laboratory ER measurement. These samples are listed in Table 3.1 with in situ and laboratory properties. Samples were designated according to their highway name and the order of sampling at each site. For example, the top sample from US-69 highway was named US-69 #1. Note that two samples were used from each of three bridges (i.e., US-73, US-24, and US-160) as there was not enough soil remaining after the erosion and soil characteristic testing to measure ER in the laboratory from the remaining bridges. Laboratory ER measurements were performed using the in situ conditions (e.g., degree of saturation, water content, and density) of each sample, followed by determining their ER under fully saturated conditions. These two measurements yielded data to compare the laboratory versus in situ ER values to verify the validity of using laboratory ER for an erosion predictor, and for using laboratory ER to measure the ER at fully saturated conditions that could not be simulated in the field.

Table 3.1 Comparison of in situ ER with laboratory ER at different degree of saturation.

Sample (I)	USCS soil type (II)	In-situ ER				Lab ER with in-situ S	Lab ER with $S \approx 100\%$	
		Water content (%) (III)	Dry density (g/cm ³) (IV)	Degree of saturation, S (%) (V)	ER (Ωm) (VI)	ER (Ωm) (VII)	ER (Ωm) (VIII)	Degree of saturation S (%) (IX)
US-73 #1	CL	27.20	1.50	93.0	5.98	7.51	6.97	99
US-73 #4	CL	27.63	1.50	94.8	6.76	6.87	5.79	98
US-69 #4	CL	29.41	1.46	94.8	7.49	7.44	6.97	99
US-160 #3	CH	26.28	1.55	95.7	9.07	9.02	8.80	98
US-160 #4	CL	24.54	1.59	96.5	9.11	9.06	8.61	100
K-58 #4	CL	27.66	1.50	95.1	12.31	10.88	10.16	99
US-24 #5	CL	29.31	1.37	82.7	13.03	13.07	10.86	98
US-75 #1	CH	23.15	1.54	82.3	14.01	12.20	10.47	100
US-24 #4	CL	30.99	1.34	82.9	14.25	14.85	13.22	98
US-54 #5	CL	25.74	1.57	98.5	14.94	12.84	12.71	99

3.4.1 Laboratory ER measurements as an alternative to in situ ERT

The ER values of the ten samples obtained by in situ ERT, laboratory ER measurements with in situ degree of saturation (S), and fully saturated condition ($S \approx 100\%$) are presented in Fig.3.6(a).

The corresponding black and yellow bars in Fig. 3.6(a) showed that the differences in ER between the in situ and the laboratory methods (with in situ S) varied from 0 to 2.10 Ωm for the ten samples.

This small difference indicated that both in situ ERT and laboratory ER results were consistent.

This was also evident from the laboratory (with in situ S) versus in situ measurements plot in Fig.

3.6(b). Among the points corresponding to the ten samples, four were located on the 1:1 line indicating approximately equal values for the in situ and laboratory methods, two were on the upper left side of the 1:1 line indicating higher laboratory values (maximum of 1.53 Ωm), and four were on the lower right side of the 1:1 line indicating lower laboratory values of ER (maximum of 2.10 Ωm) than the in situ method.

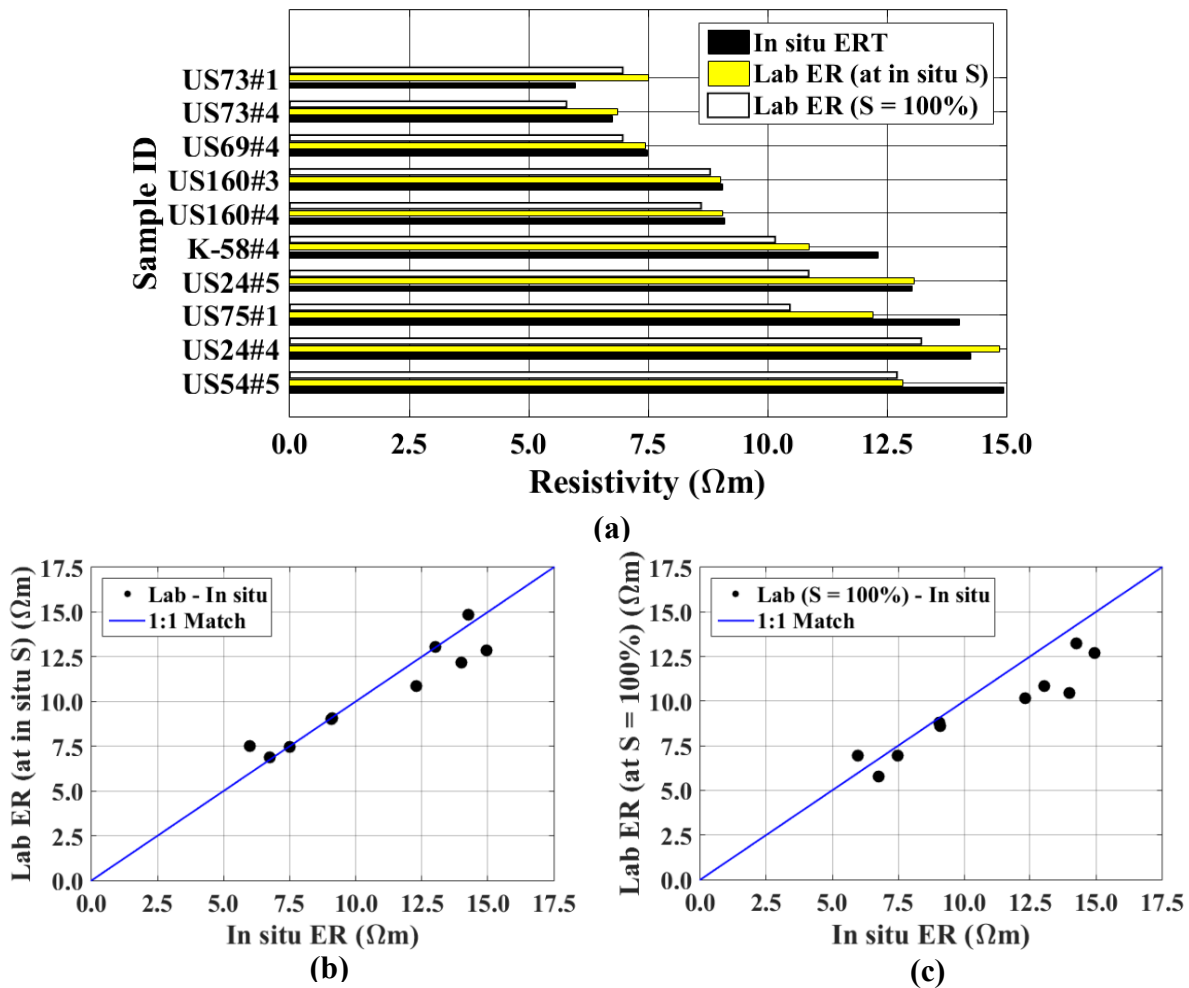


Fig. 3.6 Comparison of ER values: (a) bar chart comparing ER values as obtained from in situ ERT, laboratory ER (at the same S as in the field), and laboratory ER at fully saturated condition ($S \approx 100\%$); (b) laboratory ER (at in situ S) versus in situ ER; (c) laboratory ER ($S \approx 100\%$) versus in situ ER

Although numerical values suggested that the ER measurements were very similar, a statistical hypothesis testing between the two samples (in situ ER and laboratory ER with in situ S) was performed to verify if the in situ and laboratory measurements were statistically similar. For a small sample size of 10 (corresponding to the two populations, namely, in situ and laboratory ER values with in situ S), a t-test is suitable for hypothesis testing (Ott and Longnecker 2004). The t-tests comparing two samples can be of two types: two sample t-test (where both samples are independent) and paired t-test (where both samples are dependent). In this case, the samples were dependent since two different ER measurement methods were conducted on the same soil; hence, a paired t-test was utilized to verify the similarity in ER values between in situ ERT and laboratory ER (with in situ S) methods. A paired t-test simply calculates the difference between paired observations and then performs a one sample t-test. The observations of two samples (size = 10) are given in column VI and VII in Table 3.1. Column VII was subtracted from column VI (Table 3.1) and a single sample denoting the difference between in situ and laboratory ER values (with in situ S) was obtained as shown in Table 3.2. The single sample t-test was conducted on that sample.

Table 3.2 Sample of observations showing the differences between in situ and laboratory ER (with in situ S) (Column VI - Column VII of Table 3.1).

Difference in ER, d_1 (Ωm)	-1.527	-0.114	0.050	0.050	0.050	1.432	-0.041	1.812	-0.600	2.104
---	--------	--------	-------	-------	-------	-------	--------	-------	--------	-------

For the paired t-test, two assumptions were checked: (1) ER is a continuous variable; and (2) ER follows a normal distribution. ER is an intrinsic soil property and therefore is a continuous variable, satisfying the first assumption. To check the second assumption, a normality check was conducted. Note that a set of observations tends to follow a normal distribution when their probability density

function has a bell-shaped curve and can be described by its mean and standard deviation (Ott and Longnecker 2004). The probability density of a normal distribution can be defined as

$$f(x | \mu, \sigma^2) = \frac{1}{\sqrt{2\pi\sigma^2}} e^{-\frac{(x-\mu)^2}{2\sigma^2}} \quad (3.4)$$

where μ is the mean and σ is the standard deviation of the distribution of variable x . The mean of the differences in Table 3.2 was $\bar{d}_1 = 0.322$ with a standard deviation of $s_{d1} = 1.127$, and the p-value of the Anderson-Darling normality test was 0.105 (above 0.05), showing the observations of the differences follow a normal distribution for 95% confidence level (Ott and Longnecker 2004).

After verifying the accuracy of the assumptions, a t-test was performed with null hypothesis $H_0: \mu_{D1} = 0$ [i.e., the in situ and laboratory (with in situ S) measurements of ER are statistically equal], and $H_a: \mu_{D1} \neq 0$ [i.e., the in situ and laboratory (with in situ S) measurements are statistically different], where μ_{D1} denotes the population mean of the differences between the in situ and laboratory (with in situ S) measurements. The t-test was performed for a significance level, $\alpha = 5\%$. For the degree of freedom $df_1 = n - 1 = 9$, where, $n = 10$ was the sample size, the test statistics t_1^* was obtained as 0.90 using the relationship

$$t_1^* = \frac{\bar{d}_1 - \mu_{D1}}{s_{d1}/\sqrt{n}} \quad (3.5)$$

where, all the variables were previously defined. Using $t_1^* = 0.90$ and $df_1 = 9$, the corresponding p-value was determined as 0.39 from a t-table for the hypothesis test (Ott and Longnecker 2004). Since the p-value = 0.39 > $\alpha = 0.05$, the null hypothesis H_0 could not be rejected. In other words, the statistical analysis suggested that there was no evidence that in situ and laboratory ER measurements were different at a 95% confidence level.

Although the t-test is designed for small sample sizes, the power of the t-test was determined to verify if the sample size of ten was adequate in this hypothesis test. The power of a t-test is defined as the difference of the probability of Type II error from unity. Type II error occurs when the test fails to reject the null hypothesis, given the null hypothesis is false. For the associated standard deviation, $s_{d1} = 1.127$, significance level $\alpha = 5\%$, and an estimated difference in ER of $1.5 \Omega\text{m}$, the resulting power of the t-test was 96.16%, which was the probability of correctly rejecting the null hypothesis when the difference in ER was truly at least $1.5 \Omega\text{m}$. Due to this high power of 96.16%, a sample size of ten was considered satisfactory and the hypothesis test result was accepted. Therefore, it was proven that there was no significant difference between the in situ and laboratory ER measurements, when both methods were applied on the same soil with the same degree of saturation and density. Although in situ ERT provides mass scale geological information of the subsurface, this finding is very significant; a laboratory-based alternative of ERT will allow the users to utilize any ER based models economically.

3.4.2 Effect of Degree of Saturation on In Situ ER

ERT surveys and soil sampling (for erosion testing) were conducted on the streambanks, as erosion around the bridge abutments was the primary interest. Unfortunately, these in situ ERT measurements may not accurately characterize the fully saturated soils anticipated in a flood. The degrees of saturation for the 72 samples of this study varied between 82 to 100%. Working on fine grained soils, Kouchaki et al. (2018), Kibria and Hossain (2012) and Abu-Hassanein et al. (1996) showed that the ER decreased approximately exponentially with an increasing degree of saturation. However, as the degree of saturation crossed approximately 60-70%, the curves started to flatten out and there was a negligible change in ER with increase in the degree of saturation until full

saturation. Based on these previous studies it was assumed that in situ ER would not be significantly different in the fully saturated condition, as the minimum degree of saturation in this study was 82%. To support this information from the literature, the ER values were measured at fully saturated conditions in the laboratory and compared with their in situ ER for ten samples. Note that these ten samples were the same samples listed in Table 3.1, but this time a comparison was made between column VI (obtained at field by ERT with in situ S) and VIII (obtained at laboratory with $S \approx 100\%$).

Fig. 3.6(a) and Fig. 3.6(c) show that nine out of ten samples had a smaller value of ER in laboratory with full saturation (maximum difference of 3.54 Ωm) than what was obtained through in situ ERT. As shown in Table 3.1, only sample US-73 #1 showed slightly higher ER (6.97 Ωm) with $S \approx 100\%$ than its in situ value (5.98 Ωm), which was likely due to the different measurement devices. Comparison of the laboratory ER with in situ S (7.51 Ωm) and the laboratory ER with $S \approx 100\%$ (6.97 Ωm) confirmed that full saturation slightly reduced the ER of US-73 #1 sample too, like the nine other samples. Therefore, it is true for all ten samples that, full saturation decreased the ER as more water replaced the air within the soil pores and increased the conductivity. However, the decrease in ER due to full saturation was minor. Among the ten samples listed in Table 3.1, US-75 #1 had the lowest degree of saturation in the field ($S = 82.3\%$) with in situ ER of 14.01 Ωm , and at full saturation (17.7% increase in S) the ER was determined as 10.47 Ωm (only 3.54 Ωm decrease). The decrease of ER due to full saturation in the other nine remaining soil samples was even smaller as shown in Table 3.1. Note that the remaining 62 samples from this study had an in situ S equal to or above 82%. Table 3.3 includes these differences in ER between in situ measurements and fully saturated condition in laboratory by subtracting column VIII from column VI of Table 3.1 for the ten samples.

While ER values can be over 1,000 Ωm for many geomaterials, these small changes in ER due to full saturation likely have a negligible impact on the ER based binary classifier model for bridge scour evaluation. Therefore, to verify if this change in ER was small enough (such as 3 Ωm), a paired t-test was performed using the ten observations (differences in ER between in situ condition and fully saturated condition in the laboratory) of Table 3.3. The mean value of these observations was $\bar{d}_2 = 1.24$ with a standard deviation of $s_{d2} = 1.292$. These differences also satisfied the normality assumption (p value = 0.533 > 0.05), justifying the use of the paired t-test.

Table 3.3 Sample of observations showing the differences between in situ ER (with in situ S) and laboratory ER (with S \approx 100%) (Column VI - Column VIII of Table 3.1).

Difference in ER, d_2 (Ωm)	-0.986	0.968	0.522	0.268	0.505	2.151	2.167	3.536	1.032	2.233
--	--------	-------	-------	-------	-------	-------	-------	-------	-------	-------

The null hypothesis of the paired t-test was $H_0: \mu_{D2} \geq 3$ [i.e., the mean of differences between the in situ ER and laboratory ER (with $S \approx 100\%$) is greater than or equal to 3 Ωm], and alternative hypothesis was $H_a: \mu_{D2} < 3$ [i.e., the mean of differences between the in situ ER and laboratory ER (with $S \approx 100\%$) is less than 3 Ωm], where μ_{D2} denotes the population mean of differences between the in situ ER and laboratory ER (with $S \approx 100\%$). Note that a difference of 3 Ωm was used in the hypothesis test, because Abu-Hassanein et al. (1996) showed that the variation in ER for fine grained soils is usually less than 3 Ωm between 70 to 100% degree of saturation and the range of degree of saturation of 72 samples in this study (82 to 100%) was well within this boundary. The t-test was performed for a significance level, $\alpha = 5\%$.

For the degree of freedom $df_2 = n-1 = 9$, where, $n = 10$ was the sample size, the test statistics t_2^* was obtained as -4.31 using Eq. (3.5) with equivalent p-value = 0.001. Since p-value

$= 0.001 \ll \alpha = 0.05$, null hypothesis H_0 was rejected, signifying that the difference in ER between the partially saturated soils and fully saturated soils would be less than $3 \Omega\text{m}$. The power of the paired t-test was found to be 95.84% for the associated standard deviation $s_{d2} = 1.292$, significance level $\alpha = 5\%$, and an estimated difference in ER of $1.5 \Omega\text{m}$, meaning the probability of correctly rejecting the null hypothesis was 95.84% when the difference in ER was truly at least $1.5 \Omega\text{m}$. With a 95.84% power, it can be said that the sample size of ten was adequate for the paired t-test. Based on this hypothesis, it can be said with 95% confidence $[(100-\alpha)=95\%]$ that ER values from in situ ERT surveys were not more than $3 \Omega\text{m}$ different than what it would be if all the samples were fully saturated from the streambed. Hence, considering the typical range of ER for different geologic materials, this difference can be considered small enough to not influence the binary classifier model of ER for bridge scour evaluation.

3.5 Electrical Resistivity as a Classifier for Erodibility

Karim and Tucker-Kulesza (2018) established that soil samples falling in the high erodibility zone of the HEC-18 erodibility categorizing graph mostly corresponded to comparatively higher ER than the moderate or low erodibility samples. However, there were overlaps of ER values between samples representing “high” and “not high” (comprised of “moderate” and “low”) erodibilities. That is, there were highly erodible samples that corresponded to very low ER, and there were samples that were not highly erodible but had a very high ER. Seven new bridge sites were added in this study, as well as the ER measured in the laboratory as an alternative method. The ability for ER to distinguish bridge sites containing “high” erodibility soils from the rest of the soils (comprised of “moderate” and “low”) is a binary problem. The Receiver Operating Characteristics (ROC) curve is a popular statistical tool for illustrating the diagnostic ability of a binary classifier (Swets 1988) and was used in this study.

3.5.1 ROC Curve for Evaluating a Binary Classifier

The control variable of a binary diagnostic test (i.e., ER in this study) must be quantitative and continuous for ROC analysis. To help decide if the outcome of a binary diagnostic test is positive or negative, a cut-off value of the control variable must be estimated. The cut-off value works as a boundary and the binary outcome may be considered positive or negative when the control variable will be above or below the estimated cut-off value. Outcomes of a binary diagnostic test are leveled either positive (e.g., high erodibility, p), or negative (e.g., not high erodibility, n , comprising of low and moderate erodibility) and can be summarized in a 2 x 2 contingency table (Kumar and Indrayan 2011) (Table 3.4). The columns of Table 3.4 represent the actual erodibility results obtained from erosion testing in this study and the rows represent the binary diagnostic test results (i.e., predicted erodibility using ER).

Table 3.4 Diagnostic test results with respect to actual test results (adapted from Kumar and Indrayan 2011).

Diagnostic test results (predictions)	Actual erosion testing results		Total
	High erodibility	Not high erodibility	
High erodibility	True positive (TP)	False positive (FP)	All test positive (p)
Not high erodibility	False negative (FN)	True negative (TN)	All test negative (n)
Total	Actual high erodibility samples (H_+)	Actual not high erodibility samples (H_-)	Total sample size

In the context of identifying high erodibility using ER, true positive rate (TPR) is the probability of predicting a soil to have high erodibility when it was actually found highly erodible in erosion testing. On the other hand, false positive rate (FPR) is the probability of predicting a soil to have

high erodibility when it was actually found not highly (moderate or low) erodible in erosion testing. Mathematically,

$$TPR = \frac{TP}{TP+FN} = \frac{TP}{H_+} \quad (3.6)$$

$$FPR = \frac{FP}{FP+TN} = \frac{FP}{H_-} \quad (3.7)$$

where, all variables are defined in Table 3.4. Note that, the values of TPR and FPR will be different depending on the estimation of cut-off value of the control variable (i.e., ER) of the binary diagnostic test. The ROC curve is the graphical display of the TPR plotted against FPR for all these varying cut-off values.

3.5.2 Interpreting an ROC Space

A characteristic ROC space (that contains ROC curve) is shown in Fig. 3.7 for depicting the relative tradeoff between true positive and false positive predictions. Since, both TPR and FPR represent probabilities, the range of abscissa and ordinate of a ROC space varies between 0 to 1. For a certain cut-off value, the best possible prediction would yield a point on the top-left corner of the ROC space (0, 1) in Fig. 3.7, which is called a perfect classification (Kumar and Indrayan 2011). This point corresponds to $TPR = 1.0$ (100% probability of true positive) and $FPR = 0.0$ (zero probability of false positive). The diagonal dashed line joining (0, 0) and (1, 1) is called the no-discrimination line. For a certain cut-off value, any point falling on this line will correspond to a random guess indicating equal probability of true positive and false positive. This no-discrimination line divides the ROC space into two equal triangles. Points falling on the upper triangle represent good classification (corresponding to certain cut-off values) indicating probability of true positive is greater than false positive. Points falling in the lower triangle (corresponding to certain cut-off values) do not necessarily indicate bad classification; rather it is an indication that if the hypothesis of binary prediction was inverted, these points would represent

good classification. Therefore, the further the points are away from the diagonal in the ROC space, the better is the efficiency of the binary diagnostic test.

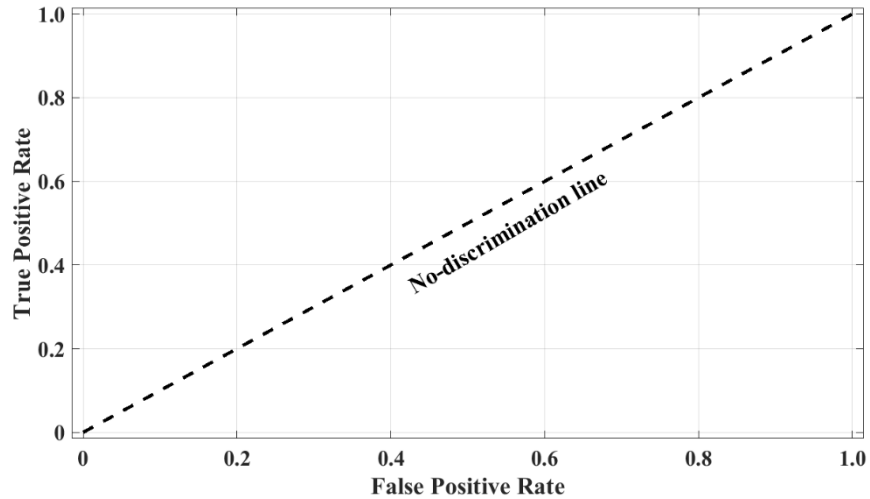


Fig. 3.7 Characteristic ROC Space.

When all the points in the ROC space corresponding to various cut-off values of the control variable (i.e., ER) are joined, the ROC curve is formed and the area it makes with the x-axis (*FPR* axis) is called the area under the curve (*AUC*). The *AUC* is a combined measure of true positive and false positive probability and it provides an effective assessment of the binary diagnostic test itself (Kumar and Indrayan 2011). The maximum value of *AUC* is 1.0, meaning the diagnostic test is perfect and high erodibility soils can be identified using ER without any probability of false prediction, for example. This would occur if there was no overlap between the probability density functions (PDF) of the ER values for high and not high erodibility soils. However, $AUC = 1.0$ is extremely unlikely to occur (Kumar and Indrayan 2011) and a rough guide for classifying the accuracy of the diagnostic test using the *AUC* value is: 0.5-0.60 = fail; 0.60-0.70 = poor; 0.70-0.80 = fair; 0.80-0.90 = good; and 0.90-1.0 = excellent (Swets 1988).

3.5.3 Efficiency of ER as a Binary Diagnostic Classifier

The hypothesis of the ROC analysis was that samples with ER value greater than the cut-off ER value would be predicted as high erodibility and vice versa. The ROC analysis was done in *SPSS Statistics* by selecting various cut-off ER values in the range of 5.5 Ωm to 327.7 Ωm . This was the range for 82 observations of measured ER (72 in situ measurements and 10 laboratory measurements at the in situ degree of saturation). The ER observations were arranged in ascending order. The smallest cut-off value was a unity less than the minimum observed value (i.e., 4.5 Ωm); the largest cut-off value was a unity greater than the maximum observed value (i.e., 328.7 Ωm). The rest of the cut-off values were the averages between two consecutive observed ER values. Although there were 83 cut-off values, only 28 are shown in Table 3.5. This was because there were high frequencies of observed data at low ER values (e.g. below 15 Ωm) and such closely spaced cut-off values would unnecessarily complicate the analysis. The samples from this study yielded 302 points in the erosion rate versus shear stress plot, with 27 falling in the high erodibility zone and 275 falling in the low-moderate erodibility zone. While calculating the *TPR* (Eq. 3.6) and the *FPR* (Eq. 3.7) corresponding to various ER cut-off values in *SPSS*, the number of high erodibility points $H_+ = 27$ and not high erodibility points $H_- = 275$ (combining moderate and low erodibility points) remained constant (as these were actual erosion test results). However, the numbers of total predicted positive (p) and total predicted negative (n) changed depending on the varying cut-off value. The *TPR* and *FPR* corresponding to various cut-off ER values, as obtained from the *SPSS* output, are also shown in Table 3.5. When the ROC curve was plotted using these *TPR* against *FPR*, the AUC value was found to be 0.902, showing ER as an “excellent” binary classifier to distinguish the high erodibility soils for bridge scour evaluation according to Swets (1988).

Table 3.5 TPR and FPR for various ER cut-off values as obtained from SPSS.

ER cut-off (Ωm)	<i>TPR</i>	<i>FPR</i>	ER cut-off (Ωm)	<i>TPR</i>	<i>FPR</i>
4.5	1	1	16.9	0.889	0.222
6.0	0.963	0.967	17.8	0.852	0.200
6.8	0.963	0.920	18.5	0.852	0.167
7.2	0.963	0.895	19.2	0.852	0.142
7.6	0.926	0.862	26.0	0.852	0.105
8.5	0.926	0.833	31.8	0.852	0.076
9.0	0.926	0.775	40.7	0.852	0.040
9.6	0.926	0.669	51.3	0.815	0.029
10.8	0.926	0.571	96.5	0.704	0.025
11.7	0.926	0.538	134.3	0.704	0.007
12.8	0.926	0.447	163.0	0.519	0.007
13.5	0.926	0.360	223.3	0.370	0.007
14.6	0.889	0.295	292.5	0.148	0.007
15.4	0.889	0.251	328.7	0.000	0.000

3.5.4 Selecting a Fixed Cut-off ER for the Binary Classifier

A fixed cut-off ER must be selected as a design guideline to implement the binary classifier model. The cut-off value of the control variable, ER should be such that the *TPR* is as high and/or *FPR* is as low as possible. This will ensure high probability of true positive and/or low probability of false positive prediction. However, for a very low cut-off ER, such as 15.4 Ωm (corresponding to very high *TPR* = 0.889), the design would be very conservative and would falsely treat many not high erodibility as high erodibility samples. On the other hand, for a very high cut-off ER, such as 163.0 Ωm (corresponding to very low *FPR* = 0.007), the design may be unsafe and many potentially high erodible sites may be neglected. Therefore, a balanced ER cut-off was required so that *TPR*

and *FPR* were still high and low respectively. Recalling the typical range of ER for different geologic materials mentioned in the introduction, a cut-off ER of 50 Ωm was selected which corresponds to *TPR* = 0.820 and *FPR* = 0.030. This cutoff ensured that most clean, coarse grained soils would be identified as high erodibility while not excluding all fine grained soils or coarse grained soils with some fines based solely on the electrical resistivity properties that may, in fact, be highly erodible. Note that the selected cut-off value of 50 Ωm is applicable for the hydrogeologic conditions of eastern Kansas (i.e., considering the gradation, density, degree of saturation, porewater conductivity), and needs to be evaluated for different conditions. The actual results of the erosion testing in this study were revised with respect to the selected cut-off ER of 50 Ωm in Table 3.6.

Table 3.6 Erosion test results with respect to recommended ER cut-off.

Erodibility Based on Actual Erosion Test	ER below 50 Ωm	ER above 50 Ωm	Total	When ER below 50 Ωm	When ER above 50 Ωm
High Erodibility	5	22	27	1.8%	73.3%
Not High (Low/Moderate) Erodibility	267	8	275	98.2%	26.7%
Total	272	30	302	100.0%	100.0%

As shown in Table 3.6, 73.3% of the samples with ER above 50 Ωm were highly erodible and 98.2% of the samples with ER below 50 Ωm were not highly erodible during actual erosion testing. This indicates that the selected cut-off ER provides a sound prediction of the erodibility. The PDFs for both high and not high erodibility (low and moderate erodibility) points are shown in Fig. 3.8 to obtain the actual probability of the erodibility based on the selected cut-off ER 50 Ωm .

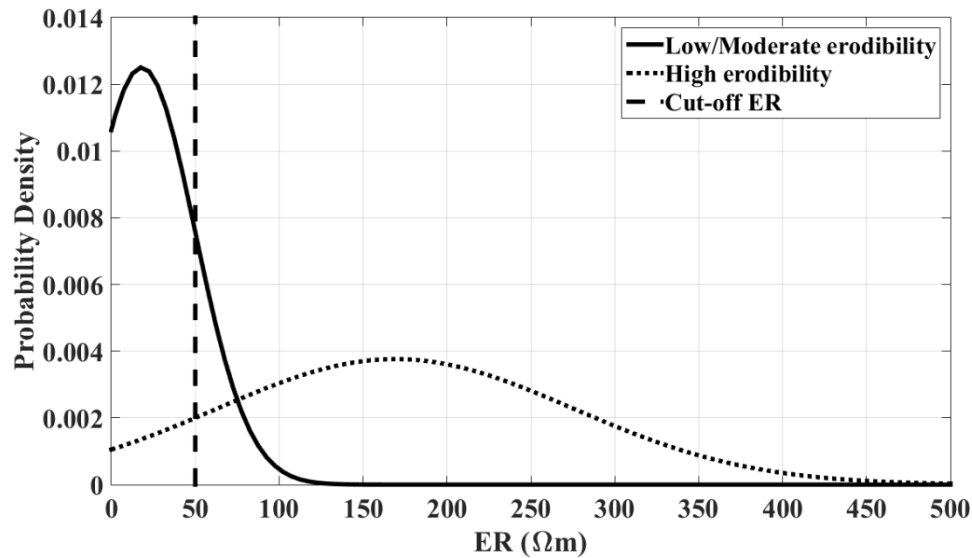


Fig. 3.8 Probability density functions for both high and not high erodibility samples.

The average ER among the 27 high erodibility points was 169.2 Ωm with a standard deviation of 106.0 Ωm , which provided the equivalent of 50 Ωm in the standard normal distribution as $z = -1.125$. Therefore, there is an 87% probability of high erodibility when the measured ER is above 50 Ωm (to the right of cut-off ER line in Fig. 3.8). On the other hand, the average ER among the 275 not high (low/moderate) erodibility points was 18.0 Ωm with a standard deviation of 31.9 Ωm and the resulting equivalence of 50 Ωm in the standard normal distribution was $z = 1.003$. As such, there is an 84% probability of low/moderate erodibility when the ER is below 50 Ωm (left to the cut-off ER line in Fig. 3.8).

3.6 Discussion

The developed model is a binary classifier that can be used to rapidly identify bridge sites with high erodibility soils. As shown by the statistical t-test, inexpensive laboratory ER measurements can also be used as an alternative if samples are collected and ERT equipment is not available. An advantage of the in situ ERT surveys is ERT provides a two-dimensional subsurface ER profile

along the entire channel cross-section as opposed to laboratory measurements which can only give ER in the localized zone of drilling. Based on the ER threshold of 50 Ωm , subsurface resistivity profiles (from in situ ERT surveys) can be converted into equivalent erodibility profiles by assigning high erodibility to soils having ER over 50 Ωm and low to moderate erodibility to soils having ER below this threshold. In this way, the entire subsurface along the cross-section of a channel, around bridge abutments, or other erodible infrastructure (e.g., levees) can be visualized with respect to erodibility. For illustration purposes, the erodibility profile of the US-24 site is shown in Fig. 3.9 based on the ER cut-off of 50 Ωm .

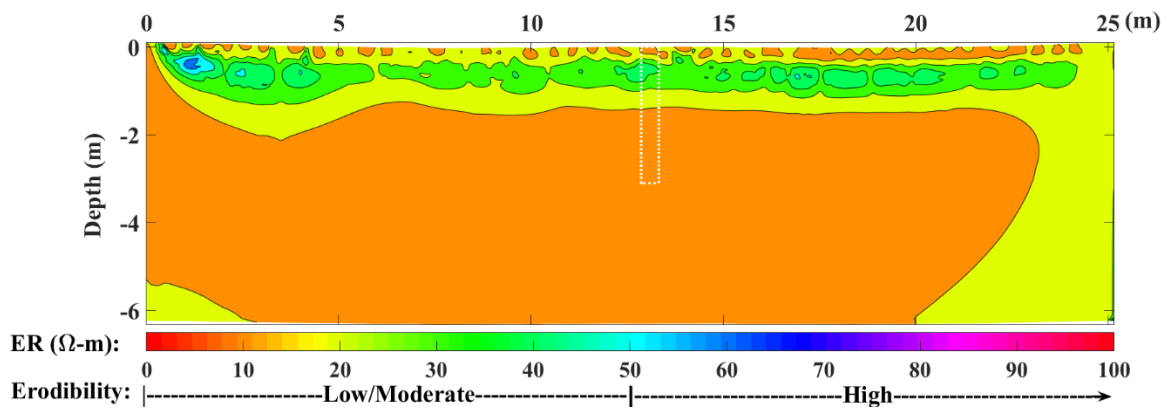


Fig. 3.9 Two dimensional ER and soil erodibility profile for US-24 site. (in color)

The white, dashed rectangle in Fig. 3.9 at 13 m along the horizontal axis shows the location where the five samples were collected for erosion testing in the laboratory. The in situ ER values of these samples varied between 13 to 35.6 Ωm . This range is below the cut-off ER of 50 Ωm indicating that these samples would be predicted to fall in the not high erodibility category. The EFA results of these samples showed moderate erodibility, agreeing with the binary classifier model. ER of two of these five samples were also determined using the laboratory ER method and were very similar to that of the in situ value (Table 3.1). This is an indication that after performing the drilling, ER values can also be measured in the laboratory to give a rapid estimate of the soil erodibility

instead of conducting a time-consuming erosion test, although the results would be limited to only two categories of erodibility.

The ER of Fig. 3.9 was relatively uniform indicating the soils at this site are likely not highly erodible; however, other sites may be more variable. For example, the subsurface ER profile of the US-36 site in Fig. 3.10 depicts how a 2-D erosion profile can identify layers or pockets (represented by yellow, orange, and red) of highly erodible soils (with ER above 50 Ωm). Fig. 3.10 highlights how even if drilling is performed and a full erosion test is conducted, the erosion risk may not be detected. The location of drilling is shown with a white, dashed rectangle in Fig. 3.10 indicating samples should exhibit low to moderate erodibility (represented by blue zone). These samples were in fact moderately erodible based on erosion testing (Karim and Tucker-Kulesza 2018). Thus, a field ERT survey can identify the location of potentially highly erodible soils where localized measurements from traditional drilling and sampling may be limited.

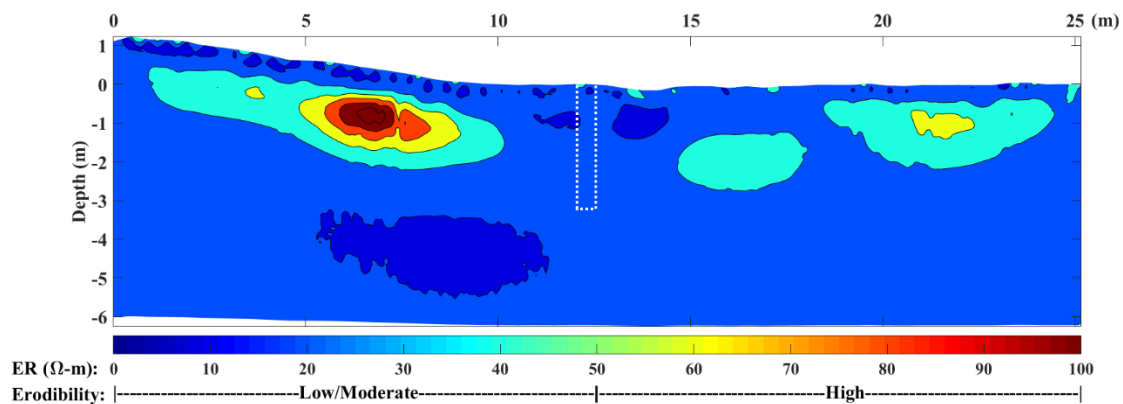


Fig. 3.10 Two dimensional ER and soil erodibility profile for US-36 site. (in color)

There remain limitations of this study. Firstly, despite the fact that 72 samples were used in the study, the range of soil types was narrow consisting mostly of high and low plasticity clays, with four clayey sands, two high plasticity silts, and two low plasticity silts. As shown in Fig. 3.5, none of the 72 samples collected for this study occupied the very high or very low erodibility zones of

the HEC-18 graph meaning that soil falling into those categories was unrepresented by this study. Therefore, there is a need to include fine sands in the model, which would likely fall in the very high erodibility zone. These sands would also likely have ER values above the cut-off of 50 Ωm ; however, there are limited data in this study to support this hypothesis. Additionally, very few studies on the erosion characteristics of intermediate geomaterials (IGM) or soft rock were found in existing literature; therefore, erosion testing on IGM's is required to include their erosion characteristics in the model. Although the soils in this study were not fully saturated in situ, statistical analysis showed that the ER values would not vary more than 3 Ωm when fully saturated. As the ER cut-off value of the developed binary classifier itself was 50 Ωm , this small variation (3 Ωm) can be considered negligible. Note that, the degree of saturation varied between 82 to 100% in this study. Hence, there is also a need to perform testing where degree of saturation is much lower because ER is greatly affected by the degree of saturation below 60%. In this way, this methodology, which was originally built for bridge scour, can be extended to partially saturated surface erosion. Finally, porewater conductivity affects ER measurements. The porewater electrical conductivity varied between 0.28 to 1.28 mS/cm with an average of 0.74 mS/cm for all the samples in this study. Soils with more conductive porewater (i.e., above 4.5 mS/cm like those found on the Arkansas River in Western Kansas) (Miller et al. 2010) may not be appropriately characterized by this methodology. Note that according to Grabowski et al. (2011), salinity also affects erodibility, therefore highly saline samples need to be investigated to further broaden potential applications.

3.7 Conclusions

There is a need for a rapid methodology to identify scour critical bridges. ER was proposed as a novel approach to this problem. Statistical similarity between in situ and laboratory (at the same

in situ degree of saturation and density) measurements of ER indicated that laboratory measurements can be conducted interchangeably where in situ ERT is not economically feasible. However, the added benefits of nondestructively acquiring spatial variation of large subsurface areas make in situ ERT preferable. The degree of saturation, one of the significant factors that affect the measured ER of soils, was investigated. This study has showed that soil ER values do not change significantly at fully saturated conditions, when compared to the ER values of partially saturated samples collected from streambanks. Note that, this was the case for the hydrogeologic conditions of eastern Kansas where the degree of saturation was not found below 82%. Therefore, ER values obtained from streambanks can be utilized for an ER based scour prediction model in similar hydrogeologic conditions. The statistical methodology of using ER (measured in the field and laboratory) as a binary classifier for bridge scour evaluation was explained as an example of applying probabilistic approaches in transportation projects. Results showed that the efficiency of this ER based binary classifier model was “excellent”. A cut-off value of 50 Ωm was selected for this model to distinguish high erodibility soils from soils with less erosion potential. Results also showed that there is an 87% probability of correctly predicting high erodibility soils using ER alone. This study was limited by a narrow range of soil types, high in situ degree of saturation, and relatively non-saline porewater. In order to expand the model for other hydrogeologic conditions, there is a need to evaluate soil at lower degrees of saturation, particularly below 60%, and where high concentration of dissolved solids increases the conductivity of porewater.

Chapter 4 - Modeling Critical Shear Stress for Bridge Abutment Scour in Cohesive Soils

This article is currently under review for publication in the ASCE's *Journal of Geotechnical and Geoenvironmental Engineering*.

Karim, M. Z., and Tucker-Kulesza, S. E. "Modeling Critical Shear Stress for Bridge Abutment Scour in Cohesive Soils." *Journal of Geotechnical and Geoenvironmental Engineering*, under review.

Abstract

Critical shear stress is an important variable when estimating scour around bridge abutments in cohesive soils. Critical shear stress is the stress exerted by the flowing water that initiates soil erosion. The objective of this study was to develop an empirical model to predict the critical shear stress in cohesive soils. A total of 70 soil samples from 26 bridge sites were used for this study. Erosion testing was performed in an Erosion Function Apparatus and 13 soil properties (independent variables) were measured. Multiple variable screening criteria determined percent fines, liquid limit, and electrical resistivity as the statistically significant model variables for predicting critical shear stress. Design factors for implementing the model to predict abutment scour were also recommended based on probabilistic analysis and its effect on scour predictions were presented. The critical shear stress model was validated using an arbitrary bridge site. If adopted by transportation agencies, this model can be used to predict abutment scour and reduce over conservative bridge scour designs.

Keywords: Soil erosion; Bridge scour; Cohesive soils; Critical shear stress; Electrical resistivity

4.1 Introduction

Scour is soil erosion around bridge supports and from the bed and bank of streams due to the hydraulic stress exerted by flowing water (Calappi et al. 2010). In 1991, the Federal Highway Administration (FHWA) established Hydraulic Engineering Circular 18 (HEC-18) to provide a conceptual framework for scour analysis, which remains the primary guideline for transportation agencies nationwide. The original empirical scour equations in HEC-18 were based on cohesionless coarse grained soils and were a function of median grain size. These equations have been proven to be over conservative for cohesive soils (Schuring et al. 2010). For example, these equations are applicable for a minimum median grain size of 0.2 mm (Arneson et al. 2012); however, median grain size is smaller than 0.075 mm for most cohesive soils. Median grain size predicts scour in cohesionless/non-cemented coarse grained soils because gravity force is the only resistive force against scour (Shields 1936, Briaud et al. 2017). In cohesive soils, cohesion and adhesion due to interparticle forces provide resistance against scour, in addition to the gravity force (Grabowski et al. 2011). In later editions of the HEC 18, equations for calculating scour were developed as a function of critical shear stress.

The critical shear stress is the threshold of applied hydraulic shear stress at which soil erosion initiates (Partheniades 1965; Hanson et al. 1999; Utley and Wynn 2008; Bernhardt et al. 2011). The excess shear stress equation is the common equation relating erosion rate and critical shear stress such that

$$\dot{E} = k_d(\tau - \tau_c) \quad (4.1)$$

where \dot{E} is the erosion rate (mm/hr), k_d is the erodibility coefficient ($\text{m}^3/\text{N}\cdot\text{s}$), τ is the hydraulic shear stress (Pa) and τ_c is the critical shear stress (Pa) (Partheniades 1965; Hanson et al. 1999).

Although equations to determine scour depth in cohesive soils are a function of critical shear stress,

site specific erosion testing is currently recommended to obtain the critical shear stress. Site specific testing is the most accurate approach, but it requires highly specialized equipment which many transportation agencies do not own, likely making this cost prohibitive. Therefore, the minimum median grain size for the given equation (developed for cohesionless soils) is often used for estimating scour in cohesive soils, leading to over conservative designs. There are numerous empirical equations to calculate critical shear stress in cohesive soils; however, these are rarely used in practice. The most prevalent critical shear stress equations for cohesive soils are as follows.

Erosion in cohesive soils is affected by various physical, biological, and geochemical properties (Grabowski et al. 2011, Paterson 1997). The relative contributions and interaction of these factors are still unknown and there has been no research to date investigating all of these factors in one empirical model. One of the earliest empirical equations for critical shear stress (τ_c) was developed by Dunn (1959),

$$\tau_c = 0.01(\tau_s + 180) \tan(30 + 1.73PI) \quad (4.2)$$

where τ_s is the shear strength and PI is the plasticity index of soil. However, the equation was intended to be used in the design of earth lined canals. Kimiaghali et al. (2015) also correlated critical shear stress and shear strength parameters, specifically cohesion, but the empirical model was based on a small number (13) of soil samples and narrow range of critical shear stress (0.31 – 10.25 Pa). Amos et al. (1997) studied the erosion mechanism of river delta sediments and established that

$$\tau_c = 7 * 10^{-4} \rho_b^{-0.47} \quad (4.3)$$

where ρ_b is the bulk density; this relationship was based on critical shear stress ranging from 0.11 to 0.50 Pa, which is a very small portion of the typical critical shear stress range in cohesive soils (Arneson et al. 2012). Julian and Torres (2006) developed a relationship based on particle size such that

$$\tau_c = 0.1 + 0.1779(SC) + 0.0028(SC) - 2.34e^{-5(SC)^3} \quad (4.4)$$

where SC is the clay-silt content. Thoman and Niezgoda (2008) used 25 soil samples collected from five different creeks in northeast Wyoming and they found that activity of clay (CA), dry density (ρ_d), specific gravity (G_s), pH , and water content (w) were significant soil properties affecting critical shear stress such that,

$$\tau_c = 77.28 + 2.20(CA) + 0.26\rho_d - 13.49G_s - 6.4pH + 0.12w. \quad (4.5)$$

Mahalder et al. (2018) developed 4 sets of equations based on physiographic regions and had poor correlation. Note that although these are likely not all of the empirical equations to predict critical shear stress, they highlight that researchers have selected different soil properties for their empirical models and there is no consensus on what controls the onset of erosion. Also, these models were not developed for bridge scour design.

Shan et al. (2015) developed an empirical equation for predicting the critical shear stress in cohesive soils, specifically to be used in the HEC-18 bridge scour design. Shan et al. (2015) found percent fines, water content, plasticity index, and unconfined compressive strength as statistically significant model variables, all of which are commonly measured by transportation agencies. Therefore, this equation allows transportation agencies to estimate critical shear stress without conducting site specific testing; however, the equation is only applicable for shear stress ranging from 3 to 15 Pa. Furthermore, the model was based upon laboratory prepared soils with

plasticity index ranging from 4 to 25, liquid limit between 15 to 50, and percent fines ranging from 10 to 90. These soils and lower shear stresses were likely chosen to focus on the worst case (i.e., more erodible) cohesive sediment in riverbeds (i.e., primarily pier and contraction scour).

Abutment scour occurs in the floodplain, outside of the river bed sediment, due to the obstruction of flow by the abutment and roadway embankment (Arneson et al. 2012). When working with cohesive soils in eastern Kansas to study abutment scour, the authors identified that most soil properties and applied hydraulic shear stresses were outside of the limits of Shan et al. (2015) model (Tucker-Kulesza and Karim 2017). Therefore, although Shan et al. (2015) is an improvement over previous equations based on cohesionless soils, there is still a need for calculating critical shear stress outside of riverbeds, where a wider range of cohesive soil properties was observed and where hydraulic stresses are higher. Broadening the soil properties and hydraulic stresses will also have the potential of using this approach for other structures where erosion is critical (i.e., dams, levees, slopes).

Karim and Tucker-Kulesza (2018) established that electrical resistivity tomography (ERT) can be used to rapidly characterize the erosion potential of a bridge site, primarily for prioritizing bridges for more advanced scour analyses. ERT is considered one of the Advanced Geotechnical Methods in Exploration (A-GaME) by the FHWA for its capacity to obtain continuous subsurface data between soil borings (FHWA 2019). In addition to site characterization, researchers have correlated electrical resistivity with geotechnical properties to reduce the number of geotechnical tests in a project (e.g., Kouchaki et al. 2018, Kibria and Hossain 2012, Abu-Hassanein et al. 1996, Ahmed et al. 2018, Chen et al. 2018). Karim and Tucker-Kulesza (2018) recommended ERT because of the overlap between physical, geochemical, and biological properties that affect both soil erodibility and electrical resistivity. Tucker-Kulesza and Karim (2017) noted that there was a

correlation between electrical resistivity and critical shear stress in cohesive soils; however, the relationship was not strong ($R^2 = 0.52$). Still, an advantage of electrical resistivity is that it is an intrinsic soil property which is influenced by non-engineering properties that also control soil behavior, like geochemical and biological factors (Friedman 2005).

Previous equations to calculate critical shear stress were limited because they did not consider the combined effects of physical, geochemical and biological factors; they focused on engineering properties. Similarly, researchers have studied the relationship between critical shear stress and geochemical or biological properties alone. For example, Ariathurai and Arulanandan (1978) showed critical shear stress increases with increasing cation exchange capacity (*CEC*). Arulanandan (1975) showed that critical shear stress decreases with increasing sodium absorption ratio. On the biological side, burrowing organisms create water filled chambers in consolidated sediment resulting in higher water content, lower shear strength and lower critical shear stress (Widdows et al., 2009). To the best of the authors knowledge, there has been no research to date on a method to calculate critical shear stress considering all biological, geochemical, and physical soil properties. This is likely because there are too many variables that may influence cohesive soil erosion identified in the literature, making the analysis too complicated and an unreasonable scope. This study included electrical resistivity as a soil property because it inherently includes the influence of geochemical and biological conditions in the measurement. For example, electrical resistivity will decrease with increasing *CEC* (Kibria 2014), and increase with increasing percentage of calcium ions (Kibria and Hossain 2012). Again, Chambers created by burrowing organisms will decrease the electrical resistivity due to increased water content (Widdows et al., 2009, Kouchaki et al. 2018). Thus, both geochemical and biological factors are captured by electrical resistivity without additional experiments for each factor. Including electrical resistivity

as a soil property is one unique aspect of this study. As will be shown, electrical resistivity was one of the three significant variables for calculating critical shear stress.

The objective of this study was to develop an empirical model to predict the critical shear stress for erosion in cohesive soils focusing bridge abutment scour. This introduction is followed by a methodology section where the field work and laboratory testing are briefly described. The results and analysis section includes the description of the variables, the selection of variables through multicollinearity analysis and variable screening technique, model building, and cross validation of the model. Next, a design factor for application of the model for calculating abutment scour is selected based on a probabilistic approach. The paper ends with the model validation, a discussion of the results, and conclusions.

4.2 Methodology

A total of 70 soil samples from 26 sites were used to develop the model to predict critical shear stress. Most of the samples (i.e., 67) were collected from 23 sites in eastern Kansas. The Kansas Department of Transportation (KDOT) identified these sites based on scour vulnerability. As expected, 20 of the Kansas sites characterized as alluvium geology (i.e., deposited during comparatively recent geologic time by streams on their floodplain or delta) (KGS 2019). Two of the sites were Dakota formation, characterized by white, gray, red, brown, and tan kaolinitic claystone, mudstone, shale siltstone, and interbedded and lenticular sandstones (Zeller 1968). The remaining Kansas site was formed by glacial drift. Glacial drift sediment was transported by glaciers and deposited directly on land (Neuendorf et al. 2011). A map of the 23 Kansas sites are shown with their surficial geologic information in Fig. 4.1. The remaining three soil samples were collected from Ohio, Nebraska, and Colorado by the FHWA for a separate study.

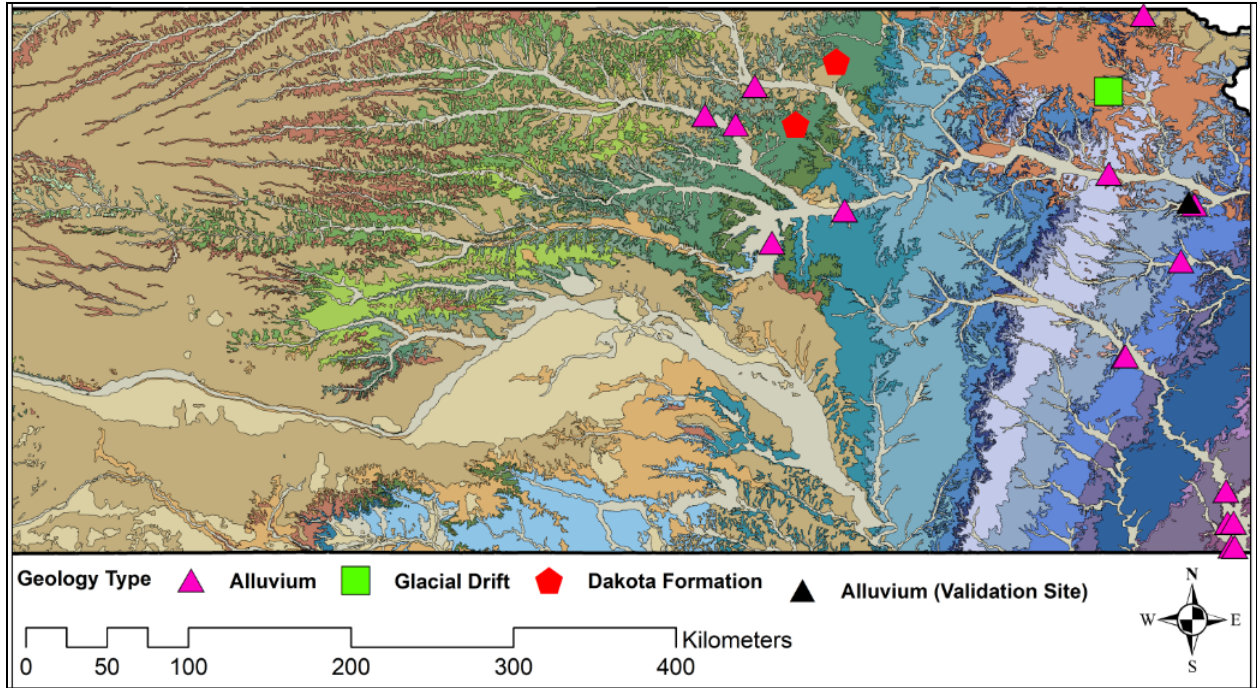


Fig. 4.1 Location of the 23 sites from eastern Kansas with their surficial geology

As shown in Table 4.1, the 26 sampling locations fell under eight different physiographic provinces (KGS 2019, ODNR 2019, KDHE 2019, CGS 2019). Physiographic provinces are divided according to their geomorphology, which is related to the processes of landforms and geologic structure. Among the physiographic provinces Smoky Hills, Central Nebraska Loess Plains, and Colorado Piedmont fall in the United States Great Plains region and are formed by sandstone, limestone and chalk (KGS 2019). The other five provinces fall in the Central Lowlands region; among them both Osage Cuestas and Flint Hills are formed by eroded shales and limestone; Cherokee Lowlands by eroded shales and sandstones; Glaciated Region by glacial drift and loess; and Derby Plain by high-lime till, carbonate rocks and shales (KGS 2019, ODNR 2019).

Table 4.1 Physiographic Origins of the Soil Samples

State	Physiographic Province	No. of Sites
Kansas	Smoky Hills	6
	Glaciated Region	4
	Osage Cuestas	7
	Flint Hills	1
	Cherokee Lowlands	5
Ohio	Darby Plain	1
Nebraska	Central Nebraska Loess Plains	1
Colorado	Colorado Piedmont	1
Total		26

All samples were collected in 610 mm long, thin-walled Shelby tubes following ASTM D1587 (ASTM 2015a), and preserved and transported following ASTM D4220 (ASTM 2014a). An ERT survey was conducted to obtain the electrical resistivity data for the 67 samples at the 23 Kansas sites. A laboratory electrical resistivity measurement was used for the three FHWA samples with a four-electrode soil box following ASTM G187 (ASTM 2018a). Note that Karim et al. (2019) showed that laboratory resistivity measurements provide statistically similar resistivity values as in situ ERT, primarily for this purpose where ERT was not possible. Additional soil property measurements included: triaxial unconsolidated undrained shear strength (ASTM D2850 2015b), water content (ASTM D2216 2019), Atterberg limits (ASTM D4318 2017a), grain size distribution (ASTM D7928 2017b, ASTM C117 2017c, and ASTM C136 2014b), and bulk density (ASTM D7263 2018b). Dry density, void ratio, porosity, and degree of saturation were calculated based on the measured properties.

Erosion testing of all 70 samples were conducted in an erosion function apparatus (EFA). The EFA is a flume-style apparatus where erosion rate (mm/hr) can be measured at different water velocities (m/s) and the corresponding shear stress, τ (Pa) applied by the water to the eroding soil surface is calculated as

$$\tau = \frac{1}{8} f \rho v^2 \quad (4.6)$$

where f is the friction factor, ρ is the density of water (kg/m^3), and v is the water velocity (m/s) (Briaud et al. 2001). The critical shear stress was determined from each EFA test as the shear stress corresponding to an erosion rate of 0.1 mm/hr (Briaud 2017). A more detailed description of the sampling, ERT surveys, and erosion testing can be found in Karim and Tucker-Kulesza (2018) and Karim et al. (2019).

A multiple linear regression (*SAS v.9.4*) was performed for modeling critical shear (dependent variable) for erosion. A total of 13 independent variables were obtained through above tests for this purpose. Variable transformation using a suitable function was done as the first step to reduce the skewness in the distribution of the variables. Next, several independent variables were removed from the model development process considering the multicollinearity (Mendenhall and Sincich 2012) among independent variables. Finally, backward elimination technique (Mendenhall and Sincich 2012) was utilized to choose the best independent variables for the multiple linear regression model of critical shear stress.

4.3 Results and Analysis

Among the 70 samples of this study, 17 classified as CH (high plasticity clays), 44 as CL (low plasticity clays), four as ML (low plasticity silts), one as MH (high plasticity silts), three as SC (clayey sands), and one as SW-SC (well graded clayey sands) as per Unified Soil Classification System (USCS) (ASTM D2487 2017d). According to Mitchell and Soga (2005), and Raudkivi (1990) soils having a minimum of 5-10% fines (passing 0.075 mm sieve) (by weight) are cohesive and their erosion behavior is controlled by the fines. All samples were cohesive by this definition and included in the analysis to predict the critical shear stress.

The results of erosion tests (erosion rate versus shear stress) for all 70 samples are shown in Fig. 4.2. The critical shear stress of these samples varied between 0.4 to 97.1 Pa and are shown using asterisks along the 0.1 mm/hr erosion rate line in Fig. 4.2. As per HEC-18 (Arneson et al. 2012), the graph is divided into six different categories of erodibility based on USCS soil types.

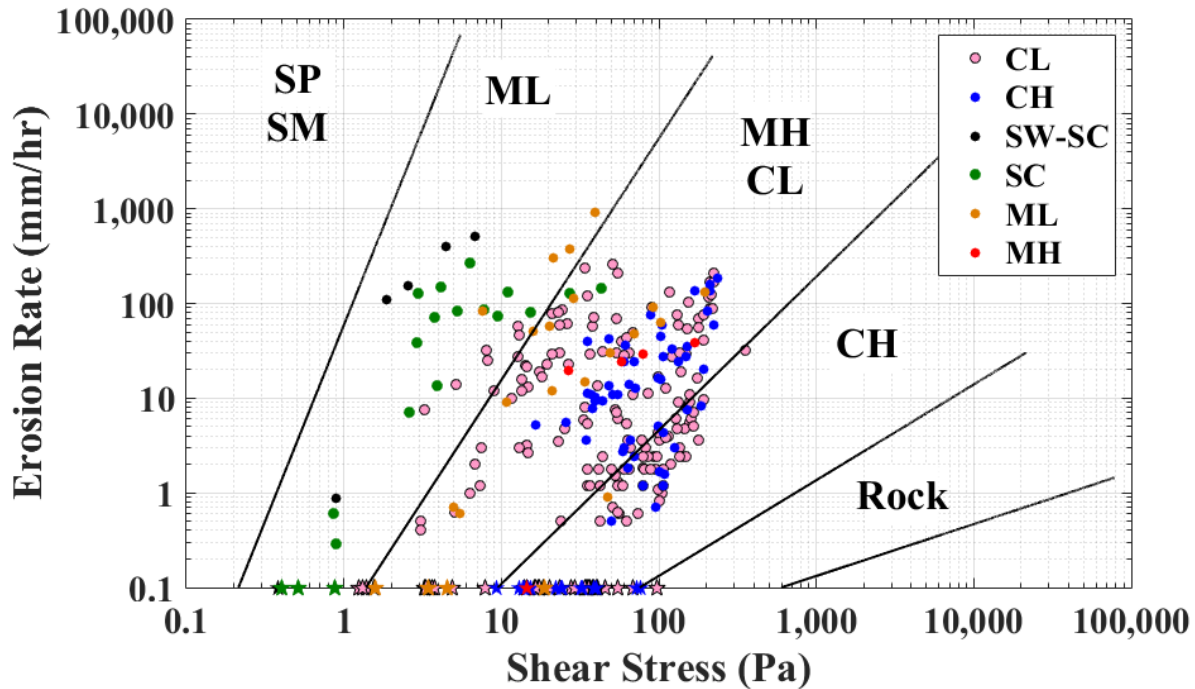


Fig. 4.2 Erosion rate versus shear stress with USCS classification for the 70 samples

As shown in Fig. 4.2 the critical shear stress of the 70 samples in this study ranged across four (out of six) different categories of erodibility. According to HEC-18, high plasticity clays is the most erosion resistant soil after rocks. It also suggests that, critical shear stress should approximately vary between 1.5 to 9 Pa for the low plasticity clays and 9 to 70 Pa for the high plasticity clays (CH). However, in this study, a low plasticity clay was the most erosion resistant soil with maximum critical shear stress of 97.1 Pa. The range, minimum, maximum, mean, median, and standard deviation of critical shear stress (dependent variable) and 13 other soil properties

(independent variables) for all 70 samples are shown in Table 4.2. Due to the difference between mean and median and large standard deviation of 20.59 Pa for a range of 96.7 Pa (Table 4.2), the distribution of the 70 observations of critical shear stress was highly skewed; hence, logarithmic transformation was used. Note that, variable transformation using a suitable function is the first step in multiple linear regression to reduce the skewness in the distribution of the variables (Mendenhall and Sincich 2012).

Table 4.2 Description of the Statistical Variables for Model Development for 70 Soil Samples

Variable	Range	Min.	Max.	Mean	Median	Std. Dev.
Critical shear stress, τ_c (Pa)	96.7	0.4	97.1	23.31	17.23	20.59
Electrical resistivity, ρ (Ω -m)	321.7	6.0	327.7	28.87	12.71	54.90
Water content, w (%)	29	11	40	26.77	27.08	4.74
Percent fines, f (%)	89	11	100	90.30	96.79	19.21
Median grain size (mm), d_{50}	1.9188	0.0012	1.9200	0.09	0.01	0.36
Liquid limit, LL (%)	54	26	80	42.72	41.50	10.25
Plastic limit, PL (%)	24	10	34	20.52	20.00	4.18
Plasticity index, PI (%)	49	3	52	22.20	22.00	10.01
Void ratio, e (dimensionless)	0.90	0.28	1.18	0.77	0.76	0.19
Porosity, n (dimensionless)	0.32	0.22	0.54	0.43	0.43	0.06
Degree of saturation, S (%)	32	67	100	90.90	90.58	6.53
Bulk density, D_b (g/cm^3)	0.58	1.75	2.32	1.93	1.91	0.11
Dry density, D_d (g/cm^3)	0.86	1.25	2.11	1.54	1.53	0.16
Undrained strength, S_u (kPa)	225.5	13.9	239.4	97.54	95.76	47.51

As shown in Table 4.2, while the electrical resistivity values varied between 6.0 Ω m to 327.7 Ω m, its mean (28.8 Ω m) and median (12.71 Ω m) indicated that the data distribution was positively skewed (i.e., more soil samples with low electrical resistivity values). The soil samples in this study were predominantly fine grained with a high degree of saturation, supporting the relatively low electrical resistivity (Everett 2013; Kouchaki et al. 2018, Kibria and Hossain 2012, Abu-

Hassanein et al. 1996). Similarly, as shown in Table 4.2 the distribution of median grain size was positively skewed, and the distribution of percent fines was negatively skewed. Typically, logarithmic or square root functions are applied to reduce the skewness of the data distribution and normalize the data as much as possible (Mendenhall and Sincich 2012). Therefore, electrical resistivity, median grain size, and percent fines were transformed using logarithmic function (base = 10) before regression analysis. The difference between mean and median for rest of the variables were small (Table 4.2); hence, no transformation was needed.

4.3.1 Variable Selection

All soil properties measured herein were previously identified as variables that impact cohesive soil erodibility (e.g., Grabowski et al. 2011, Kimiaghalam et al. 2015, Karim and Tucker-Kulesza 2018, Arneson et al. 2012). Some of these properties measure similar soil characteristics leading to multicollinearity in the dataset. Multicollinearity is the existence of near-linear to linear relationship between a pair of independent variables, and it can cause the regression coefficients to be misleading and reduce the model predictability (Mendenhall and Sincich 2012). Following variable transformation, multicollinearity among the 13 independent variables were checked to select the set of independent variables for predicting critical shear stress. Multicollinearity is measured by the coefficient correlation, r (dimensionless ratio) such that

$$r = \frac{\sum_i(x_{1i}-\bar{x}_1)(x_{2i}-\bar{x}_2)}{\sqrt{\sum_i(x_{1i}-\bar{x}_1)^2 \sum_i(x_{2i}-\bar{x}_2)^2}} \quad (4.7)$$

where, $-1 \leq r \leq 1$; x_{1i} and x_{2i} are the two variables between which r is being measured for the i -th observation (Mendenhall and Sincich 2012). A positive r denotes that the pair of variables are positively related (increasing one increases the other) and vice versa. The closer the $|r|$ value is to 1, the stronger is the relationship (i.e., multicollinearity) between two independent variables and

one of these two variables should be excluded from further consideration. A heatmap showing the r values among all available pairs of independent variables is shown in Fig. 4.3.

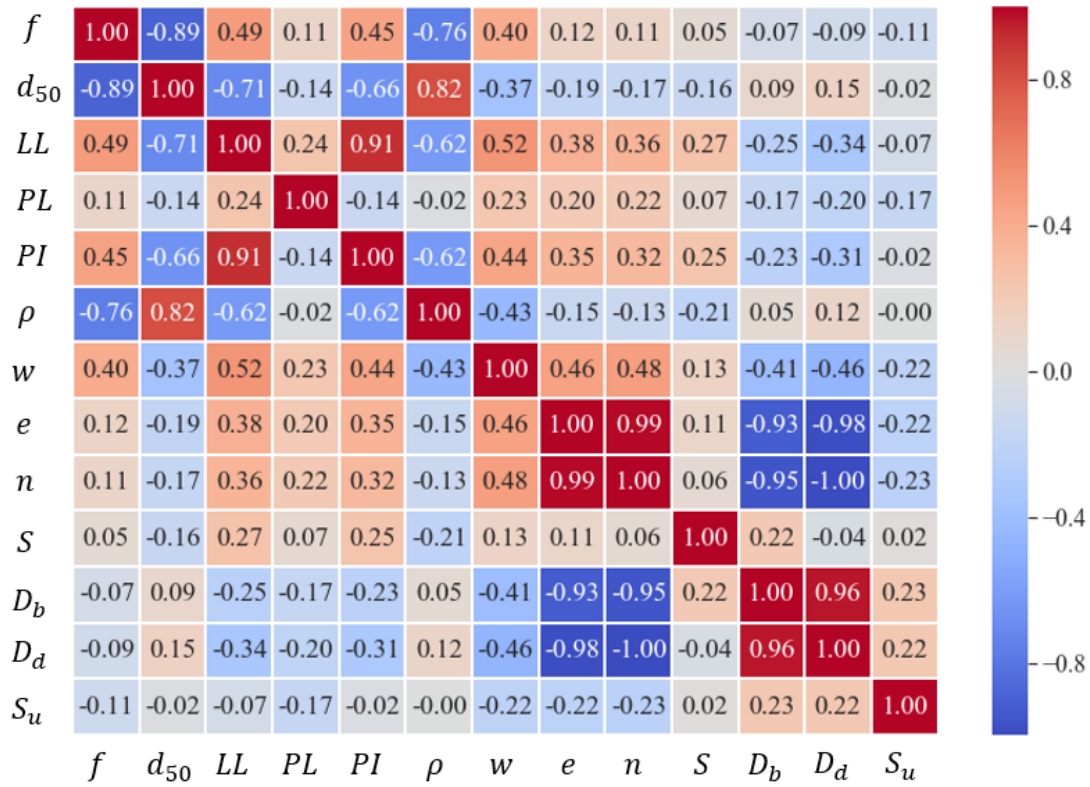


Fig. 4.3 Heatmap showing the multicollinearity among independent variables; red and blue colors denote positive and negative correlations, respectively

As shown in Fig. 4.3, bulk density, dry density, void ratio, and porosity were highly correlated with mutual $|r|$ values among them over 0.90. This was expected, because all these four variables denote how densely the soil particles are packed. Each of these variables was checked and the results did not change regardless of which was kept; therefore, dry density was kept because it is commonly measured. Rest three variables (bulk density, void ratio, porosity) were excluded from the model to avoid multicollinearity. Among the Atterberg limits, plasticity index was left out because r was found as 0.91 between plasticity index and liquid limit. Also, plasticity index is

obtained combinedly from plastic limit and liquid limit, so this information was inherently redundant. Finally, percent fines and median grain size were highly correlated with $|\tau|$ of 0.89. When plotted separately against critical shear stress both of these variables were found to affect the onset of erosion. However, because both percent fines and median grain size were obtained from the gradation curve, keeping both would induce repetitive information and ultimately have an adverse effect on the model. Note that median grain size is a good indicator of critical shear stress in clean sand and gravel where gravity forces control the erosion threshold (Shields 1936). Hence, median grain size is used in the scour equations for cohesionless soils in HEC-18 and the cohesionless equations are very accurate (Arneson et al. 2012). In cohesive soils, the erosion is not controlled by the size of the particle but rather the amount of cohesive material, or the percent fines. Furthermore, percent fines is determined more routinely than median grain size in cohesive soils because median grain size also requires a hydrometer analysis, which might not be feasible. Therefore, percent fines was considered for predicting critical shear stress and median grain size was dropped to avoid multicollinearity. After removing five independent variables considering the multicollinearity, eight variables were left for the final stage of variable selection.

The final step in variable selection was to select the optimum number of independent variables that would best describe the critical shear stress (dependent variable) using the backward elimination stepwise regression, which is one of the most widely used variable screening techniques (Mendenhall and Sincich 2012). Note that, at this stage, eight different properties were available as model variables, and liquid limit was used as a quadratic function (LL^2 , LL), adding an extra variable. Liquid limit was used as a quadratic function because, critical shear stress showed an increasing trend with increasing liquid limit up to a liquid limit value of around 50 and beyond this point the critical shear stress became somewhat constant or slightly decreased, and a

quadratic function best described this behavior. A quadratic function for plasticity index was also used in the permissible shear stress equation developed by the United States Department of Agriculture (USDA) for the purposes of evaluating channel lining stability (USDA 1987). The backward elimination technique fitted a model containing all nine independent variables in the first iteration. In successive iterations the predictive performance of a variable was evaluated based on the t-statistic (Mendenhall and Sincich 2012) and removed if not satisfactory, until all the variables existing in the model had significant t-statistic. Backward elimination was run using $\alpha = 0.10$ significance level. A significance level of 0.05 to 0.10 is commonly used (Mendenhall and Sincich 2012); 0.10 was chosen because the result of backward elimination was further verified by an additional variable screening. After the final iteration, percent fines, liquid limit as a quadratic function (i.e., LL^2 and LL), and electrical resistivity were identified as significant independent variables for predicting critical shear stress. At this stage, plastic limit, water content, saturation, dry density, and undrained shear strength were eliminated. To validate these variables in the model and ensure it was not overly constrained, an additional variable selection algorithm (Pedregosa et al. 2011) was used to detect most influential independent variables. In this method, independent variables are ranked based on their F scores such that

$$F = \frac{r^2(n-2)}{1-r^2} \quad (4.8)$$

where r is the correlation coefficient for a certain independent variable with critical shear stress and n is the total number of observations. As shown in Table 4.3, F scores of percent fines, liquid limit as a quadratic function, and electrical resistivity were higher than the remaining five variables indicating they were the most influential variables. Furthermore, this result was in agreement with backward elimination method.

Table 4.3 F Scores of the Independent Variables for Predicting Critical Shear Stress

Variable	$Log(f)$	LL^2	LL	PL	$Log(\rho)$	w	S	D_d	S_u
F score	59.7	18.8	31.1	0.5	70.9	6.1	1.5	0.001	0.7

4.3.2 Model to Predict Critical Shear Stress in Cohesive Soils

A multiple linear regression analysis was run based on the four variables that most influence soil erosion, namely, percent fines, liquid limit, liquid limit squared, and electrical resistivity. Based on these properties the regression equation was

$$Log(\tau_c) = -2.26 + 0.80 * Log(f) - 7.78 * LL^2 + 8.95 * LL - 0.40 * Log(\rho) \quad (4.9)$$

where LL is in decimal. The coefficient of determination, R^2 , of the model was 0.62. The results of the predicted versus actual critical shear stress are shown in Fig. 4.4. Among the 70 observations, 38 data points underpredicted and 32 of the data points overpredicted the critical shear stress. Although the R^2 of 0.62 was moderate to substantial (Henseler et al. 2009), this was because most of the data were underpredicted. Moreover, the amount of underprediction was very high (ratio of actual to predicted critical shear stress above 2.7) for five samples, which greatly affected the model accuracy based on R^2 . From a geotechnical design perspective, underprediction of critical shear is conservative and over prediction would initiate erosion earlier than expected. Therefore, statistical results without engineering judgement may provide wrong implications of the model.

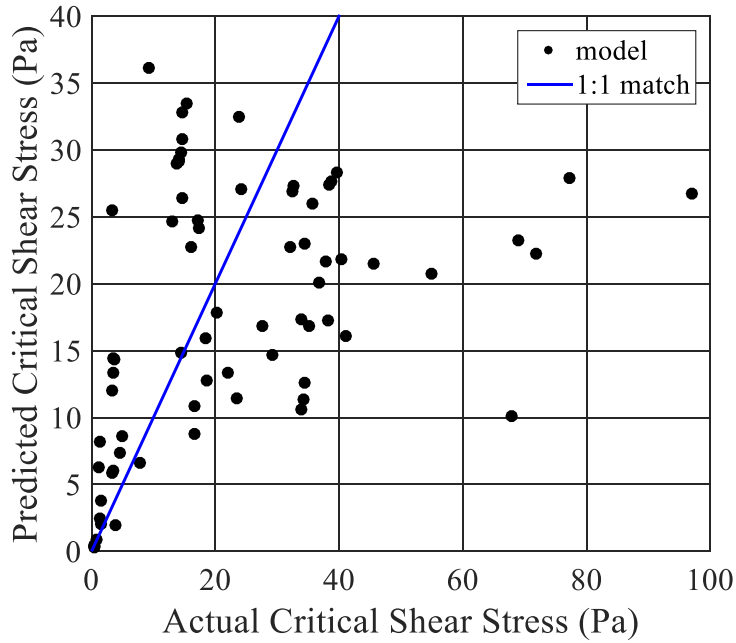


Fig. 4.4 Predicted versus actual (measured) critical shear stress

After raising both sides of Eq. (4.9) to the power of 10, the proposed model is

$$\tau_c = f^{0.80} \rho^{-0.40} 10^{-7.78LL^2 + 8.95LL - 2.26} \quad (4.10)$$

where all the variables are previously defined. Finally, cross validation was performed to verify all model coefficients would also perform well for sites not used in this dataset. Cross validation is a model evaluation method where the model is built by a portion of the dataset and the remaining portion is used for validating the model. The leave one out method, one of the most robust cross validation methods available, was used in this study (Pedregosa et al. 2011). In this technique the model was built 70 separate times using 69 observations and keeping the only other observation for validating the model each time. A total of 70 sets of intercept and coefficients of the model were obtained along with their maximum, minimum, and mean values. As presented in Table 4.4, the mean values of intercept and all four coefficients (for 70 different test models) were within 1%

of the regression analysis results shown in Eq. (4.9); therefore, no further modification of the coefficients and intercept of the model was made.

Table 4.4 Model Cross Validation Results

	Intercept	Variable Coefficients			
		$Log(f)$	LL^2	LL	$Log(\rho)$
Min.	-2.84	0.68	-11.02	7.66	-0.51
Max.	-1.85	0.89	-6.68	11.77	-0.29
Mean	-2.27	0.79	-7.81	8.97	-0.41
Selected	-2.26	0.80	-7.78	8.95	-0.40
Difference from mean	0.01	0.01	0.03	-0.02	0.01

4.4 Design Recommendations

As shown in Fig. 4.4, the developed equation over predicted 32 of the data points. In other words, the soil eroded relatively easily but was calculated to be more erosion resistant. Among these overpredicting points four points were roughly on the 1:1 line in Fig. 4.4 (indicating negligible overprediction); however, the ratio of actual and predicted critical shear stress of the remaining 28 samples were over 0.80. Therefore, a design factor, α_d , is recommended based on an acceptable level of risk by the designing engineer such that

$$\tau_{c,d} = \alpha_d * (f^{0.80} \rho^{-0.40} 10^{-7.78LL^2 + 8.95LL - 2.26}) \quad (4.11)$$

where $\tau_{c,d}$ is the design critical shear stress and α_d is the ratio of design critical shear stress and predicted critical shear stress. The purpose of using α_d was to minimize the probability of overpredicting the design critical shear stress. The α_d is selected by the engineer such that the probability of overpredicting critical shear stress is minimized while still achieving a prudent design (Tucker et al. 2015). A total of 65 observations were used to create the cumulative density function (CDF) shown in Fig. 4.5. It was determined that the five observations with extremely

high critical shear stress (above 60 Pa) should be removed so the design did not become extremely conservative as the model cannot predict critical shear stress that high. To construct the CDF, probability of failures (the ratio of over predicted observations and total observations) were calculated for many α_d values. For example, for $\alpha_d = 1$ (unfactored equation), the probability of failure was 0.49 as 32 observations (out of 65 observations) exhibited overprediction. The same procedure was repeated for varying α_d to obtain a plot of probability of failure versus α_d . A lognormal cumulative density function (CDF) was fit on these experimental data.

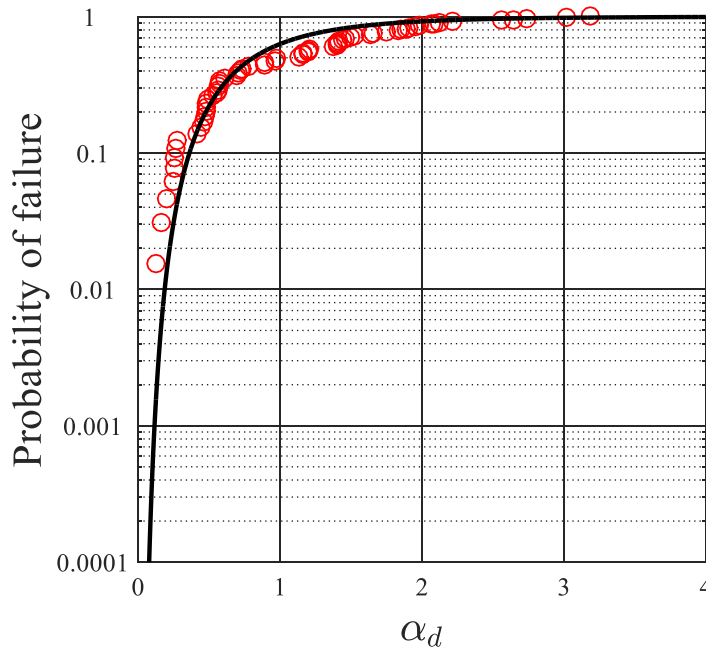


Fig. 4.5 Cumulative density function plot for α_d

The goal was to recommend α_d based on a well-judged probability of failure. Baecher and Christian (2003) provided the acceptable risk of failure for several civil engineering structures based on the accumulated data in the United States. According Baecher and Christian (2003), the acceptable probability of foundation failure is 0.01 for bridge design. Shan et al. (2015) recommended a reduction factor (α_d) so that no more than 10% critical shear stress data in cohesive soils were over predicted (probability of failure = 0.10) in the context of the FHWA's

HEC-18 framework. The design factor, α_d , is 0.20 and 0.36 for a probability of failure of 0.01 and 0.1, respectively (Fig. 4.5). Note that these are not the only permissible design factors. The design equation (Eq. 4.11) can be factored using an α_d value based on the project need. For example, for designing scour depth for a bridge along rural highways, a higher α_d may be warranted so as to not be too conservative while $\alpha_d = 0.20$ would likely be used for a major interstate where a lower risk is acceptable.

To evaluate how the design equation for critical shear stress would influence bridge scour design, the design scour depths for different α_d values were calculated using the abutment scour depth equation in cohesive soils (Arneson et al. 2012). The HEC-18 abutment scour equation (Eq. 4.12) for cohesive soils calculates the scour depth y_s (m) by

$$y_s = \alpha_B \left[\left(\frac{\gamma}{\tau_c} \right)^{\frac{3}{7}} \left(\frac{nq_{2f}}{K_u} \right)^{\frac{6}{7}} \right] - y_0 \quad (4.12)$$

where, α_B (unitless) is the scour amplification factor which is dependent on unit discharge of the stream, γ (N/m³) is the unit weight of flowing water, n (unitless) is the manning's coefficient, q_{2f} (m²/s) is the abutment unit discharge, K_u is a dimensionless factor (1 in S.I.), and y_0 is the abutment flow depth before scour. For evaluation, the design critical shear stresses were calculated using Eq. (4.11) with $\alpha_d = 0.20, 0.36,$ and 1.0 . Next, three sets of abutment scour depths were calculated with these design critical shear stresses using Eq. (4.12). These design scour depths were compared with calculated scour depths using the measured critical shear stress from the EFA tests [Fig. 4.6(a and b)]. Using $\alpha_d = 1.0$ (corresponding probability of failure 0.60 from the CDF in Fig. 4.5) allowed the evaluation of the unfactored equation. Note that the values of $\alpha_B, \gamma, n,$

q_{2f} , and y_0 were utilized from a design example defined in HEC-18 as 2.1, 9810 N/m³, 0.025, 0.94 m²/s, 1.1 m, respectively (Arneson et al. 2012).

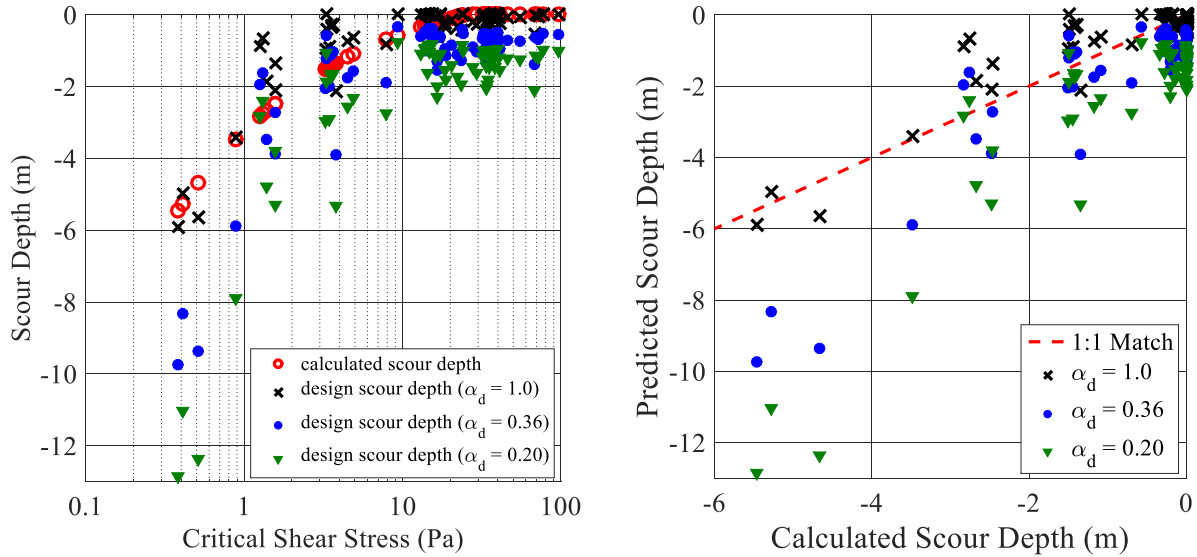


Fig. 4.6 (a) Comparison of design scour depths with calculated scour depths for varying critical shear stress; (b) Design scour depths versus calculated scour depth

As shown in Fig. 4.6(a), the calculated scour depths from measured critical shear stresses varied up to -5.5 m (hollow red circle markers) and scour depths were negligible when critical shear stress was above 24 Pa. This further supported omitting the five extremely high (i.e., greater than 60 Pa) samples from the CDF developing α_d , these samples made the reduction too conservative while also representing sites where calculated scour would be negligible. For $\alpha_d = 1.0$ (unfactored design equation), design scour depths (black 'x' markers) were over predicted 38 times and under predicted 32 times. Note that, opposite to critical shear stress, over prediction of scour depth is conservative. Most of the 32 under predictions occurred between shear stresses of 1 to 10 Pa and the maximum difference in design and calculated scour depths was 2.1 m at a critical shear stress of 1.3 Pa. As shown in Fig. 4.6 (a) and (b), the risk of under prediction was greatly reduced by

implementing both $\alpha_d = 0.36$ (blue circle markers) and 0.20 (green triangle markers). For $\alpha_d = 0.36$, there were seven observations of under predicted scour depth with a maximum difference in design and calculated scour depths of 1.1 m. For $\alpha_d = 0.20$, there were only two observations of under predicted scour depth and maximum difference between design and calculated scour depths was only 0.4 m. Overall, both design factors showed that proposed design equation was conservative. Design scour depths were obtained deeper than calculated depths for 61 and 68 observations for $\alpha_d = 0.36$ and 0.20, respectively. In many occasions these over predictions were by a big margin (e.g. in low critical shear stresses). Note that the unfactored model was very accurate (i.e., within maximum 0.98 m) at the four critical shear stresses below 1 Pa. Therefore, a design engineer may use a α_d greater than the proposed values to avoid extreme over prediction for a rural structure with low traffic volume.

4.5 Validation

The developed model was validated using a site selected by the KDOT. The site is located 6.2 km southwest of Lawrence, Kansas along Kansas 10 (K-10) highway. The drilling was conducted on the bank of Yanky Tank creek that intersects with K-10 highway. As expected, the soils at the site are characterized by the alluvium geology and the site is in the glaciated region physiographic province (KGS 2019). Sampling and ERT surveys were conducted on the same day. The subsurface electrical resistivity distribution is shown in Fig. 4.7(a). The electrical resistivity at the sample location was 8.1 Ωm . The liquid limit and percent fines for the sample was found 40 and 95.77, respectively. Using these values, the unfactored critical shear stress was predicted as 19.1 Pa using Eq. (4.10). The design equation (Eq. 4.11) yielded a critical shear stress of 3.8 Pa and 6.9 Pa for $\alpha_d = 0.2$ and 0.36, respectively. The actual critical shear stress from the EFA test was found

36.3 Pa [Fig. 4.7(b)]. Therefore, the proposed model under predicted the critical shear stress, which is conservative from design standpoint.

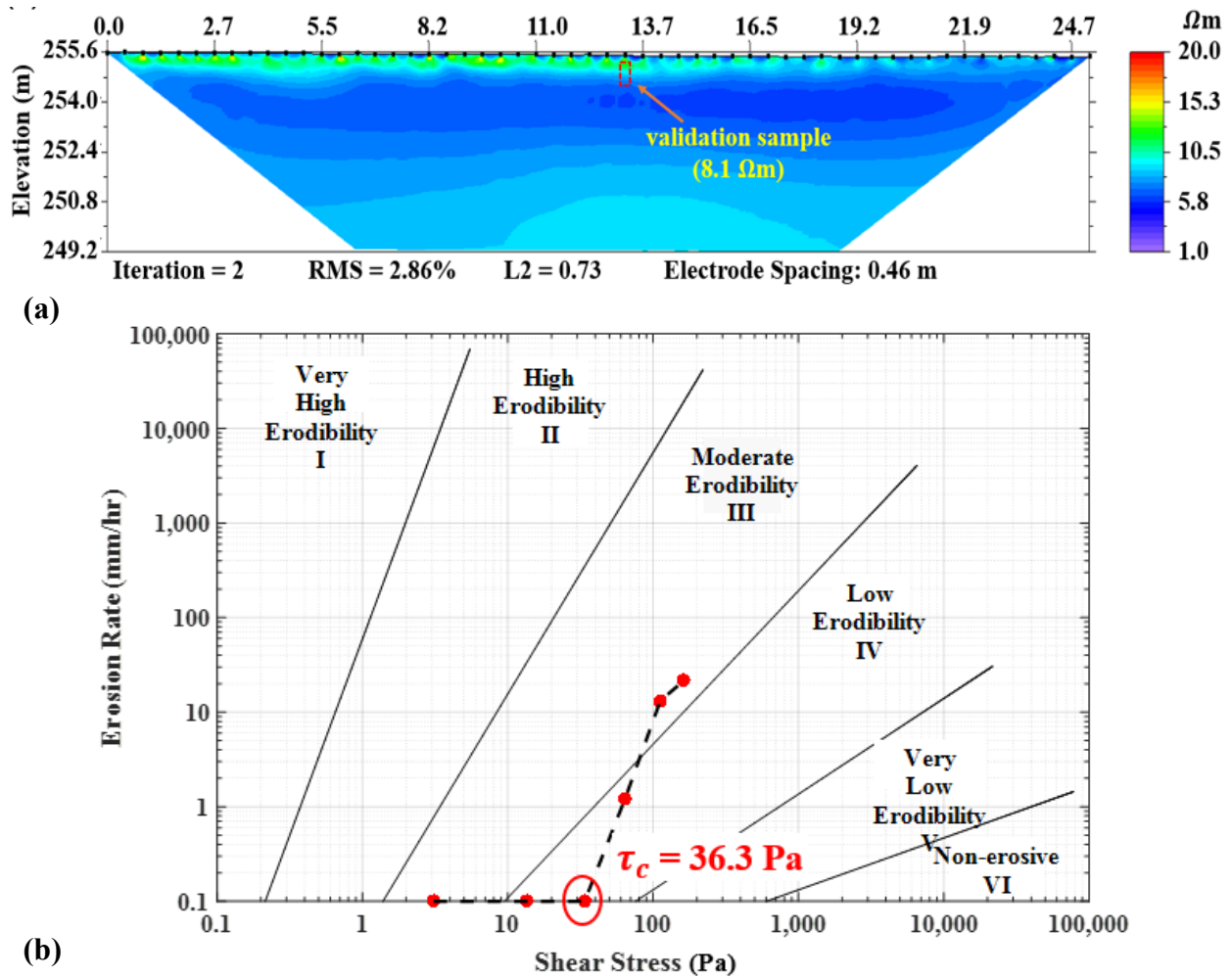


Fig. 4.7 (a) Subsurface resistivity distribution at K-10 site; (b) the EFA test result for the validation sample from K-10 site

4.6 Discussion

The primary goal of this study was to develop a model for predicting critical shear stress in cohesive soils. The final variables in the critical shear stress equation were percent fines, liquid limit, and electrical resistivity. Recent scour models such as Shan et al. (2015), Kimiaghalam et al. (2015), Mahalder et al. (2018) have been valuable contributions in understanding the effects of

many soil properties on the onset of erosion in cohesive soils. Shan et al. (2015) specifically addressed the need for incorporating the erosion behavior of cohesive soils in the context of FHWA's HEC-18 framework. Shan et al. (2015) selected percent fines, plasticity index, water content, and unconfined compressive strength to predict critical shear stress in low plasticity cohesive soil. Percent fines was also a statistically significant variable in this study and plasticity index has a high correlation with liquid limit, another significant variable in this study. Therefore, it is evident that the amount of fines and the Atterberg limits of cohesive soils are important measurable properties for predicting the onset of erosion. This is an important finding as researchers continue to work to understand and define the mechanisms of cohesive soil erosion.

A new finding of this study was that electrical resistivity was identified as a statistically significant model variable for predicting critical shear stress. Electrical resistivity is a bulk response of the soil and is affected by many physical and geochemical factors of soil. Many of the physical properties that previous researchers identified to affect critical shear stress [i.e., water content, unconfined compressive strength by Shan et al. (2015), cohesion by Kimiaghalam et al. (2015), bulk density by Amos et al. (1997)] also influence electrical resistivity (Abu-Hassanein et al. 1996, Kibria and Hossain 2012, Kouchaki et al. 2018, Chen et al. 2018). Again, erosion is affected by several geochemical factors and these properties are not routinely measured by transportation agencies, but these geochemical properties are captured utilizing electrical resistivity. For example, sodium absorption ratio and cation exchange capacity were found as significant factors affecting the onset of erosion by Kimiaghalam et al. (2015) and Mahalder et al. (2018) and electrical resistivity is highly affected by these properties (Friedman 2005). Thus, electrical resistivity may capture the physical, geochemical, and biological properties that previous researchers identified to influence the erosion separately. The contribution of electrical resistivity

can be viewed as dimensionality reduction, meaning electrical resistivity may capture the interrelated interactions and proportions of all these properties to convert to a single property. The exact components of each of these separate dimensions (i.e., various soil properties) to convert to a single dimension (i.e., electrical resistivity) is an interesting research question that should be pursued in future studies. Again, most of the previous studies on cohesive soil erosion were either based on laboratory prepared samples (e.g., Shan et al. 2015) or field samples were collected from a single physiographic location (e.g., Julian and Torres 2006). Therefore, some properties may have over constrained the model such that it would not be applicable in a different soil type or physiographic location. Electrical resistivity may capture the interrelated interactions between these properties more generally for the broader range of soil types used in this study.

The developed model exhibited an R^2 of 0.62. No other studies on cohesive soils with a better accuracy was found in the literature that used field retrieved samples and had more data points than this study. Field retrieved samples are inherently more variable than laboratory prepared samples, which may impact model accuracy. The predicted versus actual critical shear stress plot for the 70 observations of this study (Fig. 4.4) showed that 32 points were over predicted and 38 were under predicted. More data points of critical shear stress being under predicted by the developed equation is desired (conservative); however, among the underpredicted samples, critical shear stresses of five samples were very high (above 60 Pa) which greatly influenced the overall model accuracy.

The range of predicted critical shear stress by this model was 0.3 to 36.2 Pa. The lower limit of this model was very small (0.3 Pa) and therefore, this model will cover the onset of erosion for more vulnerable cohesive soils. Also, upper limit of the model (36.2 Pa) is greater than the upper limits of previous models (Shan et al. 2015, Kimiaghalam et al. 2015, Mahalder et al. 2018)

and will reduce the issue of over conservative predictions of abutment scour. However, there is still a need to understand the erosion behavior of intermediate geo materials (IGM) and soft rocks that exhibit higher critical shear stress. The authors tested a soil sample in a different study in the EFA that exhibited a critical shear stress of 109.1 Pa, which was well outside the range of this model prediction. Although it classified as low plasticity clay, the sample was drilled from a depth of 19 m, and was highly cemented. The physiographic region was characterized by the presence of shales and cemented materials. Because the depth of the sample and the cementation, the model would not be appropriate for this sample. The over consolidation due to high overburden stress most likely controlled the onset of erosion in this case; however, this highlights the need for research in erosion of IGM.

There are a few limitations of this study. Firstly, since the project goal was to reduce overconservative abutment scour predictions in cohesive soils, soil sampling and ERT surveys were performed at streambanks. As such, all samples were not fully saturated depending upon the depth of the water table. The degree of saturation was high (mean saturation of 90.91% for all 70 samples), so there is a need for separate soil sampling at streambeds to extend this model for pier scour and contraction scour. The scour behavior and other soil properties of fully saturated bed sediments may be different than the abutment soils. Kouchaki et al. (2018) showed that electrical resistivity is highly influenced by the degree of saturation at low degrees of saturation and has a negligible influence when saturation is above 60%. Therefore, there is also a need to test soils with low degrees of saturation to extend the developed model for surface erosion. Also, porewater conductivity and salinity increase critical shear stress for erosion and decrease soil electrical resistivity (Kandiah 1974, Friedman 2005). The variation of pore water conductivity was small in this study, between 0.28 to 1.28 mS/cm with a mean value of 0.74 mS/cm. Although electrical

resistivity captures the variation in salinity, the developed model should be evaluated for highly saline soils with high porewater conductivity, such as above 4.5 mS/cm found on Arkansas River in western Kansas (Miller et al. 2010). Lastly as stated before, the model prediction is limited to 36.2 Pa and will be over conservative for IGM or soft rocks. Additional testing is required for a less conservative equation incorporating these geomaterials.

4.7 Conclusions

A new model for predicting critical shear stress in cohesive soils was developed. A total of 13 different soil properties were measured; and percent fines, liquid limit and electrical resistivity were found as statistically significant independent variables for the model. The advantages of this study were that erosion testing was performed on undisturbed field samples and soil samples were collected from 26 sites across eight different physiographic provinces incorporating a broad spectrum of cohesive soils. The predicted critical shear using this model ranges between 0.3 to 36.2 Pa and the model is applicable for samples with percent fines between 11 to 100, liquid limit between 26 to 80, and plasticity index between 3 to 52. A design factor α_d was developed as a function of probability of overpredicting the critical shear stress. The design engineers may select an α_d value based on the project need and the level of uncertainty they are willing to accept, however α_d based on common levels of risk were presented.

The unique contribution of this study was to establish electrical resistivity as a measurable soil property for bridge scour estimation. Electrical resistivity is a bulk soil property and there are many common geochemical and biological properties affecting both erosion and electrical resistivity. While measurements of many of the geochemical and biological properties are uncommon for transportation agencies, the use of electrical resistivity imaging for site

characterization has been increasing. It is likely that there will be other new applications for electrical resistivity in transportation geotechnics. This study was limited to cohesive soils collected from river banks. There is a need to evaluate if the model is valid for samples collected from river beds and other geotechnical structures (i.e., levees, dams, slopes). Finally, although models to predict critical shear stress in cohesionless soils are well defined and accurate, there is very limited research on the erosion of intermediate geomaterials.

Chapter 5 - Scientific Contributions

The goals of this study were to develop a rapid methodology for priority based monitoring of scour critical bridges and an empirical model of critical shear stress to predict the onset of erosion. On the process of achieving these goals several scholarly contributions have been made in the science and engineering field; these are outlined below.

5.1 Establishing resistivity as a measurable soil property

To the best of the authors' knowledge, this study is the first to utilize electrical resistivity to predict soil erosion in the literature. Electrical resistivity has traditionally been used for qualitative subsurface characterization. In these applications, an anomaly in electrical resistivity values would indicate any irregularities in the subsurface. In this study, electrical resistivity was used both qualitatively and quantitatively. Qualitative use of electrical resistivity included constructing two dimensional soil erosion profiles. After using electrical resistivity as a binary classifier, it was possible to make a "map" of soil erodibility. As shown in Karim and Tucker-Kulesza (2017), and Karim et al. (2019), these erosion maps may be used to identify where to place a bridge foundation, where to sample for a more detailed erosion analysis, or to roughly estimate a potential scour depth. The most unique contribution of this study was to use electrical resistivity as a continuous numerical model variable. It was verified that resistivity works as an *excellent* binary classifier to distinguish bridge sites with high erodibility.

Electrical resistivity was also found as a statistically significant model variable for predicting critical shear stress. Therefore, electrical resistivity can be measured like other soil index properties. This is a novel finding because electrical resistivity is a bulk soil response and influenced by various soil properties such as particle size, soil type, water content, degree of saturation, unit weight, specific surface area, porosity, hydraulic conductivity, density, Atterberg

limits, temperature, ionic concentration, salinity, sodium absorption ratio (Kouchaki et al. 2018, Kibria and Hossain 2012, Abu-Hassanein et al. 1996, Friedman 2005). It may not be feasible to obtain all these properties separately for a single project, but using resistivity as a measurable soil property will provide a new information of how and at what proportions all these variables are affecting the onset of erosion. While many researchers are still correlating resistivity with other soil properties (Kouchaki et al. 2018, Chen et al. 2018), this was the first time electrical resistivity itself was used as a measurable soil property in a model. Finding resistivity as a significant measurable property was also crucial, because its use in transportation projects will only increase in near future (FHWA 2019) and numerical models may be developed to better characterize a site using electrical resistivity as a soil property.

5.2 A binary classifier for rapid erosion monitoring

More than 25,000 bridges were identified as scour critical after a 15 year investigation by the FHWA from 1988 to 2003. Since 2005, state DOTs are required to implement a plan of action for fixing these scour critical bridges by a federal mandate. For states like Kansas, which has over a thousand bridges on the scour critical list, this would be time consuming and not economically feasible to remediate these bridges at once. Therefore, a priority based system was needed. This research has established that ERT, which takes approximately an hour to conduct, can be used as a rapid and nondestructive methodology to distinguish potentially more vulnerable bridges on the scour critical bridge list. In HEC-18, the erodibility of all geologic materials is divided into six categories, namely, non, very low, low, medium, high, and very high erodibility (Arneson et al. 2012). Receiver operating characteristics curve showed that the efficiency of an ERT based binary classifier model was *excellent* to distinguish bridge sites with high and very high erodibility from rest of the bridges (i.e., non, very low, low, and medium erodibility). A cut-off resistivity value

of 50 Ωm was recommended for the binary classifier. If this cut-off value is used in practice, there is an 87% probability of high or very high erodibility when the measured resistivity is above 50 Ωm . Hence, this binary classifier model will allow the bridge engineers to prioritize their scour critical bridges and conduct detailed investigation only on bridges that are identified as more vulnerable. Ultimately, if accepted in practice, this methodology may also be used to remove bridges from the scour critical list that were identified based on HEC-18 calculations.

5.3 A new critical shear stress equation for cohesive soils

The HEC-18 is the primary tool for scour depth estimation, which is based on cohesionless soils. Equations to estimate scour depth as a function of critical shear stress for cohesive soils were added in the latest edition of HEC-18; however, no equations to calculate critical shear stress was given. Site specific erosion testing was recommended to obtain the critical shear stress in cohesive soils instead. Since site specific testing is time consuming and needs special equipment, transportation agencies are continuing to use the equation based on cohesionless soils resulting over conservative scour depths. Among many studies to develop critical shear stress in cohesive soils, only the Shan et al. (2015) model was developed on the context of HEC-18. However, the use of new model was limited by plasticity index ranging between 4 to 25, liquid limit between 15 to 50, percent of fines below 90, and the model only works within hydraulic shear stresses between 3 to 15 Pa. Basically, this equation covered critical shear stress for low plastic silts and clays, which is a small portion cohesive soils. With a view to incorporating a broader spectrum of cohesive soils in the model, a new model to predict the critical shear stress for cohesive soils was developed. A total of 70 field retrieved soil samples from 26 sites (falling under 8 different physiographic regions) were included in the model. The resulting R^2 of the model was 0.62. No other studies were found on cohesive soils with better accuracy that used field retrieved samples. Also, this study had the most samples than previous research, including

random samples from three other states (i.e., Ohio, Nebraska, and Colorado). Thus, the ranges of various soil properties were much wider than previous models. For example, percent fines varied between 11 to 100, liquid limit between 26 to 80, and plasticity index between 3 and 52. Hence, this model will incorporate both low high plastic silts and clays. Most notably, this new model will predict critical shear stress from 0.3 to 36.2 Pa, which is broader than previous ranges. Note that, the sole purpose of developing a separate critical shear stress equation for cohesive soils was that scour depths were very conservative using equations based on cohesionless soils in HEC-18. The increase of upper limit from 15 Pa to 36.2 Pa signifies that transportation agencies will be able to use less conservative scour depths for very erosion resistant cohesive soils and provide economical design. Also, more accurately predicting high levels of critical shear stress will further help to identify fundamental mechanisms of cohesive soil erosion, which are still largely unknown. While correlation for erosion in cohesionless soils was developed as early as 1936 (Shields 1936), researchers are still studying the cohesive soils erosion. As discussed, two significant variables of this study (percent fines and liquid limit) were also found significant by Shan et al. (2015), and resistivity, the third variable is indirectly related to variables that other researchers found significant. Perhaps, this contribution, i.e., better understanding the mechanism of erosion in cohesive soils, is more important than the statistical model development itself.

5.3 Implementing robust probabilistic and statistical approaches in geotechnical engineering

The efficiency of the binary classifier model was evaluated using receiver operating characteristics curve. A Receiver Operating Characteristics (ROC) curve is a statistical tool for illustrating the diagnostic ability of a binary classifier (Egan 1975, Swets 1988, Williams et al. 1999). This methodology was first developed for radar signal detection during the 1940s and has since been

utilized in fields like machine learning, atmospheric sciences, geosciences, biosciences, finance, experimental psychology and sociology (Krzanowski and Hand 2009). Only a few studies were identified in the literature where ROC curves were used for geologic studies (Brenning 2005, Gorsevski et al. 2006, Holliday et al. 2006); however, there have been no engineering applications. The example of utilizing this methodology for evaluating bridges can be utilized for other site characterization purposes by the geo-engineering community because many of the design problems are binary (e.g., over prediction versus underprediction, structurally safe versus unsafe). Additionally, the critical shear stress model was developed following a robust statistical analysis. Typically, in engineering applications, multiple regression analysis is done using the independent variables that show best correlation with dependent variables and transformation functions (e.g., power relationship) are iterated to obtain the best R^2 . On the other hand, several steps were followed to perform the regression analysis in this study. Multicollinearity among different independent variables were checked, and geotechnical judgement was applied to exclude extra variables, even if they showed “good” correlation with the dependent variable (i.e., critical shear stress). The findings of stepwise regression were cross checked using the F scores of each statistically significant independent variables. The regression coefficients were also finalized based on the results of “leave one out” cross validation. Furthermore, the design factor was chosen from its log-normal cumulative distribution function. This systematic approach can be an example of performing robust statistical analysis to the geo-engineers for building empirical relationships of soil parameters which are often interrelated.

Chapter 6 - Conclusions

The goal of this study was to improve current practices for evaluating scour at bridges by transportation agencies nationwide and expand the FHWA's initiative of using electrical resistivity as one of the advanced geotechnical methods in exploration (A-GaME) for site characterization purpose. Ultimately, the findings from this study can be applied for a two-stage scour evaluation at existing structures: detecting potentially vulnerable sites for remediation prioritization and determining critical shear stress for scour depth predictions. They can also be used in the same way at the design phase: using ERT to identify highly erodible soils during the initial hydraulic study for a new bridge and for determining the critical shear stress once the foundation locations are selected.

An electrical resistivity based binary classifier model was developed to categorize the erodibility level at a bridge site. Among the 616, 094 existing bridges listed in the national bridge inventory, over 20, 000 are scour critical. Nationwide DOTs are required to maintain a plan of actions (POA) to maintain these scour critical bridges. However, many states have thousands of bridges in the scour critical list (including Kansas). Therefore, a rapid site characterization methodology was warranted to characterize the level of erodibility at these scour critical bridges and prioritize their scour vulnerability based on the level of erodibility. As per HEC-18 erodibility categorization, soils exhibiting high or very high erodibilities have more potential to erode than other soils. It was showed that soils with resistivity over $50 \Omega\text{m}$ had 87% probability of classifying as high or very high erodibility. It takes approximately an hour perform resistivity survey; therefore, scour critical bridges can be rapidly prioritized for monitoring. For example, sites with subsurface resistivity above $50 \Omega\text{m}$ can be given more priority for monitoring and vice versa. Furthermore, ERT surveys provide spatial distributions of variability in the subsurface. For

example, although the boreholes were up to 3.35 m deep with a diameter of 89 mm in this study, the ERT profiles contained the subsurface distribution of ER for a 2D section of $25 \times 6.4 \text{ m}^2$ area. This methodology can be used to map the extent of highly erodible soils parallel to a bridge, future bridge site, or other infrastructure where surface erosion estimates are needed. When present at the surface, bridge designers may elect to consider the entire high erodibility layer thickness as the minimum potential scour zone. Localized zones of highly erodible soils that may have been missed with traditional boreholes will also be identified using the continuous ERT profiles.

A new critical shear stress model for cohesive soils was developed in this study. One of the advantages of this model was that soil samples were collected from eight different physiologic provinces incorporating a broad range of cohesive soils. The model is applicable for percent fines between 11 to 100, liquid limit between 26 to 80, and plasticity index between 3 to 52. As a result, the range of predicted shear stress was much greater than previous models. Higher predicted critical shear stress is equivalent to lower predicted scour depth; therefore, if this model is utilized by transportation agencies more economic design can be achieved in cohesive soils than before. Percent fines, liquid limit, and resistivity were found as statistically significant variables for the critical shear stress model in this study. Among these variables percent fines and liquid limit are commonly measured by transportation agencies. Electrical resistivity is a bulk soil property and there are many common physical and geochemical properties affecting both erosion and electrical resistivity. While measurements of many of the geochemical properties are uncommon for transportation agencies, the use of electrical resistivity imaging for site characterization has been increasing. Recently, the FHWA has taken an initiative to conduct increased geophysical surveys including electrical resistivity for various aspects of site characterization. Since, ERT survey takes approximately an hour to nondestructively image the subsurface, the FHWA note that introducing electrical resistivity survey in

geotechnical projects will provide reduced risk, improved quality and accelerated project delivery. Furthermore, electrical resistivity contains a new information of how many physical and geochemical factors are interrelated. While many researchers have been still correlating resistivity with other soil properties, finding resistivity as a measurable property by itself was a unique scientific contribution of this study.

The coefficient of determination of the critical shear stress model was 0.62. A comparison of predicted versus actual critical shear stress showed that the model equation over predicted 32 observations of critical shear stress and under predicted 38 observations of critical shear stress. A plot of probability of failure for different design factors were constructed. This will allow the design engineers to choose a design factor depending upon the uncertainty they are willing to accept for a certain project. For example, for designing scour depth for a bridge along rural highways, a higher design factor may be warranted so as to not be too conservative, while a smaller factor would likely be used for a major interstate where a lower risk is acceptable.

One of the limitations of this study was that soil samples and measured resistivity represented partially saturated condition at most of the bridge sites depending on the depth to the groundwater table. This was because abutment scour is prominent in Kansas, and soil sampling and ERT surveys were performed on the streambank (as opposed to streambed) at all sites. However, the degree of saturation was very high (mean value of 90.91%) for all 70 samples. As shown in Chapter 3, the difference in resistivity values compared to fully saturated condition was negligible at these high degrees of saturation. However, there is a need to collect samples from streambeds to extend this model for pier scour and contraction scour estimation because riverine sediments are expected to have different soil properties than stream bank soils. Future researches may also consider the erosion of geostructures other than bridge foundations. For example, there is a need to evaluate if the model is valid for

erosion in levees, dams, and slopes. As electrical resistivity is highly controlled by the degree of saturation, additional testing is required at lower degrees of saturation. This study was also limited by low conductivity, non-saline porewater. Thus, the electrical conductivity of the porewater was measured to establish boundaries of using electrical resistivity on this context. Porewater salinity also affects soil erosion, thus the potential remains for the model in more saline soils, however this must be established. Finally, the developed critical shear stress equation can predict up to a critical shear stress of 36.2 Pa which was found over conservative for cemented soils. Very few studies on the erosion characteristics of IGM, soft rock, shale or cemented materials were found in existing literature; therefore, future studies should include the erosion characteristics of these geomaterials in the model.

References

- AASHTO. (2012). "Standard method of test for determining minimum laboratory soil resistivity."
AASHTO Standard T 288-12, American Association of State Highway and Transportation
Officials, Washington, DC.
- Abu-Hassanein, Z., Benson, C., and Blotz, L. (1996). "Electrical resistivity of compacted clays."
J. Geotech. Eng., 10.1061/(ASCE)0733-9410 (1996)122:5(397), 397–406.
- AGI (Advanced Geosciences, Inc.). (2009). *Instruction Manual for EarthImager 2D Version 2.4.0
Resistivity and IP Inversion Software*, Advanced Geosciences, Inc., Austin, TX.
- Ahmed, A., Hossain, S., and Khan, M. S. (2018). "Monitoring of Moisture Variation in Highway
Slope through Resistivity Imaging." *IFCEE 2018*, ASCE, Reston, VA, 435-444.
- Amaryan, L. S. (1993). *Soft soil properties and testing methods*. A. A. Balkema, Rotterdam, 180.
- Amos, C. L., Feeney, T., Sutherland, T. F., and Luternauer, J. L. (1997). "The stability of fine-
grained sediment from the Frase River Delta." *Estuarine, Coastal and Shelf Science*, 45,
507–524.
- Arato, A., Cosentini, R. M., Della Vecchia, G., Foti, S., Godio, A., and Musso, G. (2013).
"Electrical Resistivity Tomography: combined field and laboratory experiments for the
characterization and monitoring of hydrocarbon pollution." *Geotechnical and Geophysical
Site Characterization: Proceedings of the 4th International Conference on Site
Characterization ISC-4*, Taylor & Francis Books Ltd., 1, 1789-1796.
- Ariathurai, C.R. (1974). "A finite element model for sediment transport in estuaries." PhD-thesis,
University of California, Berkley, CA.

- Ariathurai, R., and Arulanandan, K. (1978). "Erosion rates of cohesive soils." *Journal of the hydraulics division*, 104(2), 279-283.
- Arjwech, R., Everett, M. E., Briaud, J. L., Hurlbauss, S., Medina-Cetina, Z., Tucker, S., and Yousefpour, N. (2013). "Electrical resistivity imaging of unknown bridge foundations." *Near Surface Geophysics*, 11(6), 591-598.
- Arulanandan, K. (1975). "Fundamental aspects of erosion of cohesive soils." *Journal of the Hydraulics Division*, 101(5), 635-639.
- Arneson, L. A., Zevenbergen, L. W., Lagasse, P. F., and Clopper, P. E. (2012). "Evaluating scour at bridges." *Rep. No. FHWA-HIF-12-003*, U.S. Dept. of Transportation, Washington, DC.
- ASCE. (2017). "Report card for American infrastructure." (<http://www.infrastructurereportcard.org/wp-content/uploads/2017/01/Levees-Final.pdf>) (Jun. 30, 2017).
- ASTM. (2007a). "Standard test method for erodibility determination of soil in the field or in the laboratory by the jet index method (withdrawn 2016)." *ASTM D5852-00*, West Conshohocken, PA.
- ASTM. (2007b). "Standard test method for particle-size analysis of soils." *ASTM D422-63*, West Conshohocken, PA.
- ASTM. (2010). "Standard test methods for liquid limit, plastic limit, and plasticity index of soils." *ASTM D4318-10*, West Conshohocken, PA.

- ASTM. (2013). “Standard test method for materials finer than 75- μm (No. 200) sieve in mineral aggregates by washing.” *ASTM C117-13*, West Conshohocken, PA.
- ASTM. (2014a). “Standard practices for preserving and transporting soil samples.” *ASTM D4220/D4220M-14*, West Conshohocken, PA.
- ASTM. (2014b). “Standard test method for sieve analysis of fine and coarse aggregates.” *ASTM C136/C136M-14*, West Conshohocken, PA.
- ASTM. (2014c). “Standard Test Methods for Specific Gravity of Soil Solids by Water Pycnometer.” *ASTM D854-14*, West Conshohocken, PA.
- ASTM. (2015a). “Standard practice for thin-walled tube sampling of finegrained soils for geotechnical purposes.” *ASTM D1587/D1587M-15*, West Conshohocken, PA.
- ASTM. (2015b). “Standard Test Method for Unconsolidated-Undrained Triaxial Compression Test on Cohesive Soils.” *ASTM D2850-15*, West Conshohocken, PA.
- ASTM. (2017a). “Standard Test Methods for Liquid Limit, Plastic Limit, and Plasticity Index of Soils.” *ASTM D4318-17e1*, West Conshohocken, PA.
- ASTM. (2017b). “Standard Test Method for Particle-Size Distribution (Gradation) of Fine-Grained Soils Using the Sedimentation (Hydrometer) Analysis.” *ASTM D7928-17*, West Conshohocken, PA.
- ASTM. (2017c). “Standard Test Method for Materials Finer than 75- μm (No. 200) Sieve in Mineral Aggregates by Washing.” *ASTM C117-17*, West Conshohocken, PA.

- ASTM. (2017d). “Standard Practice for Classification of Soils for Engineering Purposes (Unified Soil Classification System).” *ASTM D2487-17*, West Conshohocken, PA.
- ASTM. (2018a). “Standard Test Method for Measurement of Soil Resistivity Using the Two-Electrode Soil Box Method.” *ASTM G-187-18*, West Conshohocken, PA.
- ASTM. (2018b). “Standard Test Methods for Laboratory Determination of Density (Unit Weight) of Soil Specimens.” *ASTM D7263-09(2018)e2*, West Conshohocken, PA.
- ASTM. (2019). “Standard Test Methods for Laboratory Determination of Water (Moisture) Content of Soil and Rock by Mass.” *ASTM D2216 - 19*, West Conshohocken, PA.
- Baecher, G.B., Christian J.T. (2003). *Reliability and Statistics in Geotechnical Engineering*. New York, John Wiley & Sons.
- Bai, W., Kong, L., and Guo, A. (2013). “Effects of physical properties on electrical conductivity of compacted lateritic soil.” *Journal of Rock Mechanics and Geotechnical Engineering*, 5(5), 406-411.
- Bale, A. J., Stephens, J. A., and Harris, C. B. (2007). “Critical erosion profiles in macro-tidal estuary sediments: Implications for the stability of intertidal mud and the slope of mud banks.” *Continental shelf research*, 27(18), 2303-2312.
- Bernhardt, M., Briaud, J., Kim, D., Leclair, M., Storesund, R., Lim, S., Bea, R. G., and Rogers, J. D. (2011). “Mississippi river levee failure: June 2008 flood.” *International Journal of Geoengineering case history*, 2(3), 127-162.

- Binley, A., and Kemna, A. (2005). “DC resistivity and induced polarization methods.” *Hydrogeophysics*, Springer, Netherlands, 129-156.
- Bloomquist, D., Sheppard, D. M., Schofield, S., and Crowley, R. W. (2012). “The rotating erosion testing apparatus (RETA): A laboratory device for measuring erosion rates versus shear stresses of rock and cohesive materials.” *Geotech. Test. J.*, 35(4), 641-648.
- Brenning, A. (2005). “Spatial prediction models for landslide hazards: review, comparison and evaluation.” *Natural Hazards and Earth System Science*, 5(6), 853-862.
- Briaud, J., Ting, F., Chen, H., Cao, Y., Han, S., and Kwak, K. (2001). “Erosion function apparatus for scour rate predictions.” *J. Geotech. Geoenviron. Eng.*, 10.1061/(ASCE)1090-0241(2001)127:2(105), 105–113.
- Briaud, J. L. (2008). “Case histories in soil and rock erosion: Woodrow Wilson Bridge, Brazos River Meander, Normandy Cliffs, and New Orleans Levees.” *J. Geotech. Engrg.*, 10.1061/(ASCE)1090-0241(2008)134:10(1425).
- Briaud, J.L., Chen, H.C., Chang, K.A., Oh, S.J., Chen, S., Wang, J., Li, Y., Kwak, K., Nartjaho, P., Gudaralli, R., Wei, W., Pergu, S., Cao, Y.W., and Ting, F. (2011). “The Sricos – EFA Method.” Summary Report, Texas A&M University, College Station, TX.
- Briaud, J. L., Govindasamy, A. V., and Shafii, I. (2017). “Erosion charts for selected geomaterials.” *J. Geotech. Geoenviron. Eng.*, 10.1061/(ASCE)GT.1943-5606.0001771, 04017072.

- Calappi, T., Miller, C., and Carpenter, D. (2010). "Revisiting the HEC-18 scour equation." *Scour and Erosion*, ASCE, Reston, VA, 1102–1109.
- Carlson, E. J., and Enger, P. F. (1962). "Studies of tractive forces of cohesive soils in earth canals." *Rep. No. Hyd-504*, US Department of the Interior Bureau of Reclamation, Denver, CO.
- CGS (Colorado Geological Survey). (2019). "Physiographic Provinces of Colorado." (<http://coloradogeologicalsurvey.org/colorado-geology/topography/physiographic/>) (Aug. 7, 2019).
- Chambers, J. E., Wilkinson, P. B., Penn, S., Meldrum, P. I., Kuras, O., Loke, M. H., and Gunn, D. A. (2013). "River Terrace Sand and Gravel Deposit Reserve Estimation using Three-Dimensional Electrical Resistivity Tomography for Bedrock Surface Detection." *Journal of Applied Geophysics*, 93(0), 25-32.
- Chen, Y., Wei, Z., Irfan, M., Xu, J., and Yang, Y. (2018). "Laboratory investigation of the relationship between electrical resistivity and geotechnical properties of phosphate tailings." *Measurement*, 126, 289-298.
- Clark, L. A., and Wynn, T. M. (2007). "Methods for determining streambank critical shear stress and soil erodibility: implications for erosion rate predictions." *Transactions of the ASABE*, 50(1), 95-106.
- Constable, S. C., Parker, R. L., and Constable, C. G. (1987). "Occam's inversion: A practical algorithm for generating smooth models from electromagnetic sounding data." *Geophysics*, 52(3), 289-300.

- Crowley, R. W., Bloomquist, D. B., Shah, F. D., and Holst, C. M. (2012). "The Sediment Erosion Rate Flume (SERF): A New Testing Device for Measuring Soil Erosion Rate and Shear Stress." *Geotechnical Testing Journal*, 35(4), 649-659.
- Dahlin, T. (2001). "The development of DC resistivity imaging techniques." *Computers & Geosciences*, 27(9), 1019-1029.
- Debnath, K., and Chaudhuri, S. (2010). "Cohesive sediment threshold: a review." *ISH Journal of Hydraulic Engineering*, 16(1), 36–56.
- Dunn, I. S. (1959). "Tractive resistance of cohesive channels." *Journal of the Soil Mechanics and Foundations Division*, 85(3), 1-24.
- Egan, J. P. (1975). *Signal Detection Theory and ROC Analysis*, Academic Press, Cambridge, MA.
- Everett, M. E. (2013). "Electrical Resistivity Method." Chapter 4, *Near-Surface Applied Geophysics*, Cambridge University Press, New York, NY, 70-102.
- FHWA (Federal Highway Administration). (2017). "Download NBI ASCII Files 2016." <<https://www.fhwa.dot.gov/bridge/nbi/ascii.cfm?year=2016>> (Feb. 20, 2017).
- FHWA (Federal Highway Administration). (2019). "Advanced Geotechnical Methods in Exploration (A-GaME)." <https://www.fhwa.dot.gov/innovation/everydaycounts/edc_5/geotech_methods.cfm> (Aug. 7, 2019).
- Friedman, S. P. (2005). "Soil properties influencing apparent electrical conductivity: a review." *Computers and electronics in agriculture*, 46(1-3), 45-70.

- Gorsevski, P. V., Gessler, P. E., Foltz, R. B., and Elliot, W. J. (2006). "Spatial prediction of landslide hazard using logistic regression and ROC analysis." *Transactions in GIS*, 10(3), 395-415.
- Grabowski, R. C., Droppo, I. G., and Wharton, G. (2011). "Erodibility of cohesive sediment: the importance of sediment properties." *Earth-Science Reviews*, 105(3), 101-120.
- Grisso, R., Alley, M., Holshouser, D., and Thomason, W. (2009). "Precision farming tools: Soil electrical conductivity." *Publication 442-508*, Virginia Cooperative Extension, Blacksburg, VA.
- Hanson, G. J., Cook, K. R., and Simon, A. (1999). "Determining erosion resistance of cohesive materials. In *Proc.*" *ASCE Intl. Water Resources Eng. Conf.*, ASCE, Reston, VA.
- Hanson, G. J., and Cook, K. R. (2004). "Apparatus, test procedures, and analytical methods to measure soil erodibility in situ." *Appl. Eng. Agric.*, 20(4), 455-462.
- Hanson, G. J., and Temple, D. M. (2002). "Performance of bare-earth and vegetated steep channels under long-duration flows." *Transactions of the ASAE*, 45(3), 695-701.
- Henseler, J., Ringle, C. M., and Sinkovics, R. R. (2009). "The use of partial least squares path modeling in international marketing." *New challenges to international marketing*, Emerald Group Publishing Limited, 277-319.
- Holliday, J. R., Rundle, J. B., Turcotte, D. L., Klein, W., Tiampo, K. F., and Donnellan, A. (2006). "Space-time clustering and correlations of major earthquakes." *Physical review letters*, 97(23), 238501.

- Hossain, M. S., Khan, M. S., Hossain, J., Kibria, G., and Taufiq, T. (2011). "Evaluation of unknown Foundation depth using different NDT Methods." *J. Geotech. Geoenviron. Eng.*, 10.1061/(ASCE)CF.1943-5509.0000268.
- Kansas Mesonet. (2018). "Agriculture, Soil Temperature." <<http://mesonet.k-state.edu/agriculture/soiltemp/>> (accessed multiple dates during 2015 through 2018).
- Inazaki, T., Hayashi, K., Watanabe, F., Tokumaru, K. M. T., and Imamura, S. (2008). "Ground truth verification of an integrated geophysical investigation for the assessment of an earthen levee." *Symposium on the Application of Geophysics to Engineering and Environmental Problems*, Environment and Engineering Geophysical Society, Tulsa, OK, 731-738.
- Julian, J. P., and Torres, R. (2006). "Hydraulic erosion of cohesive riverbanks." *Geomorphology*, 76(1), 193-206.
- Kandiah, A. (1974). "Fundamental aspects of surface erosion of cohesive soils." Ph.D. thesis, Univ. of California, Davis, CA.
- Karim, M. Z. (2016). "Characterizing soil erosion potential using electrical resistivity imaging." M.S. thesis, Kansas State University, Manhattan, KS.
- Karim, M. Z., and Tucker-Kulesza, S. E. (2017). "Two Dimensional Soil Erosion Profile Using Electrical Resistivity Surveys." *Geotechnical Frontiers 2017*, ASCE, Reston, VA, 50-58, 10.1061/9780784480465.006.

- Karim, M. Z., and Tucker-Kulesza, S. E. (2018). “Predicting soil erodibility using electrical resistivity tomography.” *J. Geotech. Geoenviron. Eng.*, 10.1061/(ASCE)GT.1943-5606.0001857, 04018012.
- Karim, M. Z., Tucker-Kulesza, S. E., and Bernhardt-Barry, M. (2019). “Electrical resistivity as a binary classifier for bridge scour evaluation.” *Transportation Geotechnics*, 19, 146-157. <https://doi.org/10.1016/j.trgeo.2019.03.002>.
- Karim, M. Z., Tucker-Kulesza, S. E., Rutherford, C., and Bernhardt-Barry, M. (2019). “Geophysical Engineering to Identify Seepage Channels in the Hager Slough Levee.” *Geo-Congress 2019: Engineering Geology, Site Characterization, and Geophysics*, ASCE, Reston, VA, 345-353, 10.1061/9780784482131.035.
- KDHE (Kansas Department of Health and Environment). (2019). “Ecoregions of Nebraska and Kansas.” (http://www.kdheks.gov/befs/download/bibliography/ksne_ecoregions.pdf) (Aug. 7, 2019).
- KGS (Kansas Geological Survey). (2019). “Surficial Geology of Kansas.” (http://maps.kgs.ku.edu/state_geology/) (Aug. 7, 2019).
- Kibria, G., and Hossain, M. S. (2012). “Investigation of geotechnical parameters affecting electrical resistivity of compacted clays.” *J. Geotech. Geoenviron. Eng.*, 10.1061/(ASCE)GT.1943-5606.0000722, 1520–1529.
- Kibria, G. (2014). “Evaluation of physico-mechanical properties of clayey soils using electrical resistivity imaging technique.” Ph.D. dissertation, Univ. of Texas at Arlington, Arlington, TX.

- Kimiaghalam, N., Clark, S. P., and Ahmari, H. (2015). "An experimental study on the effects of physical, mechanical, and electrochemical properties of natural cohesive soils on critical shear stress and erosion rate." *Int. J. Sediment Res.*, 31(1), 1–15.
- Knapen, A., Posen, J., Govers, G., Gyssels, G., and Nachtergaele, J. (2007). "Resistance of soils to concentrated flow erosion: A review." *Earth-Science Reviews*, 80, 75–109.
- Knight, R. J., and Endres, A. L. (2005). "An Introduction to Rock Physics Principles for Near-Surface Geophysics." *Near Surface Geophysics*, Society of Exploration Geophysics, Tulsa, Ok, 31-70.
- Koehn, W. J., Tucker-Kulesza, S. E., and Steward, D. R. (2018). "Developing a Hydrogeologic Conceptualization of River-Aquifer Interactions with Electrical Resistivity Tomography." *AGU Fall Meeting Abstracts*, <http://adsabs.harvard.edu/abs/2018AGUFMNS33A..06K>.
- Kouchaki, B., Bernhardt-Barry, M. L., Wood, C. M., and Moody, T. (2018). "A laboratory investigation of factors influencing the resistivity of different soil types", *ASTM Geotechnical Testing Journal*, 42(4), 829-853.
- Krzanowski, W. J., and Hand, D. J. (2009). *ROC curves for continuous data*, CRC Press, Boca Raton, FL.
- Kumar, R., and Indrayan, A. (2011). "Receiver operating characteristic (ROC) curve for medical researchers." *Indian pediatrics*, 48(4), 277-287.

- Larionov, G. A., Bushueva, O. G., Dobrovol'skaya, N. G., Kiryukhina, Z. P., Krasnov, S. F., and Litvin, L. F. (2014). "Effect of the Water Temperature and Soil Moisture on the Erodibility of Chernozem Samples: A Model Experiment." *Eurasian Soil Sci.*, 47(7), 734-739.
- Léonard, J., and Richard, G. (2004). "Estimation of runoff critical shear stress for soil erosion from soil shear strength." *Catena*, 57(3), 233-249.
- Lin, C., Han, J., Bennett, C., and Parsons, R. L. (2014). "Case history analysis of bridge failures due to scour." *Climatic effects on pavement and geotechnical infrastructure*, 204-216.
- Liu, X., Jia, Y., Zheng, J., Shan, H., and Li, H. (2013). "Field and laboratory resistivity monitoring of sediment consolidation in China's Yellow River estuary." *Engineering geology*, 164, 77-85.
- Loke, M. H. (1999). "Electrical Imaging Surveys for Environmental and Engineering Studies." <http://moho.ess.ucla.edu/~pdavis/ESS135_2013/LITERATURE/%20LokeDCREsistivity.pdf> (Feb. 22, 2017).
- Lucius, J. E., Langer, W. H., and Ellefsen, K. J. (2007). *An Introduction to Using Surface Geophysics to Characterize Sand and Gravel Deposits*, US Geological Survey, Reston, VA.
- Mahalder, B., Schwartz, J. S., Palomino, A. M., and Zirkle, J. (2018). "Relationships between physical-geochemical soil properties and erodibility of streambanks among different physiographic provinces of Tennessee, USA." *Earth Surface Processes and Landforms*, 43(2), 401-416.

- McClerren, M. A., Hettiarachchi, H., and Carpenter, D. D. (2012). “An investigation on erodibility and geotechnical characteristics of fine grained fluvial soils from Lower Michigan.” *Geotechnical and Geological Engineering*, 30(4), 881-892.
- Mendenhall, W., and Sincich, T. (2012). *A second course in statistics: Regression analysis* (7th ed.), Prentice Hall, Boston, MA.
- Meng, X. M., Jia, Y. G., Shan, H. X., Yang, Z. N., and Zheng, J. W. (2012). “An experimental study on erodibility of intertidal sediments in the Yellow River delta.” *International Journal of Sediment Research*, 27(2), 240-249.
- Miller, L. D., Watts, K. R., Ortiz, R. F., and Ivahnenko, T. (2010). *Occurrence and distribution of dissolved solids, selenium, and uranium in groundwater and surface water in the Arkansas River Basin from the headwaters to Coolidge, Kansas, 1970-2009*. U. S. Geological Survey.
- Mitchell, J. K., and Soga, K. (2005). *Fundamentals of soil behavior*, 3rd edn., John Wiley & Sons, Inc., Hoboken, NJ.
- Moody, L. F. (1944). “Friction factors for pipe flow.” *Trans. Am. Soc. Mech. Eng.*, 66(8), 671–684.
- Moore, W. L., and Masch, F. D. (1962). “Experiments on the scour resistance of cohesive sediments.” *J. of Geophysical Research*, 67(4), 1437-1446.

- Nassif, H., Ertekin, A. O., and Davis, J. (2002). "Evaluation of bridge scour monitoring methods." *United States Department of Transportation, Federal Highway Administration, Trenton.*
- Neuendorf, K. K. E., Mehl, J. P., Jr., and Jackson, J. A. (2011). *Glossary of Geology*, 5th Edition, Revised, American Geological Institute, Alexandria, Virginia.
- ODNR (Ohio Department of Natural Resources). (2019). "Physiographic Regions of Ohio." (https://geosurvey.ohiodnr.gov/portals/geosurvey/PDFs/Misc_State_Maps&Pubs/physio.pdf) (Aug. 7, 2019).
- Ott, R. L., and Longnecker, M. (2004). *A first course in statistical methods*, Brooks/Cole – Thomson Learning, Belmont, CA.
- Owen, M. W. (1975). "Erosion of Avonmouth mud (Report No. INT 150)." *Wallingford: Hydraulics Research Station.*
- Partheniades, E. (1965). "Erosion and deposition of cohesive soils." *J. Hydraul. Div.*, 91(1), 105–139.
- Paterson, D. M. (1997). Biological mediation of sediment erodibility: ecology and physical dynamics. In: N. Burt, R. Parker, and J. Watts (Eds.), *Cohesive sediments*, John Wiley and Sons, New York, 215–229.
- Pedregosa, F., Varoquaux, G., Gramfort, A., Michel, V., Thirion, B., Grisel, O., Blondel, M., Prettenhofer, P., Weiss, R., Dubourg, V., Vanderplas, J., Passos, A., Cournapeau, D.,

- Brucher, M., Perrot, M., and Duchesnay, E. (2011). "Scikit-learn: Machine learning in Python." *Journal of machine learning research*, 12(Oct), 2825-2830.
- Raudkivi, A. J. (1990). *Loose Boundary Hydraulics*, 3rd edn., Pergamon Press, New York, NY.
- Ravens, T. M. (2007). "Comparison of two techniques to measure sediment erodibility in the Fox River, Wisconsin." *J. Hydraul. Eng.*, 133(1), 111-115.
- Reddi, L. N., and Bonala, M. V. (1997). "Critical shear stress and its relationship with cohesion for sand-kaolinite mixtures." *Canadian Geotechnical Journal*, 34(1), 26-33.
- Rinaldi, V. A., and Cuestas, G. A. (2002). "Ohmic conductivity of a compacted silty clay." *Journal of Geotechnical and Geoenvironmental Engineering*, 128(10), 824-835.
- Richardson, E. V., and Davis, S. R. (2001). "Evaluating Scour at Bridges, Hydraulic Engineering Circular No. 18 (HEC-18)." *Rep. No. FHWA NHI*, 01-001.
- SAS version 9.4* [Computer software]. SAS Institute Inc., Cary, NC.
- Schuring, J. R., Dresnack, R., Golub, E., Khan, M. A., Young, M. R., Dunne, R., and Aboobaker, N. (2010). "Review of bridge scour practice in the US." *Scour and Erosion*, ASCE, Reston, VA, 1110-1119.
- Shan, H., Shen, J., Kilgore, R. and Kerényi, K. (2015). "Scour in Cohesive Soils." *Rep. No. FHWA-HRT-15-033*, Federal Highway Administration, McLean, VA.
- Sherard, F., Dunnigan, L., Decker, R. and Steele, E. (1976). "Pinhole test for identifying dispersive soils." *Proc. Amer. Soc. Civ. Engrs* 102, GTI, 69-85.

- Shields, A. (1936). “Anwendung der Aenlichkeitsmechanik und der Turbulenzforschung auf die Geschiebebewegung.” *Mitteilungen der Preussischen Versuchsanstalt fur Wasserbau und Schiffbau*, W. P. Ott and J. C. Van Uchelen, translators, California Institute of Technology, Pasadena, Calif.
- Shirole, A. M., and Holt, R. C. (1991). “Planning for a comprehensive bridge safety assurance program.” *Transportation Research Record*, 1290, 39-50.
- Siddiqui, F. I., and Osman, S. B. A. B. S. (2013). “Simple and multiple regression models for relationship between electrical resistivity and various soil properties for soil characterization.” *Environmental earth sciences*, 70(1), 259-267.
- Sirieix, C., Genelle, F., Barral, C., Touze-Foltz, N., Riss, J., and Bégassat, B. (2015). “Characterizing the ageing of a geosynthetic clay liner through electrical resistivity.” *Canadian Geotechnical Journal*, 53(3), 423-430.
- Smerdon, E. T., and Beasley, R. P. (1961). “Critical tractive forces in cohesive soils.” *Agricultural Engineering*, 42(1), 26-29.
- Snapp, M., Tucker-Kulesza, S., and Koehn, W. (2017). “Electrical resistivity of mechanically stabilized earth wall backfill.” *Journal of Applied Geophysics*, 141, 98-106.
- SPSS Statistics version 22.0* [Computer software]. IBM, Armonk, NY.
- Swets, J. A. (1988). “Measuring the accuracy of diagnostic systems.” *Science*, 240(4857), 1285-1293.

- Thoman, R. W., and Niezgodna, S. L. (2008). "Determining erodibility, critical shear stress, and allowable discharge estimates for cohesive channels: Case study in the Powder River basin of Wyoming." *Journal of hydraulic engineering*, 134(12), 1677-1687.
- Thorn, M. F. C., and Parsons, J. G. (1980). "Erosion of cohesive sediments in estuaries: an engineering guide." In *Proc. of the Int. Symp. on Dredging Technol*, 349-358.
- Tucker, S. E., Briaud, J. L., Hurlebaus, S., Everett, M. E., and Arjwech, R. (2015). "Electrical resistivity and induced polarization imaging for unknown bridge foundations." *J. Geotech. Geoenviron. Eng.*, 10.1061/(ASCE)GT.1943-5606.0001268, 04015008.
- Tucker-Kulesza, S., and Karim, M. Z. (2017). *Characterizing soil erosion potential using electrical resistivity imaging* (No. K-TRAN: KSU-15-4). Kansas. Dept. of Transportation.
- USDA (U.S. Department of Agriculture). (1987). "Stability of Grassed-lined Open Channels," *Agricultural Handbook Number 667*, Agricultural Research Service.
- Utley, B. C., and Wynn, T. M. (2008). "Cohesive soil erosion: Theory and practice." *World Environmental and Water Resources Congress 2008: Ahupua'A*, ASCE, Reston, VA, 1-10.
- Vaudelet, P., Schmutz, M., Pessel, M., Franceschi, M., Guérin, R., Atteia, O., Blondel, A., Ngomseu, C., Galaup, S., Rejiba, F., and Bégassat, P. (2011). "Mapping of Contaminant Plumes with Geoelectrical Methods. A Case Study in Urban Context." *Journal of Applied Geophysics*, 75(4), 738-751.
- Wan, C.F., and Fell, R. (2004). "Investigation of rate of erosion of soils in embankment dams." *J. Geotech. Geoenviron. Eng.*, 10.1061/(ASCE)1090-0241(2004)130:4(373).

- Whitney, D.A. (1998). "Soil Salinity." *In: Brown JR, editor. Recommended Chemical Soil Test Procedures for the North Central Region. North Central Regional Publication Number 221 (revised)*, Missouri Ag. Exp. Station SB 1001., Univ. of Missouri, Columbia, MO, 59-60.
- Widdows, J., Brinsley, M. D., and Pope, N. D. (2009). "Effect of *Nereis diversicolor* density on the erodability of estuarine sediment." *Marine Ecology Progress Series*, 378, 135-143.
- Williams, C. J., Lee, S. S., Fisher, R. A., and Dickerman, L. H. (1999). "A comparison of statistical methods for prenatal screening for Down syndrome." *Applied Stochastic Models in Business and Industry*, 15(2), 89-101.
- Wu, N. C., and Chase, S. (2010). "An exploratory data analysis of national bridge inventory." *Rep. No. UVA-2009-03*, U.S. Dept. of Transportation, Washington, DC.
- Zeller, D. E. (1968). "The stratigraphic succession in Kansas.", *Bulletin 189*, Kansas Geological Survey.
- Zhu, Y. H., Lu, J. Y., Liao, H. Z., Wang, J. S., Fan, B., and Yao, S. M. (2008). "Research on cohesive sediment erosion by flow: An overview." *Science in China Series E: Technological Sciences*, 51(11), 2001–2012.
- Zonge, K., Wynn, J., and Urquhart, S. (2005). "Resistivity, Induced Polarization, and Complex Resistivity." *Near Surface Geophysics*, Society of Exploration Geophysics, Tulsa, OK, 265-300.

Appendix A - Full dataset

Table A.1 Values of all soil properties

Critical Shear Stress	Electrical Resistivity	Water Content	Percent Fines	Median Grain Size	Liquid Limit	Plastic Limit	Plasticity Index	Void Ratio	Porosity	Degree of Saturation	Wet Density	Dry Density	Shear Strength
Pa	Ohm-m	%	%	mm	%	%	%	unitless	unitless	%	g/cm ³	g/cm ³	kPa
14.60	9.52	39.65	96.50	0.0100	55	18	37	0.8531	0.4604	88.99	1.87	1.47	143.64
3.53	18.19	30.23	92.37	0.0140	40	17	23	0.8531	0.4604	88.99	1.87	1.47	119.70
1.25	19.38	23.23	90.41	0.0160	31	19	12	0.8531	0.4604	88.99	1.87	1.47	110.12
3.27	18.81	24.39	91.28	0.0170	30	20	10	0.8531	0.4604	88.99	1.87	1.47	191.52
7.87	17.94	27.25	91.71	0.0170	31	17	14	0.8531	0.4604	88.99	1.87	1.47	119.70
35.18	11.13	21.32	89.22	0.0120	41	14	27	0.6158	0.3811	94.89	2.02	1.65	143.64
32.55	12.51	20.96	96.75	0.0068	53	16	37	0.6158	0.3811	94.89	2.02	1.65	143.64
14.49	9.68	23.23	96.37	0.0065	53	15	38	0.6158	0.3811	94.89	2.02	1.65	71.82
27.57	12.62	24.50	95.30	0.0120	41	14	27	0.6158	0.3811	94.89	2.02	1.65	107.73
1.38	131.93	21.32	73.38	0.0190	31	22	9	0.7457	0.4272	89.72	1.91	1.53	239.40
0.88	327.67	18.18	48.81	0.0820	28	18	10	0.7457	0.4272	89.72	1.91	1.53	71.82
0.51	257.31	24.93	17.46	1.8000	26	18	8	0.7457	0.4272	89.72	1.91	1.53	59.85
0.41	189.37	16.76	17.62	1.6400	27	20	7	0.7457	0.4272	89.72	1.91	1.53	23.94
0.38	136.69	23.54	11.37	1.9200	26	19	7	0.7457	0.4272	89.72	1.91	1.53	239.40
12.97	16.21	36.17	98.67	0.0148	53	23	30	0.7586	0.4314	90.08	1.93	1.54	59.85
24.17	14.09	28.41	98.76	0.0110	58	23	35	0.7586	0.4314	90.08	1.93	1.54	35.91
17.14	10.64	25.41	98.28	0.0150	47	24	23	0.7586	0.4314	90.08	1.93	1.54	47.88
32.72	10.20	29.84	96.48	0.0094	50	26	24	0.7586	0.4314	90.08	1.93	1.54	35.91
3.30	5.98	27.24	95.21	0.0100	43	16	27	0.9170	0.4784	89.52	1.82	1.39	131.67
23.75	6.73	28.21	96.74	0.0062	50	17	33	0.9170	0.4784	89.52	1.82	1.39	131.67

9.28	6.76	26.63	98.45	0.0066	56	17	39	0.9170	0.4784	89.52	1.82	1.39	131.67
15.30	6.76	27.63	97.61	0.0042	51	17	34	0.9170	0.4784	89.52	1.82	1.39	59.85
14.69	7.04	28.49	95.91	0.0102	45	16	29	0.9170	0.4784	89.52	1.82	1.39	59.85
3.66	35.58	33.36	95.97	0.0225	46	21	25	0.7421	0.4260	87.16	1.91	1.54	67.86
3.52	17.52	30.89	95.95	0.0225	41	24	17	0.7421	0.4260	87.16	1.91	1.54	119.70
3.30	13.03	29.31	97.38	0.0230	36	19	17	0.7421	0.4260	87.16	1.91	1.54	155.61
22.11	8.73	32.50	99.54	0.0012	80	28	52	1.1799	0.5413	98.41	1.78	1.25	107.73
32.10	8.68	32.44	99.55	0.0014	72	22	50	1.1799	0.5413	98.41	1.78	1.25	107.73
16.07	8.68	25.99	99.72	0.0102	43	16	27	1.1799	0.5413	98.41	1.78	1.25	107.73
54.96	12.31	27.66	99.79	0.0070	44	14	30	1.1799	0.5413	98.41	1.78	1.25	52.67
29.20	18.54	29.69	97.58	0.0145	41	25	26	1.1799	0.5413	98.41	1.78	1.25	67.03
1.57	39.77	16.30	60.53	0.0310	32	29	3	0.4904	0.3290	95.94	2.14	1.83	167.58
36.82	14.59	30.81	98.47	0.0082	45	10	35	0.4904	0.3290	95.94	2.14	1.83	107.73
14.04	7.84	30.10	99.43	0.0052	48	20	28	0.4904	0.3290	95.94	2.14	1.83	107.73
45.65	7.49	29.41	99.19	0.0064	41	24	17	0.4904	0.3290	95.94	2.14	1.83	131.67
38.32	9.28	26.40	99.37	0.0103	48	17	21	0.4904	0.3290	95.94	2.14	1.83	131.67
38.73	12.65	28.10	98.71	0.0055	54	19	35	0.8738	0.4663	92.78	1.88	1.45	131.67
41.07	12.03	27.75	94.46	0.0110	40	23	17	0.8738	0.4663	92.78	1.88	1.45	95.76
18.49	10.37	29.15	93.91	0.0140	39	16	23	0.8738	0.4663	92.78	1.88	1.45	47.88
39.74	9.65	29.00	97.94	0.0068	50	20	30	0.8738	0.4663	92.78	1.88	1.45	95.76
40.32	9.36	29.40	98.30	0.0090	43	21	22	0.8738	0.4663	92.78	1.88	1.45	131.67
33.86	12.77	22.91	98.94	0.0074	41	20	21	0.5402	0.3507	78.03	2.01	1.74	167.58
20.25	13.50	23.89	98.61	0.0082	42	22	20	0.5402	0.3507	78.03	2.01	1.74	155.61
34.49	14.16	24.50	97.52	0.0067	37	19	18	0.5402	0.3507	78.03	2.01	1.74	119.70
34.17	14.70	25.52	95.94	0.0110	36	20	16	0.5402	0.3507	78.03	2.01	1.74	83.79
16.62	14.94	25.74	91.88	0.0120	36	16	20	0.5402	0.3507	78.03	2.01	1.74	83.79
14.03	9.04	28.34	98.35	0.0032	50	26	24	0.8911	0.4712	90.58	1.86	1.44	47.21
34.41	9.26	29.69	98.13	0.0051	44	22	22	0.8911	0.4712	90.58	1.86	1.44	107.73
13.82	9.07	26.28	97.88	0.0060	50	24	26	0.8911	0.4712	90.58	1.86	1.44	107.73
17.33	9.11	24.54	97.39	0.0061	45	20	25	0.8911	0.4712	90.58	1.86	1.44	107.73

35.63	9.36	28.50	97.79	0.0050	47	22	25	0.8911	0.4712	90.58	1.86	1.44	95.76
1.56	41.69	22.41	53.11	0.0620	27	16	11	0.8152	0.4491	78.33	1.83	1.48	43.20
23.53	10.39	28.68	99.16	0.0290	34	23	11	0.6820	0.4055	96.93	1.98	1.59	71.12
3.46	61.00	32.84	98.28	0.0330	35	27	8	0.9581	0.4893	95.64	1.86	1.39	13.94
77.18	11.42	26.28	98.65	0.0044	52	25	27	0.7859	0.4400	94.14	1.93	1.52	82.40
18.67	22.18	21.52	96.79	0.0140	40	26	14	0.9542	0.4883	72.00	1.75	1.39	35.31
33.84	36.46	27.09	98.74	0.0190	40	22	18	0.7983	0.4439	67.50	1.79	1.49	52.06
97.09	7.66	25.40	96.13	0.0100	46	26	20	0.7414	0.4257	99.15	1.96	1.54	116.95
71.91	17.56	24.71	97.91	0.0057	50	23	27	0.7779	0.4375	91.82	1.93	1.53	68.18
67.91	23.40	26.16	95.90	0.0100	37	22	15	0.6545	0.3956	94.26	1.99	1.62	37.80
1.31	19.53	27.08	90.32	0.0170	34	22	12	0.6396	0.3901	94.02	2.00	1.63	61.10
4.90	22.76	18.91	93.64	0.0270	35	22	13	0.5417	0.3514	90.73	2.08	1.76	95.33
69.02	11.16	25.14	97.73	0.0038	46	26	20	0.6640	0.3990	96.58	1.99	1.61	179.55
37.84	12.40	25.87	99.33	0.0042	45	21	24	0.6640	0.3990	96.58	1.99	1.61	95.76
38.30	12.96	26.93	99.59	0.0082	41	21	20	0.6640	0.3990	96.58	1.99	1.61	47.88
14.44	13.03	27.78	96.78	0.0100	39	19	20	0.6640	0.3990	96.58	1.99	1.61	83.79
16.62	13.04	29.41	89.56	0.0150	33	18	15	0.6640	0.3990	96.58	1.99	1.61	71.82
3.79	31.27	10.84	52.07	0.0570	26	15	11	0.2819	0.2199	98.54	2.32	2.11	108.30
4.51	16.72	32.90	91.14	0.0210	32	24	8	1.0180	0.5045	86.39	1.76	1.32	35.62
14.63	7.20	38.14	93.55	0.0070	62	34	28	0.9987	0.4997	99.76	1.85	1.35	35.48